R-12-19-69

FLUIDIC LOW SPEED WIND SENSOR RESEARCH STUDY

FINAL REPORT

December 1969

by

V. F. Neradka
R. F. Turek

Prepared Under Contract NAS 12-2038

for

NASA/ELECTRONICS RESEARCH CENTER
575 Technology Square
Cambridge, Massachusetts 02109

by

Bowles Fluidics Corporation
9347 Fraser Avenue
Silver Spring, Maryland 20910

R-12-19-69

FLUIDIC LOW SPEED WIND SENSOR RESEARCH STUDY

FINAL REPORT

December 1969

by

V. F. Neradka
R. F. Turek

Prepared Under Contract NAS 12-2038

for

NASA/ELECTRONICS RESEARCH CENTER
575 Technology Square
Cambridge, Massachusetts 02109

by

Bowles Fluidics Corporation
9347 Fraser Avenue
Silver Spring, Maryland 20910

FOREWORD

This report of a "Fluidic Low Speed Wind Sensor, Research Study" presents the work performed under NASA Contract NAS 12-2038, by the Bowles Fluidics Corporation, Silver Spring, Maryland, during the period from October, 1968 to October, 1969. This work was accomplished under the technical direction of Mr. Richard J. Miner of the NASA/Electronics Research Center, Cambridge, Massachusetts.

ABSTRACT

Two basic concepts of fluidic wind speed sensors were experimentally investigated. One concept, a cross flow configuration, operates on the principle of momentum interaction between the wind and a perpendicular air jet. The second concept, a parallel flow configuration, operates on the principle of shear interaction between the wind and a parallel air jet.

The results of this investigation reveal that the parallel flow concept has the better potential for a practical instrument. It has better linearity, requires less supply pressure to measure the same maximum air speed, and it operates over a wider range with constant supply pressure than the cross flow concept. Both approaches, however, demonstrated threshold speeds less than 1 ft/sec.

A demonstration model of the parallel flow configuration was built and tested over a wind speed range of 0.3 to 160 ft/sec. Good linearity over this range was achieved with a supply pressure of 5 psig.

A part of this research included the design and fabrication of a special low speed wind tunnel for investigating the velocity range of 0.3 to 15 ft/sec.

TABLE OF CONTENTS

LIST OF FIGURES

LIST OF SYMBOLS

V	Wind Velocity
V_+	Supply Jet Velocity
P_+	Supply Pressure
ΔP	Output Differential Pressure
P_{CL}	Jet Centerline Pressure
P_{O_L}	Fluidic Amplifier Output Pressure, Left Side of Element
P_{O_R}	Fluidic Amplifier Output Pressure, Right Side of Element
P_{C_L}	Fluidic Amplifier Control Pressure, Left Side of Element
P_{C_R}	Fluidic Amplifier Control Pressure, Right Side of Element
d	Nozzle Diameter
y	Distance Between Supply Nozzle and Receiver
x	Distance Measured in Direction of Wind
w	Jet Width, Measured Where $P = P_{\mathrm{CL}}/2$
ρ	Air Density

SECTION I

INTRODUCTION AND SUMMARY

A. Background

The development of vertical and short takeoff and landing aircraft (V/STOL's) has generated the need for special instrumentation and control components unique to the operation of these aircraft. One of the measurements which would be particularly useful during takeoff and landing is relative wind speed. Because of the nature of these aircraft, very low air speeds in all three orthogonal directions occur during their operation near the ground. At present, no practical wind sensing instruments are available for this purpose. The conventional Pitot tube air speed sensor (References 1 and 2) is simple and reliable and performs very well down to the takeoff and landing speeds of conventional aircraft. However, it is generally unsuited for measuring air speeds below about 20 or 30 mph.

Several other concepts have been developed for sensing low air speeds, including the hot wire or film instruments. These devices make use of the cooling capacity of air which varies with the wind velocity. By electrically heating the wire, its temperature, and therefore it resistance, will change with air velocity. This can be measured and calibrated electrically to yield air speed data. Experience has shown, however, that these devices have reliability problems when operated in an aircraft environment due to vibration, rain, debris and natural burning out.

Other sophisticated electronic devices also exist or are being developed. These devices use ultrasonic pulse, transit time, or Doppler techniques for interrogating acoustic signals to measure relative wind speed. Measuring the wind induced motion of ion tracers in an electrostatic field has also been investigated. These types of equipment, however, are complex and quite expensive.

Mechanical devices for measuring wind speed and direction include vane or cup anemometers and weather vanes. However, these instruments have slow response speeds. Furthermore, they are subject to frictional effects which in practice result in threshold speeds of about 2 mph. While this is considerably better than that achieved by Pitot sensors, their relative complexity tends to rule against their use on board aircraft.

Another type of a mechanical low speed sensor employs two Pitot tubes mounted on the ends of a spinning boom. By superimposing the wind speed on the spin velocity, the sensitivity of the Pitot tubes is enhanced. Magnitude and direction of the wind speed are determined from the amplitude and phase of the oscillatory pressure signals developed at the Pitot sensors. Decoding is done electronically. Good linearity and low thresholds have been demonstrated with this approach, but this concept also is relatively complex, expensive and cumbersome.

In summary, then, it is concluded that the present techniques for measuring air speed do not satisfactorily meet the needs of low speed operation as required by V/STOL aircraft. What is needed is a technique for measuring very low wind velocities which is sufficiently rugged for the V/STOL application, yet markedly lower in cost and complexity than an equivalent electronic or electro-mechanical technique.

B. Objectives

Two concepts using fluidic techniques were formulated for measuring very low wind speeds. In these concepts, the wind is impressed on an air jet which produces an amplified pressure signal directly related to wind speed. The two concepts are categorized as:

- Parallel Flow Sensors - in which an air power stream is directed parallel to the wind component being measured.
- Cross Flow Sensors - in which an air power stream is directed perpendicular to the wind component being measured.

The configurations of these sensor concepts are simple and offer the advantages of ruggedness and reliability provided by conventional Pitot tubes. However, preliminary tests indicated that these concepts can provide a marked improvement in sensitivity and linearity over the Pitot sensors.

It was, therefore, an objective of this research study to further verify the feasibility of these concepts and to experimentally obtain engineering data on their performance. It was a further objective to compare the potential of each approach and select the one which seems better suited for aircraft use. And finally, it was an objective to fabricate a model of the selected configuration for demonstrating the concept.

The following design goals were used as the technical objectives for a future wind sensor. They served as guidelines for testing and evaluating the various configurations fabricated during the study.

Air Speed Magnitude

Range:	0 to 60 mph
Accuracy:	± 1/3 ft/sec at 0 mph ± 5% at 60 mph

Air Speed Direction

Range:	Over total spherical coordinates
Accuracy:	± 5 degrees

C. Summary

This study consisted of two Phases.

Phase 1. Testing of variable geometry models of both the parallel and cross flow configurations was conducted. Basic performance characteristics and expectations were determined from these tests.

Phase 2. The parallel flow concept was selected to be better suited for aircraft use. A second generation model was fabricated and tested. This was a fixed geometry model with an optimum configuration as determined by the data obtained in Phase 1.

In the Phase 1 effort, testing was conducted over a wind speed range of 0 to 90 ft/sec (0 to 60 mph). A special low speed tunnel was built to provide a testing capability in the range of 0 to 15 ft/sec. Testing from 10 to 90 ft/sec was conducted in a wind tunnel at the University of Maryland. Several models of both concepts were built and tested. Geometry variables included power nozzle diameter, nozzle-to-receiver spacing and receiver lateral location. Supply pressure was also varied during these tests.

In both configurations a threshold of less than 1/3 ft/sec was realized. The parallel flow sensor, however, was more linear, had a wider range, and required less supply pressure than the cross flow sensor. Therefore, it was chosen for further investigation in Phase 2 of the study. A cross flow model was incorporated into a feedback loop using a fluidic operational amplifier. A test of this system indicated that this would be a feasible means for extending the range of the cross flow sensor if required.

In the Phase 2 study effort, the parallel flow sensor was tested over an increased wind speed range of 0 to 160 ft/sec (0 to 106 mph). Good sensitivity and a sufficiently low threshold were demonstrated at supply pressures from 1 to 5 psig. With a 5 psig supply, saturation had not occurred at 160 ft/sec which indicates that higher ranges are feasible. This suggests that this concept might be used not only for low speeds, but for speeds well into the subsonic region. Furthermore, this could be achieved with a single instrument thereby avoiding the need for multiple sensors.

The tests in Phase 1 were conducted at zero angle-of-attack with all configurations. The tests of the parallel flow demonstration model in Phase 2 included varying angles-of-attack from 0 to 90 degrees. The sensor was located inside a simple collecting tube. Results showed that this configuration was essentially insensitive to angles-of-attack up to 40 degrees.

Section II of this report presents the test results of the demonstration model conducted in Phase 2. Section III describes the preliminary testing of the parallel and cross flow concepts conducted in Phase 1. Section IV presents conclusions of this research study and presents recommendations for further development.

SECTION II

SUMMARY OF TEST RESULTS OF FINAL PARALLEL FLOW MODEL

A. General

This section describes the model of parallel flow sensor and presents the test results conducted under Phase 2 of this study. The selection of the parallel flow approach was based on a trade-off between the two concepts investigated in Phase 1. (Details of the comparison are presented in Section III - D of this report.)

B. Model Description

The model is shown in Figure 1a, b. Flow entering the power supply port, P_+, divides evenly between two nozzles mounted on a common centerline. Separated from these nozzles at a fixed distance are two signal pressure receivers. This subassembly is mounted within a flow straightening tube so that the wind velocity vector is parallel to the nozzle and receiver assembly. To further insure parallel flow, honeycomb flow straighteners are mounted at each end of the tube. By virtue of the different jet mixing in the power jets into and with the wind, which flows along the axis of the tube, a differential pressure, ΔP, is recorded at the receivers. This is shown schematically below.

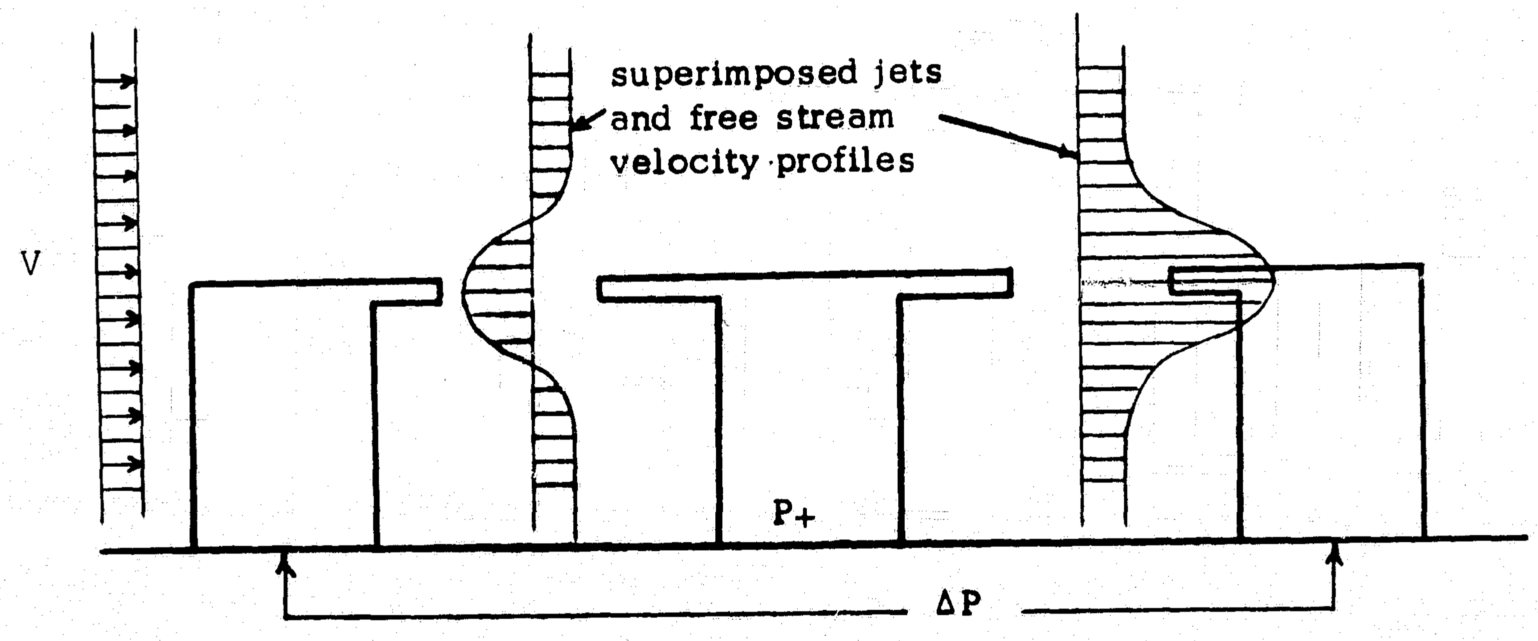

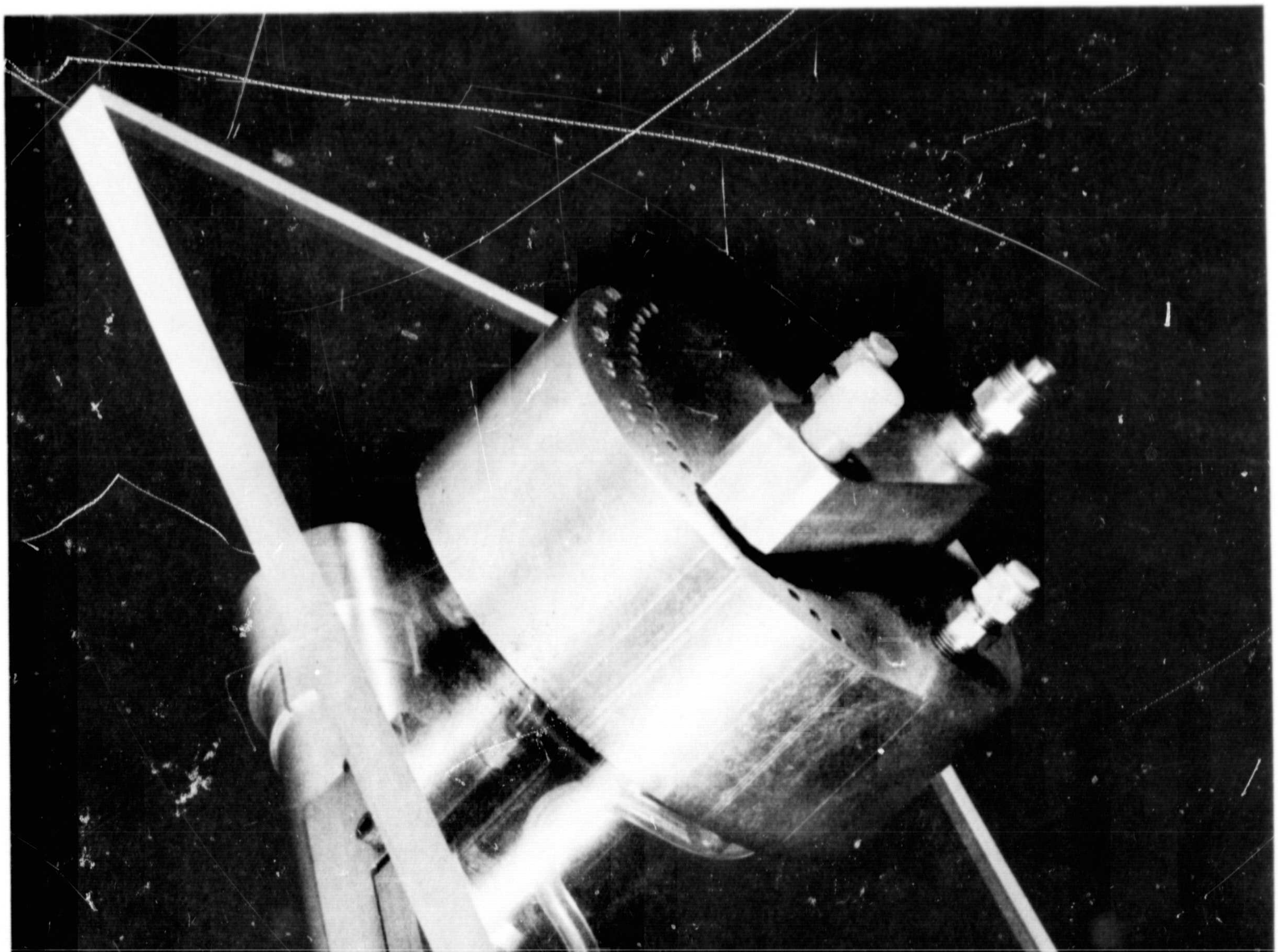

Figure 1a. BOWLES FLUIDICS CORPORATION PARALLEL FLOW WIND SENSOR

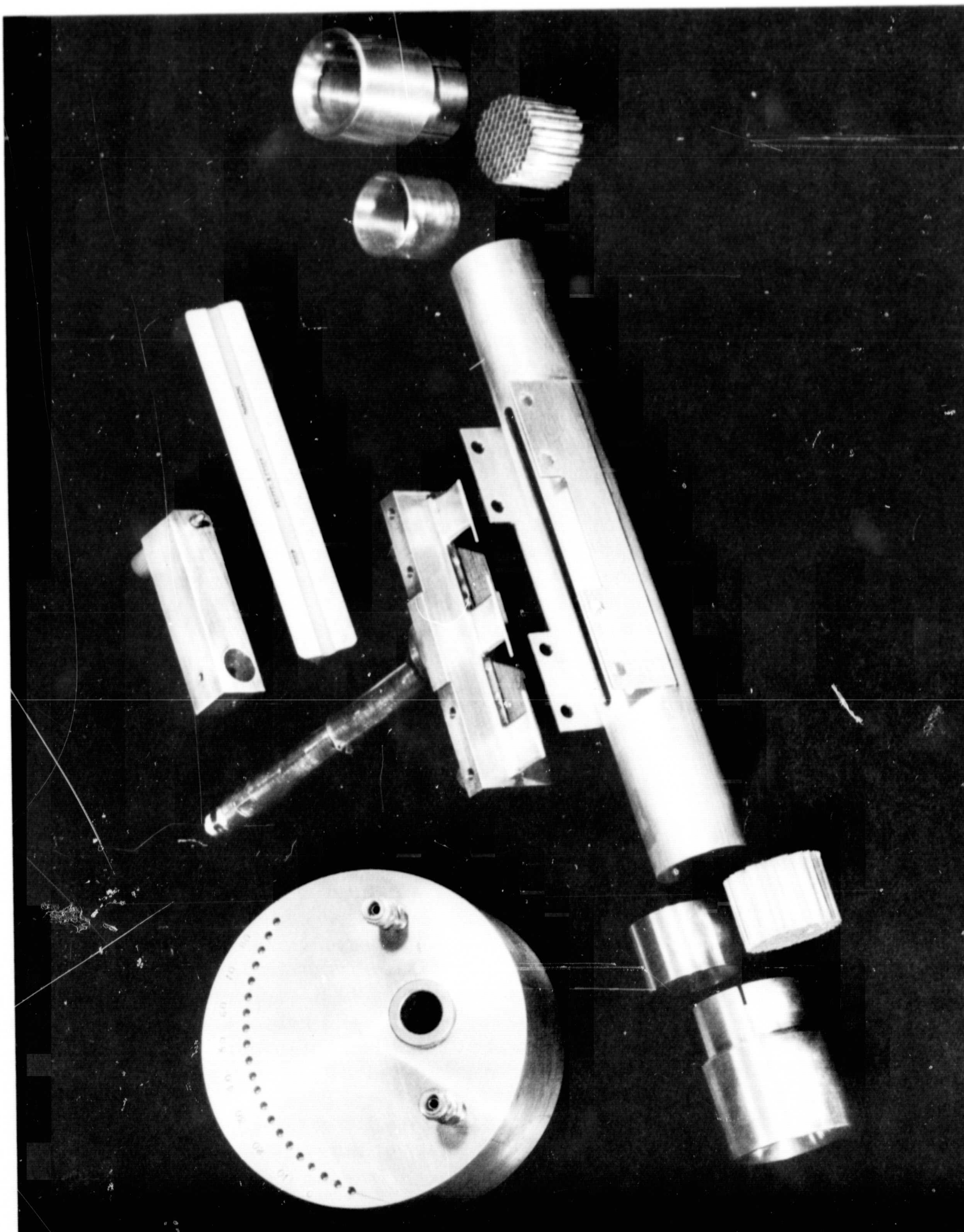

Figure 1b. BOWLES FLUIDICS CORPORATION PARALLEL FLOW WIND SENSOR

C. Description of Testing and Results

1. 0 to 15 ft/sec Range

Testing began in the low speed wind tunnel at Bowles Fluidics Corporation. The model is mounted on the centerline of the tunnel, 4 inches from the wall to insure its being out of the wind tunnel boundary layer. As shown in Figures 1a and 1b, the angle-of-attack of the sensor, with respect to the approach flow, can be varied from -10^{o} to 90^{o} in 5^{o} increments. The tests were run at constant velocity and supply pressure while the angles were traversed. Next, the supply pressure was varied and angles were again traversed. Finally, the velocity was varied. In this way, a complete set of data similar to that of Figure 2a, b, could be obtained.

2. 10 to 160 ft/sec Range

Testing was next conducted at the University of Maryland Low Speed Wind Tunnel. Runs at 10 and 15 ft/sec were recorded to provide a cross-check of the data recorded in the BFC tunnel. Correlation is quite good as can be seen in Figure 3. Tests were subsequently run in 10 ft/sec increments from 20 ft/sec to the limit of the tunnel, 160 ft/sec. Although this is beyond the range specified by the design goals, Phase 1 tests indicated that 90 ft/sec was not the limit of the sensor. Therefore, the test plan was extended to cover the increased range. The output of the wind sensor as a function of velocity is shown in Figure 4.

3. Saturation Effects

These tests show that the upper limit of the wind sensor has again not been reached, particularly for the higher supply pressures. However, an estimate of the saturation of the sensor output can be estimated from the existing data. The saturation characteristic for a given supply pressure is not defined by a sharp break. But Figure 4 shows a pseudo-saturation effect at about a wind velocity of 80 ft/sec with $P_+ = 1$ psig and at about 140 ft/sec with $P_+ = 3$ psig. At the receivers, which are 18 power nozzle diameters away from the power nozzle, the jet centerline velocity is approximately $0.6\,V_+$ as derived from the Bernoulli equation, $P = 1/2\,\rho V^2$. (V_+ is the power jet velocity.) For the supply pressures of 1 and 3 psi, the jet velocity at the receivers, V_+, are 348 and 602 ft/sec respectively. Forming the ratio

FIGURE 2a.

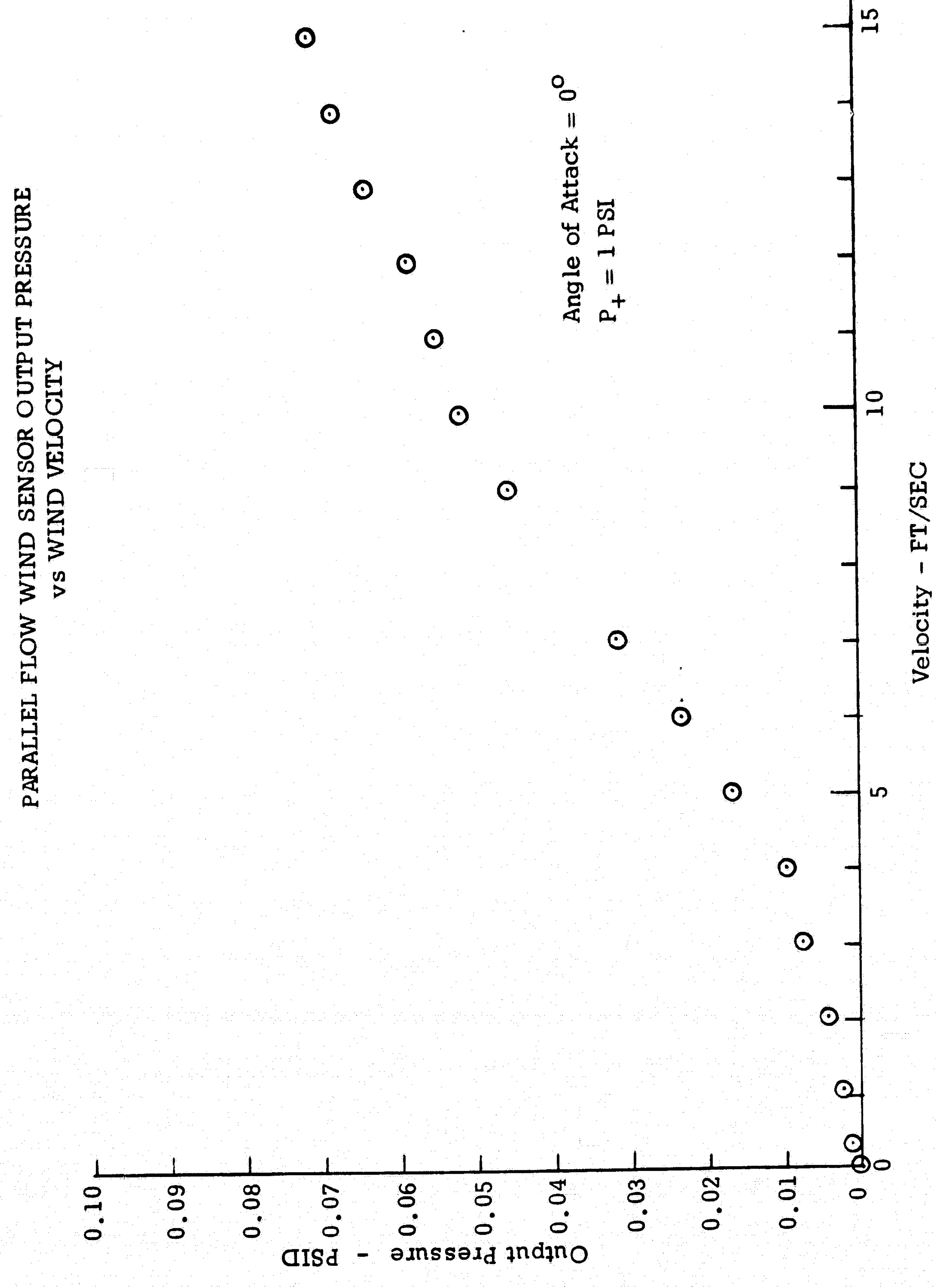

31176

PARALLEL FLOW WIND SENSOR OUTPUT
PRESSURE VS ANGLE OF ATTACK

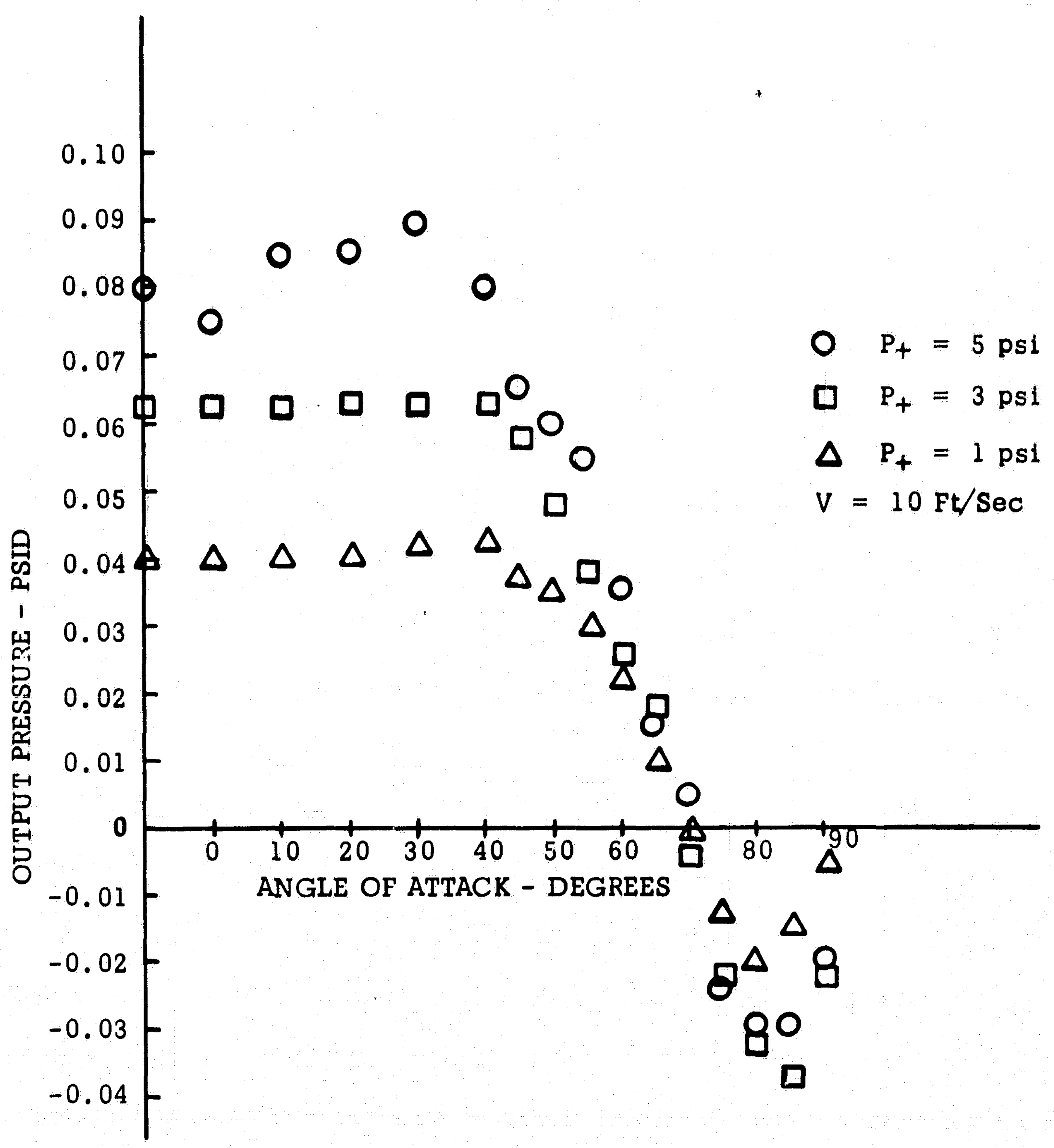

COMPARISON OF BOWLES FLUIDICS
AND UNIVERSITY OF MARYLAND
WIND TUNNEL TESTS

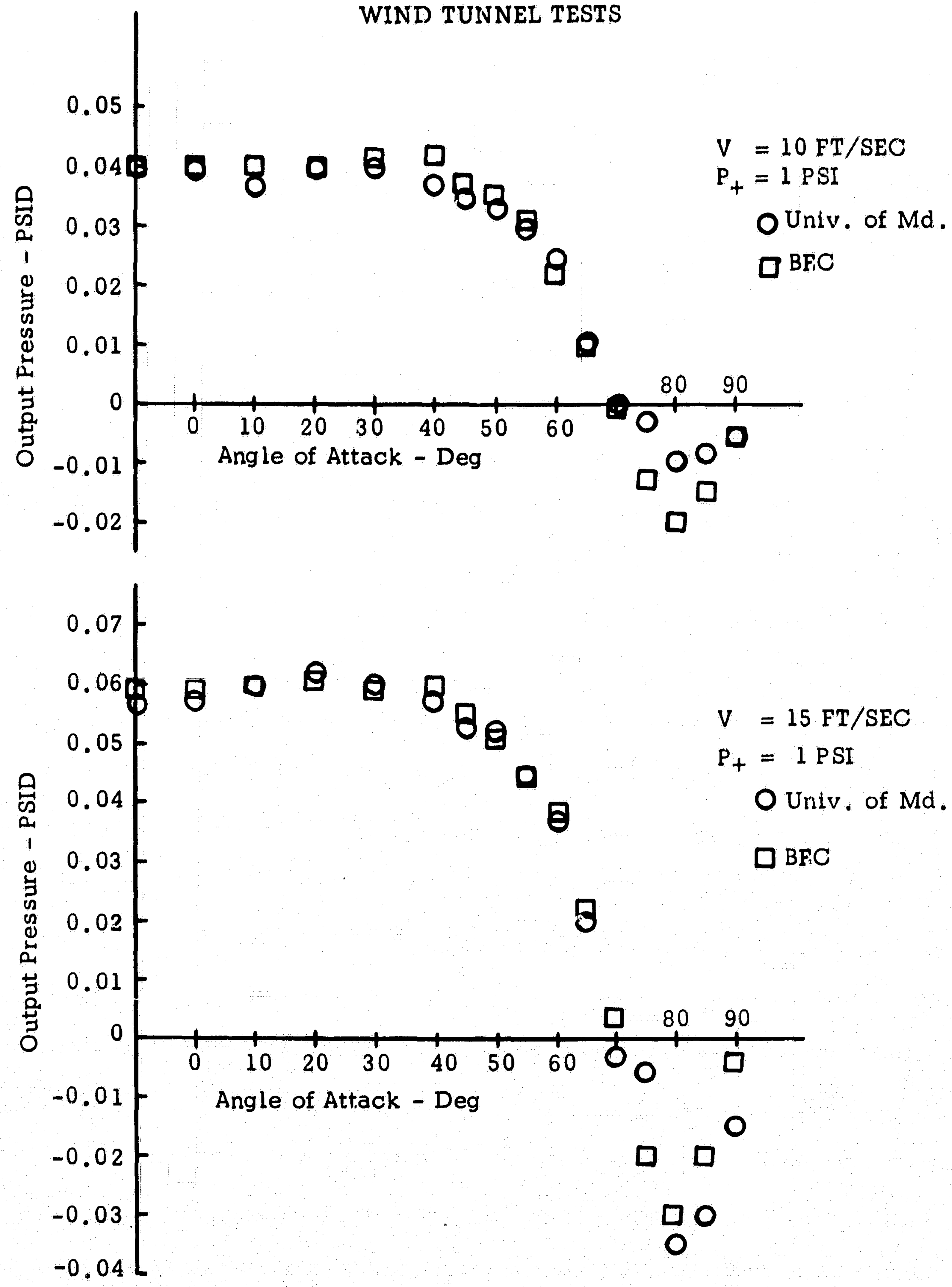

Figure 4.

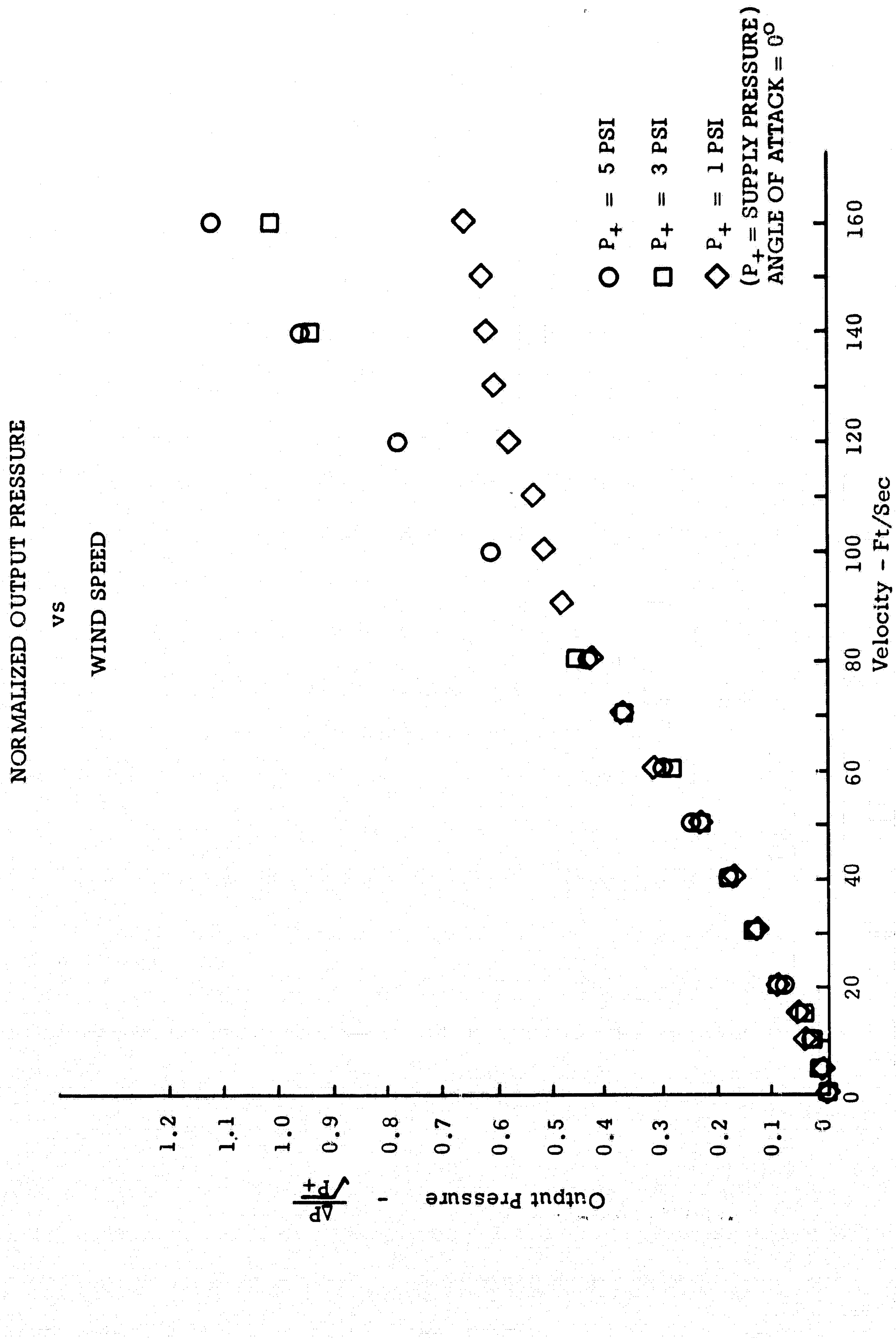
NORMALIZED OUTPUT PRESSURE
vs
WIND SPEED
Output Pressure - ΔP/P+
Velocity - Ft/Sec
0
0.1
0.2
0.3
0.4
0.5
0.6
0.7
0.8
0.9
1.0
1.1
1.2
0
20
40
60
80
100
120
140
160
P+ = 5 PSI
P+ = 3 PSI
P+ = 1 PSI
(P+ = SUPPLY PRESSURE)
ANGLE OF ATTACK = 0°

of the saturation velocity and the jet velocity, viz. 80/348 = 0.23 and 140/602 = 0.23, it can be inferred that the saturation velocity, V_{sat}, for any supply pressure is given by

$$\frac{V_{sat}}{V_+} = \frac{V_{sat}}{\sqrt{\frac{2\,P_+}{\rho}}} = 0.23 \quad .$$

which, for P_+ = 5 psig, yields V_{sat} = 178 ft/sec. Extrapolation of Figure 4 with the rolloff typified by the 1 psi curve at this velocity seems entirely reasonable. Actual testing of this effect has not been done, but the emperical estimation presented here is useful for preliminary design purposes. It is emphasized that this "saturation" does not imply that the gain, $\Delta P/V$ vanishes, but merely that it decreases while remaining finite.

4. Angle-of-Attack

The variation of output pressure with varying angle-of-attack is shown in Figure 5.

5. Other Testing

Because of the wide velocity range over which this sensor is to operate, the possibility of effectively reducing this range through the use of nonlinear resistance at the inlet of the sensor was considered. In such an application the honeycomb which was used solely for its flow straightening capability would be replaced by one of considerable length to cell diameter ratio. The resistance to the flow through the honeycomb is nonlinear, posing slight resistance at low velocity. Therefore, when the wind velocity is small, the effect of the honeycomb (as a resistor) is negligible. When the velocity is great, the resistance is high, and less flow from the free stream enters the flow straightening tube, and the velocity in the tube is correspondingly less.

The experimental verification of this is presented in Figure 6. Observe that the trend of the data is the same in both cases and that the honeycomb reduces the characteristic output pressure signal only at high velocities, thereby demonstrating the nonlinear resistance effect.

A set of runs were also recorded with the end caps of the flow straightening cylinder removed. In this way, a square edged inlet to the sensor was tested in place of the curved radius of the end cap. No significant changes were detected.

Figure 5

VARIATION OF OUTPUT PRESSURE WITH
ANGLE OF ATTACK

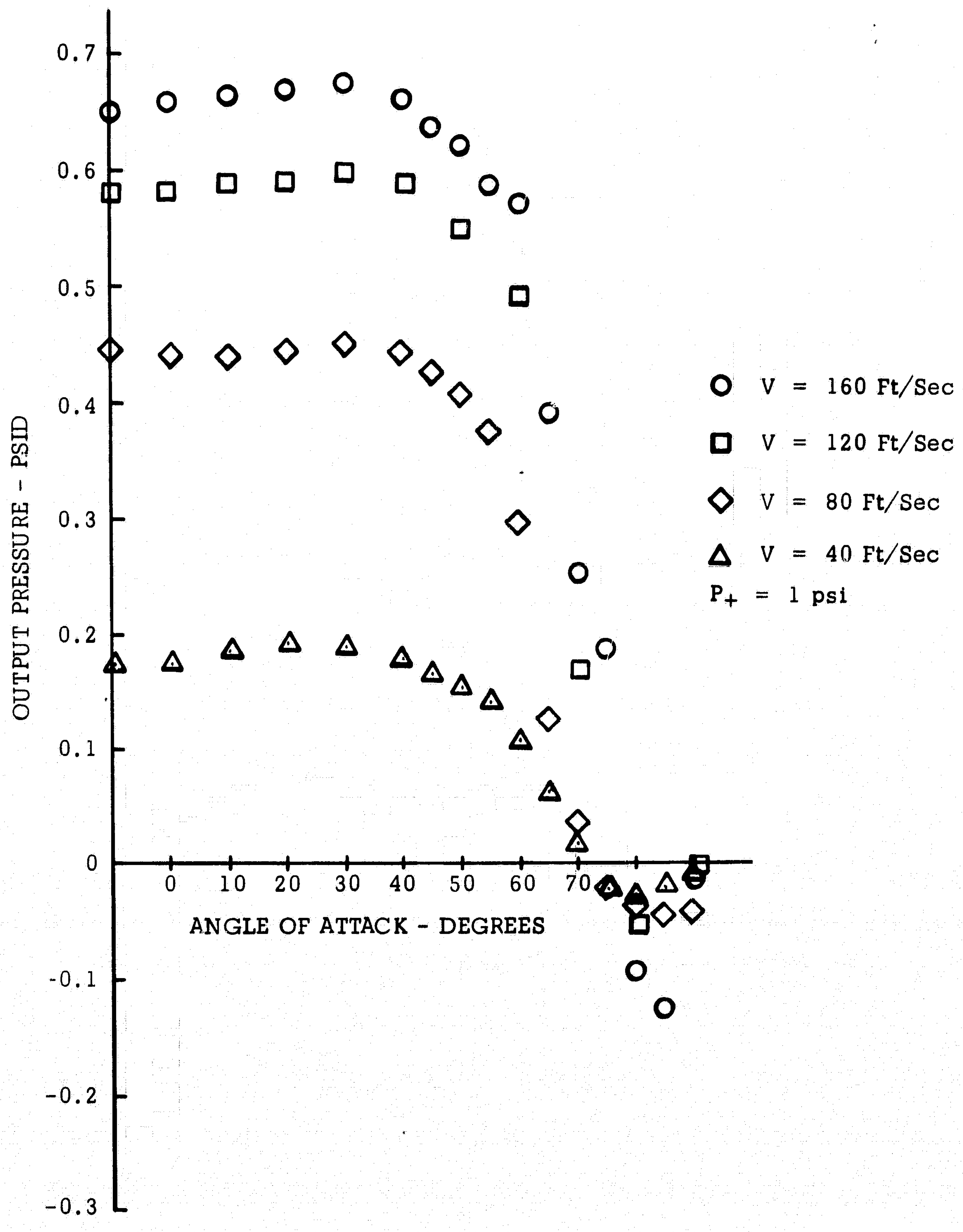

EFFECT OF HONEYCOMB FLOW STRAIGHTENERS
ON OUTPUT PRESSURE

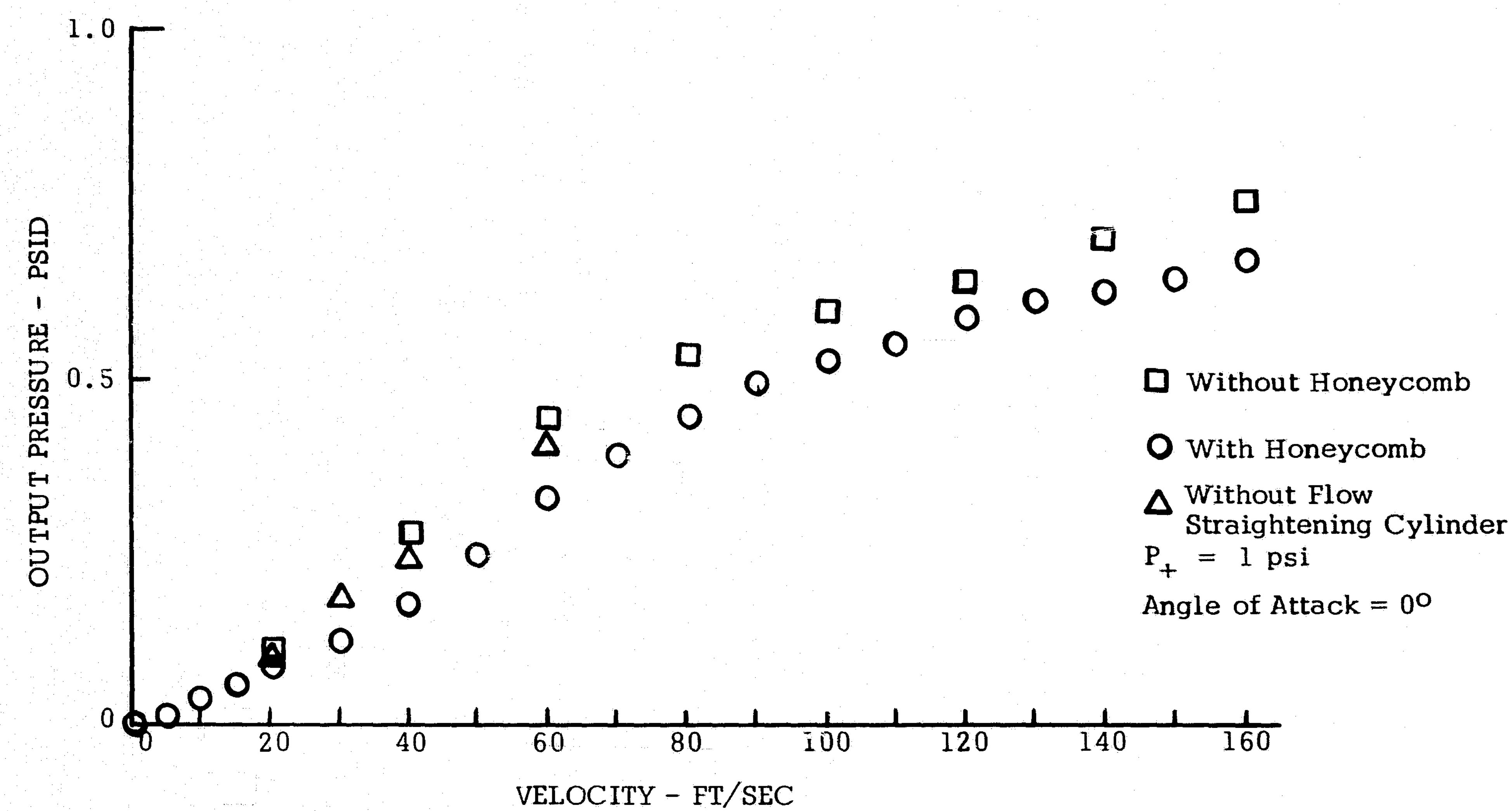

Figure 6

31370

The final test was one which was conducted with the flow straightening cylinder removed. Figure 6 shows that at zero angle-of-attack, the output pressure is the same as that obtained without the honeycomb in place. However, when the angle-of-attack is varied while holding velocity constant, there is no correlation of the data (see Figure 7). This indicates the need for the flow straightening function of the tube.

D. Summary Discussion

The testing of the demonstration model of the parallel flow sensor concept has shown that this device has good sensitivity and a linear output over the full range tested (0 to 160 ft/sec).

Because of the flow straightening tube employed with this sensor, the output is substantially constant for angles-of-attack up to 40°. This is comparable to the performance of the similarly configured Kiel probe (Reference 3) which is widely used for aerodynamic pressure measurements. A Kiel probe is shown schematically below:

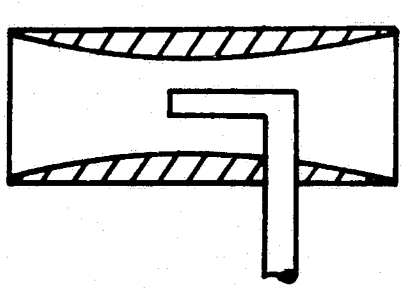

If the Fluidic wind sensor is to be used for directly measuring the wind component along a specified direction, a different external configuration may be required. This matter and intrinsic of noise of the output represent topics for further work and are discussed more fully in Section IV, Conclusions and Recommendations.

OUTPUT PRESSURE VS ANGLE OF ATTACK
WITH CYLINDER REMOVED

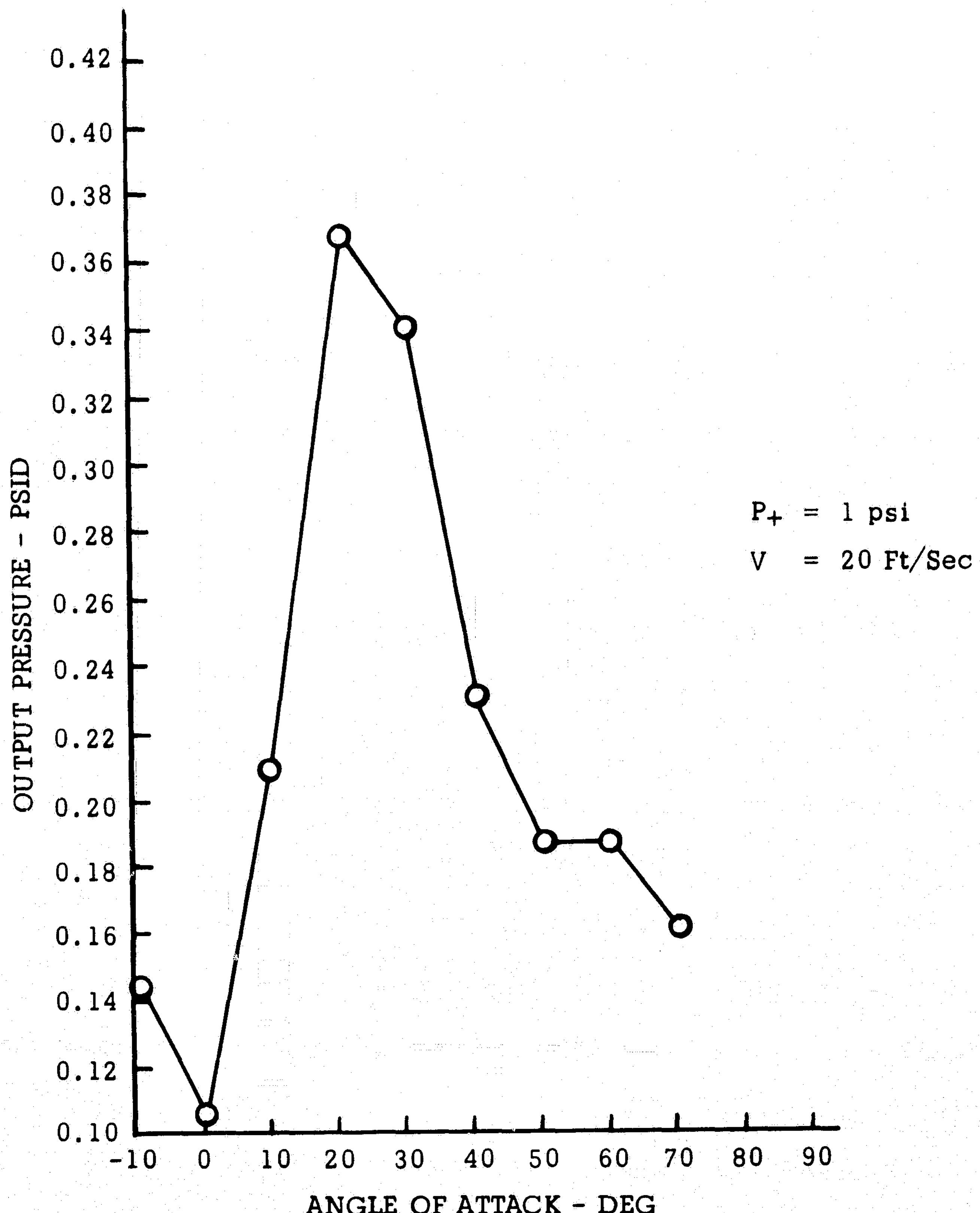

SECTION III

CONCEPT DESCRIPTION AND PHASE I TESTING

A. General

Fluidic technology is, in part, based on the concept that by interacting one fluid stream with another, amplification of pressure and flow signals can be achieved without moving mechanical parts. As an example, consider Figure 8, which shows a basic fluidic amplifier. In Figure 8a, the supply pressure, P+, creates a moving fluid stream which is evenly divided between the right and left outputs, P_{O_R} and P_{O_L}, respectively. With the issuance of a control signal on the left, P_{C_L}, (P_{C_L} < P+), the jet is deflected by jet momentum summation toward the right side of the amplifier. The decrease in flow toward the left leg of the amplifier decreases its output pressure, P_{O_L}, and the simultaneous increase in flow in the right leg increases the output pressure, P_{O_R}, on that side. The net result is a differential output pressure.

The application of fluidics in wind sensing is a natural extension of this conventional fluidic approach. The wind itself can be impressed on an air stream to perform the modulating function of P_{C_L} in Figure 8. Thus, amplification can be achieved without the use of any intermediate sensing device, and the output may be directly connected to a pressure gage or transducer. A sensor based on this principle offers the simplicity and ruggedness of the convetional Pitot sensor while providing amplification.

B. Cross Flow Wind Sensor

The basic cross flow wind sensor configuration is depicted in Figure 9. The similarity between this and the conventional fluidic amplifier is apparent. The only difference is that the wind, which acts as the control, operates on the power jet over its entire span thereby increasing the deflection of the jet centerline.

This configuration can be operated in both open and closed loop control modes. As an open loop component, the output differential pressure is the measure of the wind velocity directly. In a closed loop configuration, the differential output pressure, ΔP, drives a high gain amplifier which in turn varies the supply pressure, P+, to the sensor. When the ΔP differs from some null position, the amplifier increases or decreases the supply pressure to the wind sensor to restore the ΔP to a constant value. The supply pressure is, therefore, a measure of the wind velocity.

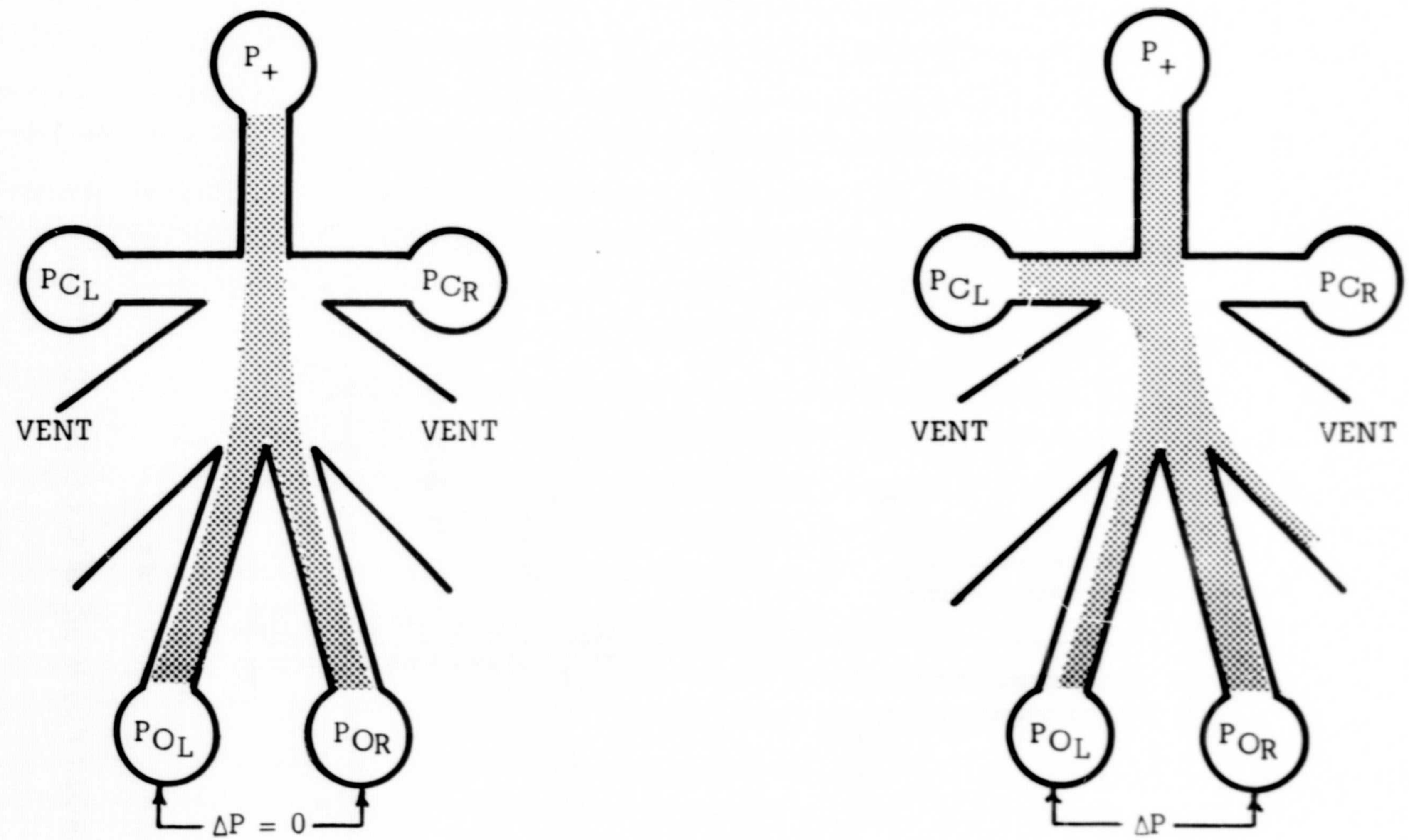

Figure 8a.

Figure 8b.

Figure 8.
FLUIDIC ANALOG AMPLIFIER

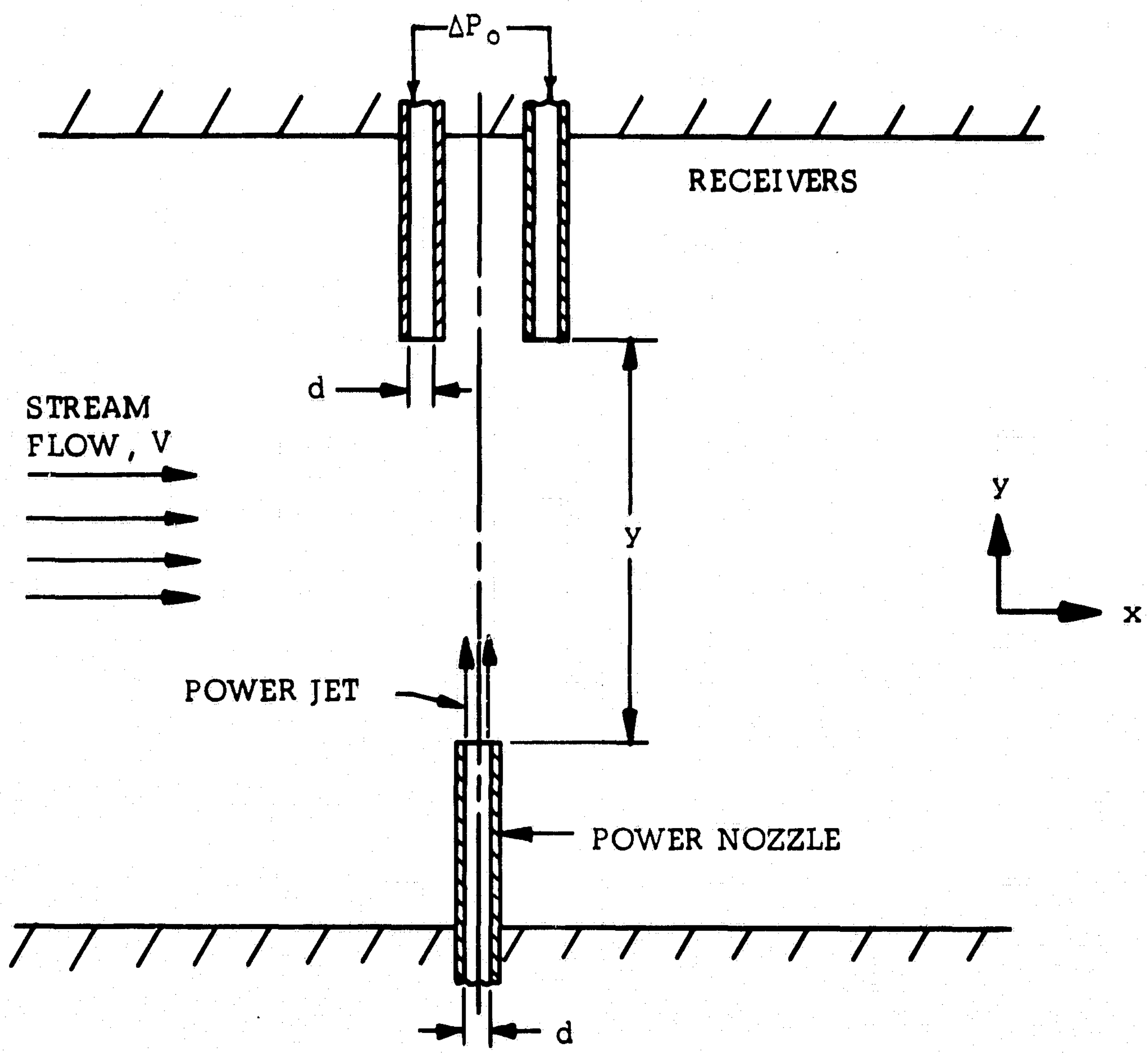

Figure 9.

CROSS FLOW SENSOR CONFIGURATION

1. Open Loop Operation

Because of the uniqueness of sensing extremely low velocities, Bowles Fluidics Corporation built a test apparatus expressly to test in the velocity range $0.3 < V < 15$ ft/sec. The wind tunnel is described in detail in the Appendix. For higher velocities ($15 < V < 90$ ft/sec) testing was carried out at the University of Maryland's 18" x 42" low speed wind tunnel.

Relatively little information is available regarding the behavior of a jet issuing transverse into a moving stream (References 4, 5, 6) and therefore, the approach taken was to record the actual jet profile while varying: 1) supply pressure, 2) distance between power nozzle and receiver, 3) velocity, and 4) power nozzle diameter.

a. Cross Flow Models

Three cross flow wind sensors were fabricated in an evolutionary process. The first two were used to collect basic information and had easily varied geometry. The third was a fixed geometry model which was used to measure the velocity threshold (i.e., lowest velocity which could be detected).

The first model consisted of a power nozzle perpendicular to a thin, flat plate and a series of 10 equally spaced receivers located in another plate parallel to the first. See Figure 10.

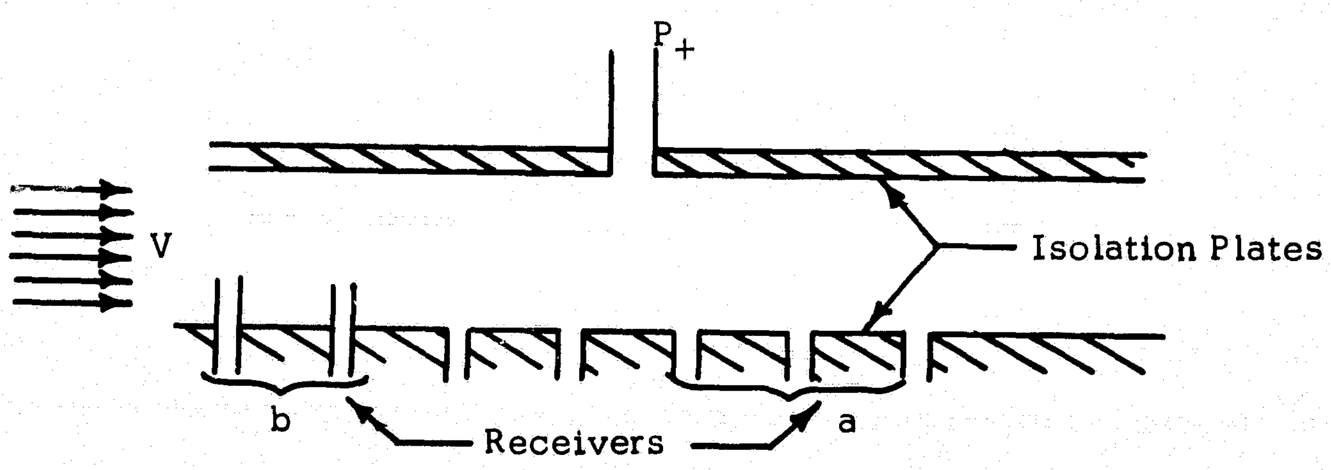

Figure 10.

CROSS FLOW WIND SENSOR

These plates were employed because they themselves have negligible effect on the main flow, yet isolate the power nozzle and receiver supports from the interaction region. The receivers were adjustable and could be flush with the surface, or project into the stream (receivers a and b, respectively). The tests with this model showed that the receivers could not be spaced sufficiently close to each other to accurately determine the jet pressure profile. The model was useful, however, in showing that except when the isolation plates were close together (in the order of a few power nozzles diameters), no difference can be observed whether the receivers were flush with the isolation plate or protruding into the stream. When the plates are close together, the difference is believed to be caused by the isolation plates themselves, because they generate a secondary stream flow pattern as shown (it is assumed here that the wind velocity is zero):

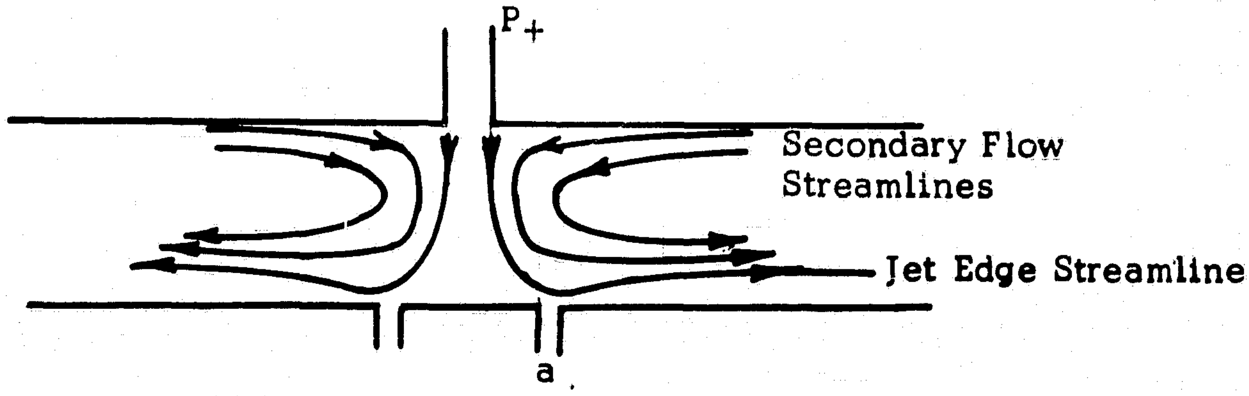

The plane at the receivers forces a 90° turning of the power jet. The viscous action of the jet sets up a strong secondary flow pattern. At point "a" the jet velocity is high because the total jet mass flow must efflux radially, and the secondary flow "squeezes" the jet edge streamline downward. The pressure in this high velocity region is correspondingly low. When the receivers protrude into the stream (as shown by station point "b" in Figure 10), they extend beyond this localized low pressure region and therefore, exhibit the usual jet pressure profile, Figure 11. With large spacing between the power nozzle and receivers, the secondary flow pattern in weaker. In this case, the secondary flow does not "squeeze" the radially effluxing jet and the characteristic jet profile appears (Figure 11).

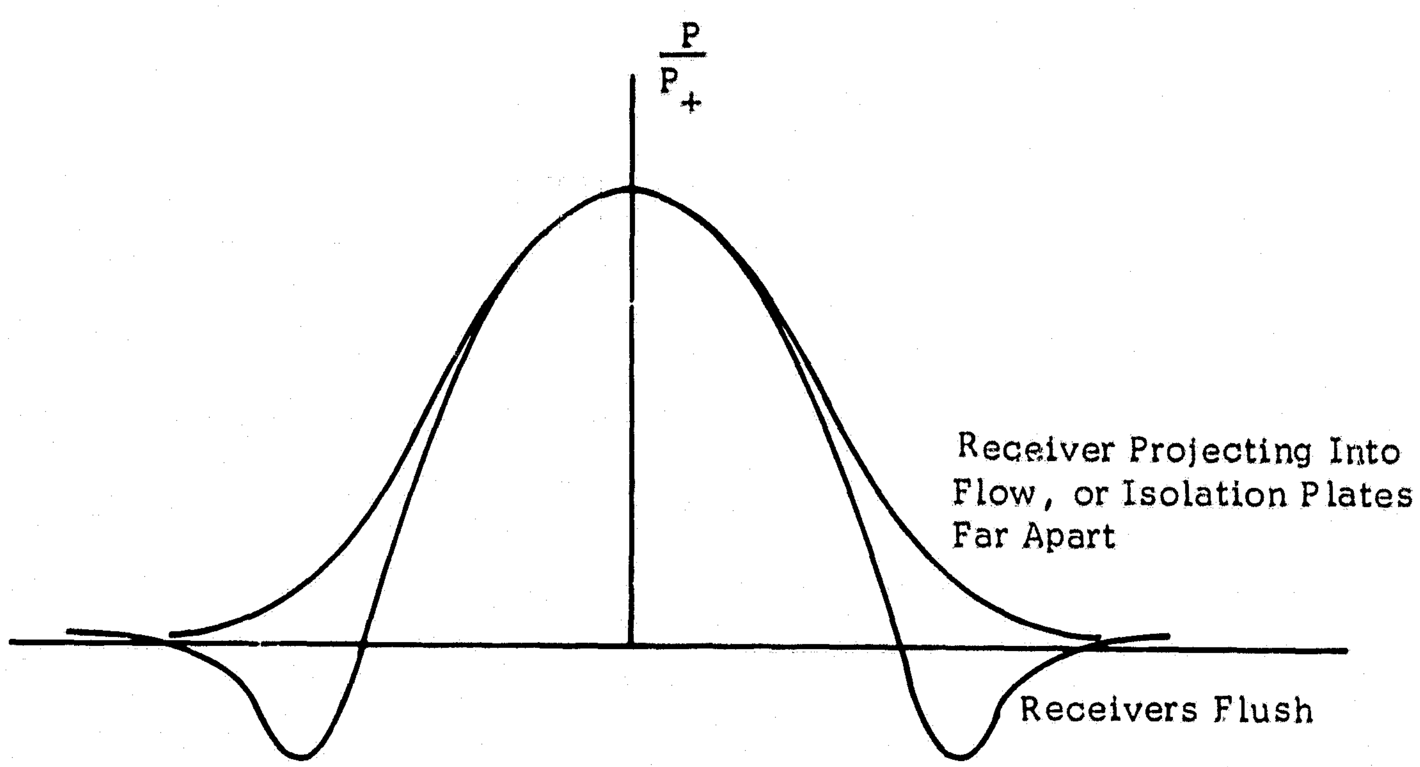

Figure 11.

JET PRESSURE PROFILES

In order to improve the accuracy of measuring the pressure profile, a second model was made. This model permitted continuous recording of the pressure, and therefore, no ambiguity of the profile exists. The model is shown in Figure 12a, b. Figure 12a shows the assembly mounted on the wind tunnel door. Figure 12b shows the supply pressure nozzle, P_+, and the receiver pressure tap, P_R. This pressure tap is mechanically moved across the jet, and the position of the tap is recorded on an X-Y recorder using a linear motion potentiometer. The pressure of the jet is simultaneously recorded on the other axis of the recorder. The test arrangement is shown schematically in Figure 13.

b. Cross Flow Test Results

A typical test result thus obtained is shown in Figure 14. Tests were run for a prescribed geometry at fixed wind velocity while varying supply pressure. As the supply pressure decreases, the deflection of the jet increased as can be observed from curves numbered 7 through 2 in Figure 14. In order to determine the actual deflection of the jet, a zero-deflection datum profile was recorded with the wind tunnel off. This was arbitrarily run at $P_+ = 3.5$ psig, and is Curve #1 in the figure.

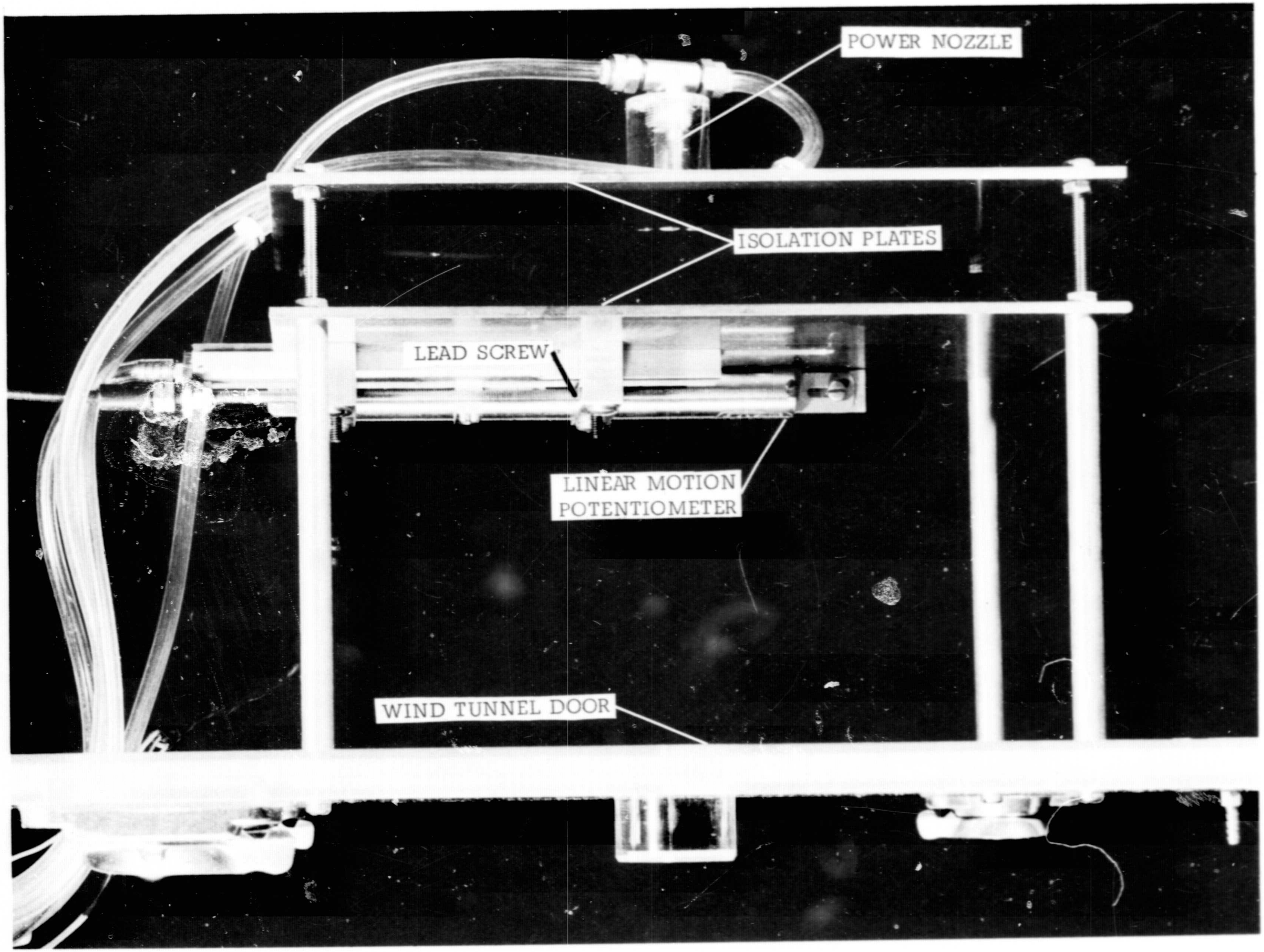

FIGURE 12a. PHOTOGRAPH - CROSS FLOW WIND SENSOR

31179

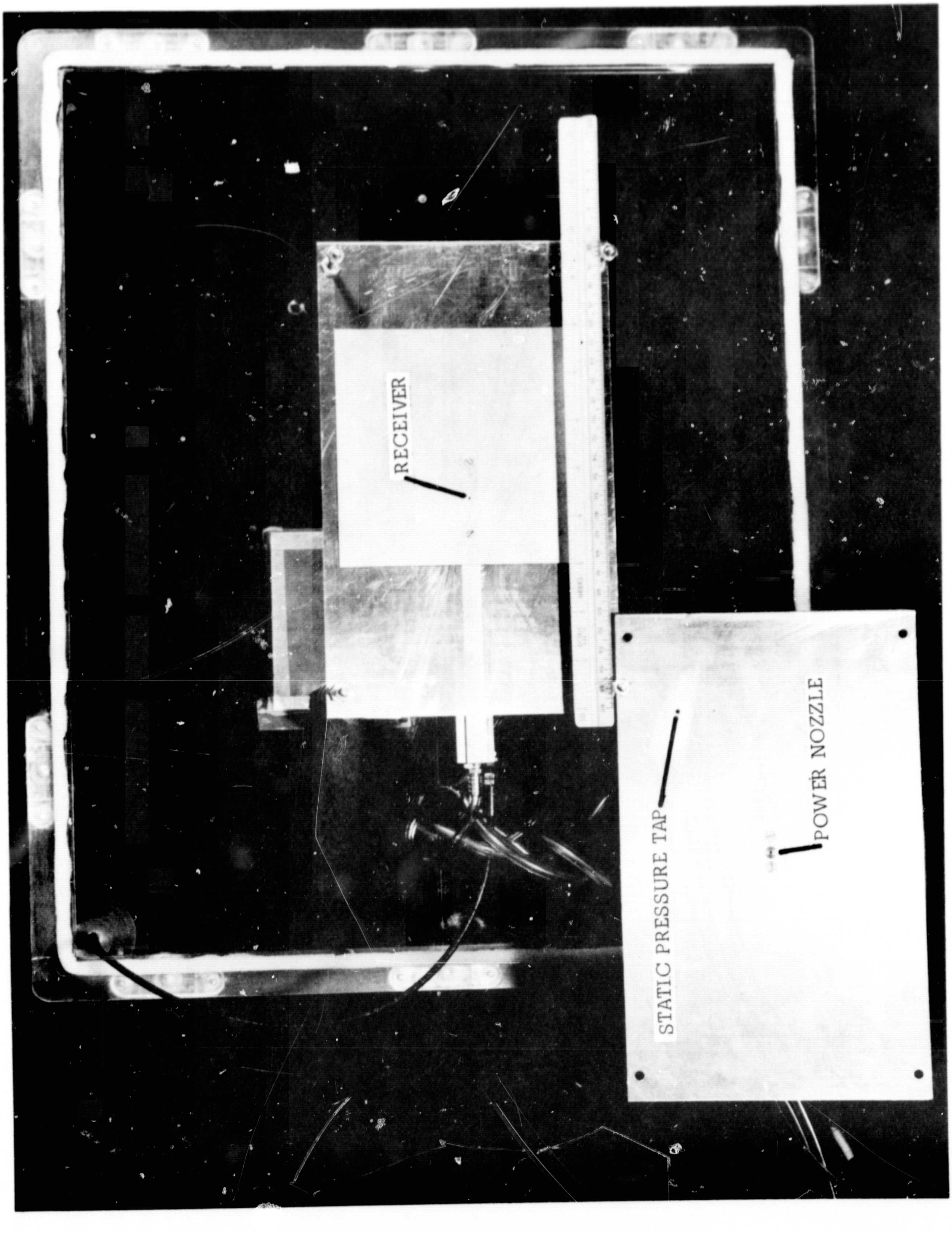

FIGURE 12b. PHOTOGRAPH - CROSS FLOW WIND SENSOR

31180

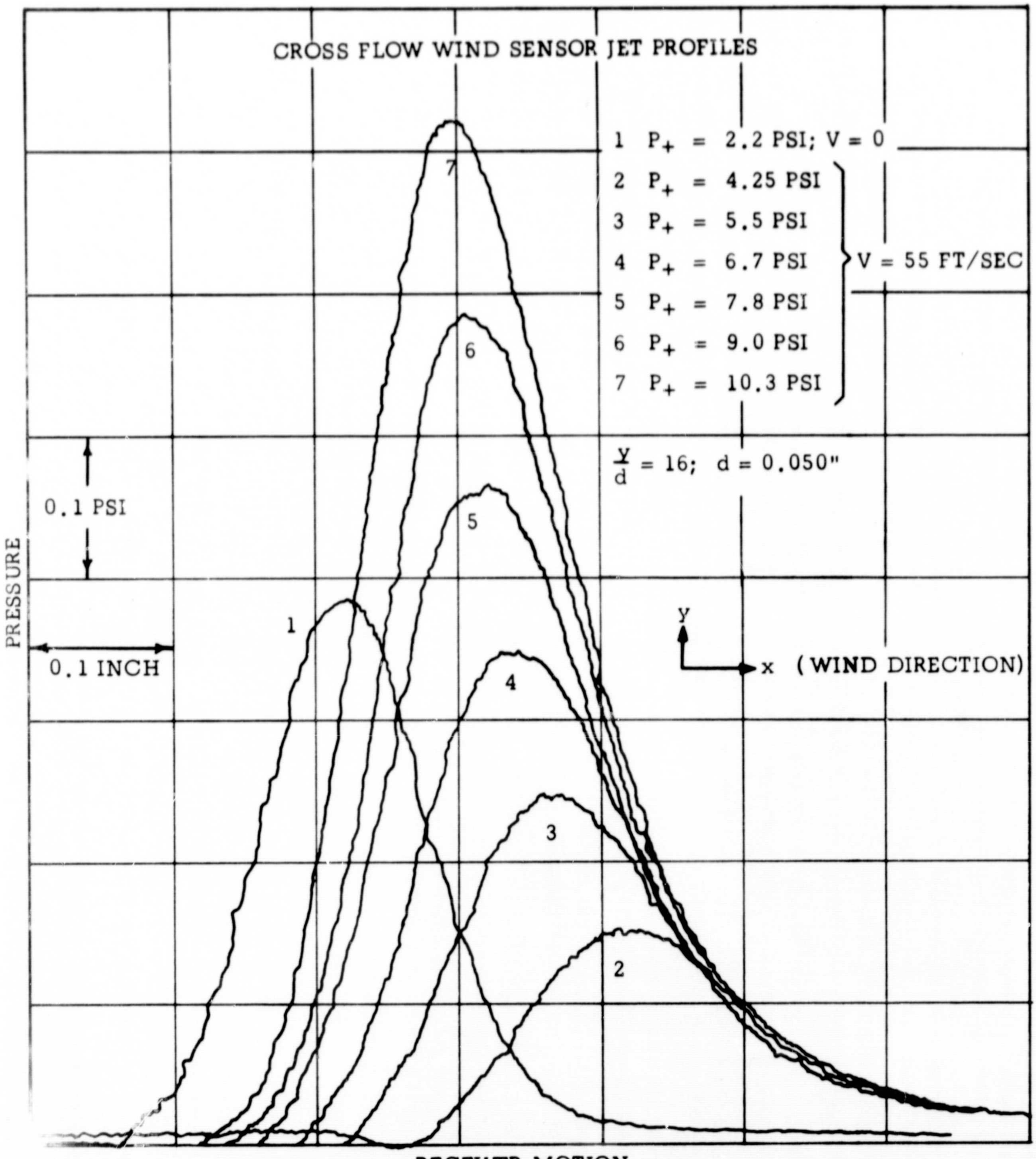
CROSS FLOW WIND SENSOR JET PROFILES
1 P+ = 2.2 PSI; V = 0
2 P+ = 4.25 PSI
3 P+ = 5.5 PSI
4 P+ = 6.7 PSI
5 P+ = 7.8 PSI
6 P+ = 9.0 PSI
7 P+ = 10.3 PSI
V = 55 FT/SEC
y/d = 16; d = 0.050"
0.1 PSI
PRESSURE
0.1 INCH
y
x (WIND DIRECTION)
1
2
3
4
5
6
7
RECEIVER MOTION

Figure 14.

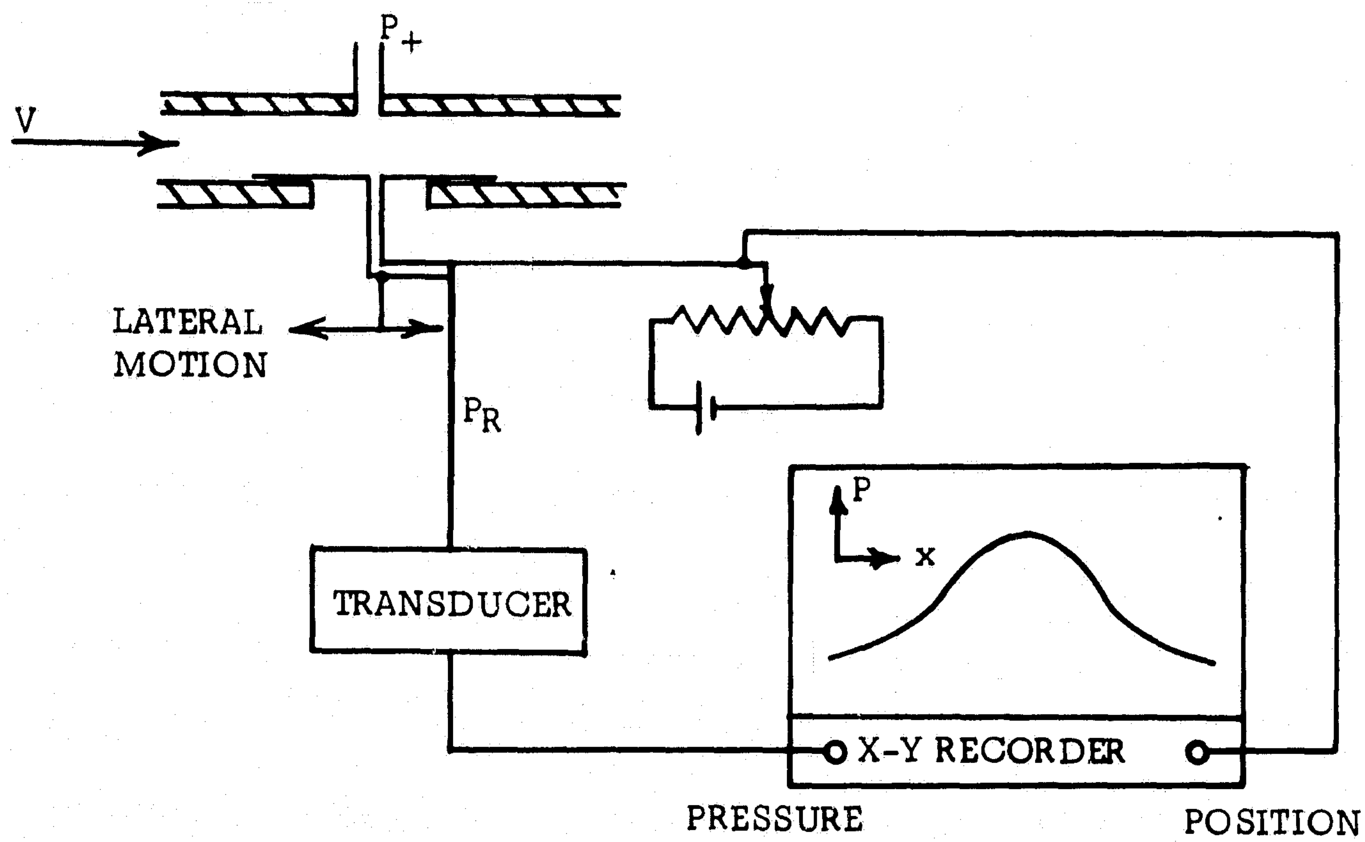

Figure 13.

EXPERIMENTAL ARRANGEMENT

From this fundamental data such information as the jet spreading, decay, and deflection is obtained throughout the flow field for the velocities of interest. From the complete set of such data, the appropriate geometry and supply pressures can be determined. The complete set of wind tunnel data has been reduced and compiled into a concise set of jet characteristics.

Figure 15 shows the deflection of the jet, x , in the wind direction. For the particular test under discussion the distance between isolation plates, y , was 0.7 in. The power nozzle diameter, d , was 0.05 in. It is useful to relate all dimensions in terms of power nozzle diameters. This same figure shows excellent agreement in the velocity range overlap between the two tunnels employed. Of particular interest in this curve is that a simple empirical equation can be written for the downstream deflection as a function of supply pressure:

$$\frac{x}{d} = \frac{K}{P_+} \qquad (1)$$

CROSS FLOW WIND SENSOR DEFLECTION OF JET

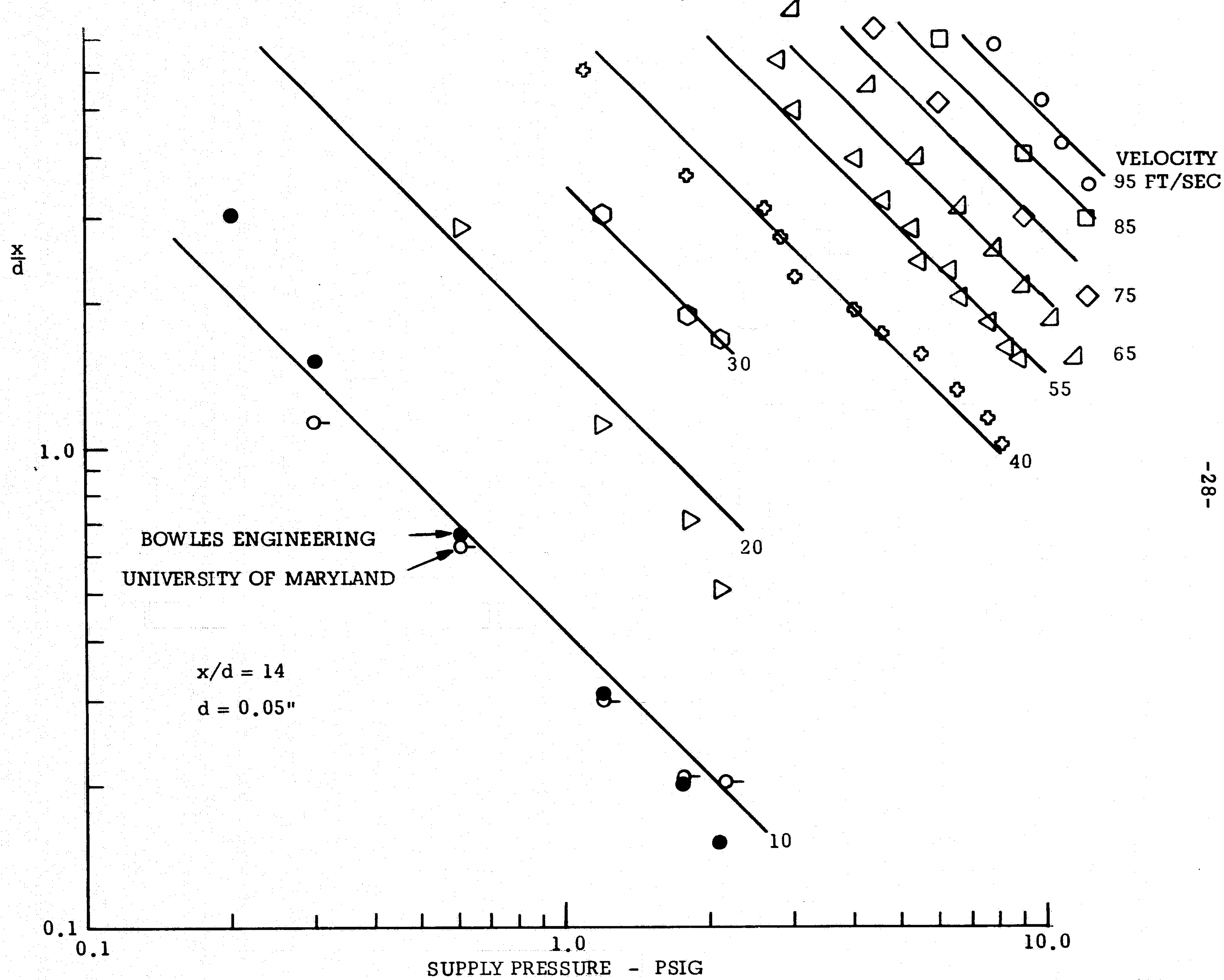

Figure 15.

31115

The constant, K, depends on the wind velocity. This has been plotted for the entire set of data and is shown in Figure 16, for various values of spacing between the isolation plates and power nozzle diameters. For wind velocities greater than a few feet per second, the curves can be quite accurately given empirically as

$$K = a V^2 \qquad (2)$$

Incorporating equation 2 in equation 1,

$$\frac{x}{d} = \frac{a V^2}{P_+} \qquad (3)$$

Equation 3 shows that the downstream shift of the jet profile varies parabolically with velocity and inversely with the supply pressure. It will be shown that this equation is useful in predicting the gain of the sensor. The constant "a" represents empirical coefficients in the equations of Figure 16, and shows that deflection increases with increased spacing between the plates. This is, of course, to be expected since the power jet is under the influence of the wind for a longer time. The final conclusion which may be drawn from Figure 16 is that the results appear to be independent of the particular power nozzle diameter. This suggests that the non-dimensionalization by power nozzle diameter is especially useful.

Figure 17 shows the jet width and its variation as the geometry, supply pressure, and velocity are changed.

There is a general trend that the jet width is greater with higher supply pressure and that the jet width decreases with increases wind velocity. Figure 18 shows that for a constant velocity, the jet widths normalized by the power nozzle diameter, fall on a single curve.

Another jet characteristic which changes radically under the influence of the wind is the slope of the pressure profile, $\Delta P/\Delta(x/d)$. This can be seen in Figure 19. An order of magnitude change exists as the velocity of the wind triples. This large degradation of the profile occurs without a drastic change in the jet width. This is the result of extremely high shear stresses existing between the jet and the wind and results in a high dissipation of jet energy.

CROSS FLOW WIND SENSOR EMPIRICAL CONSTANT
FOR DEFLECTION OF JET

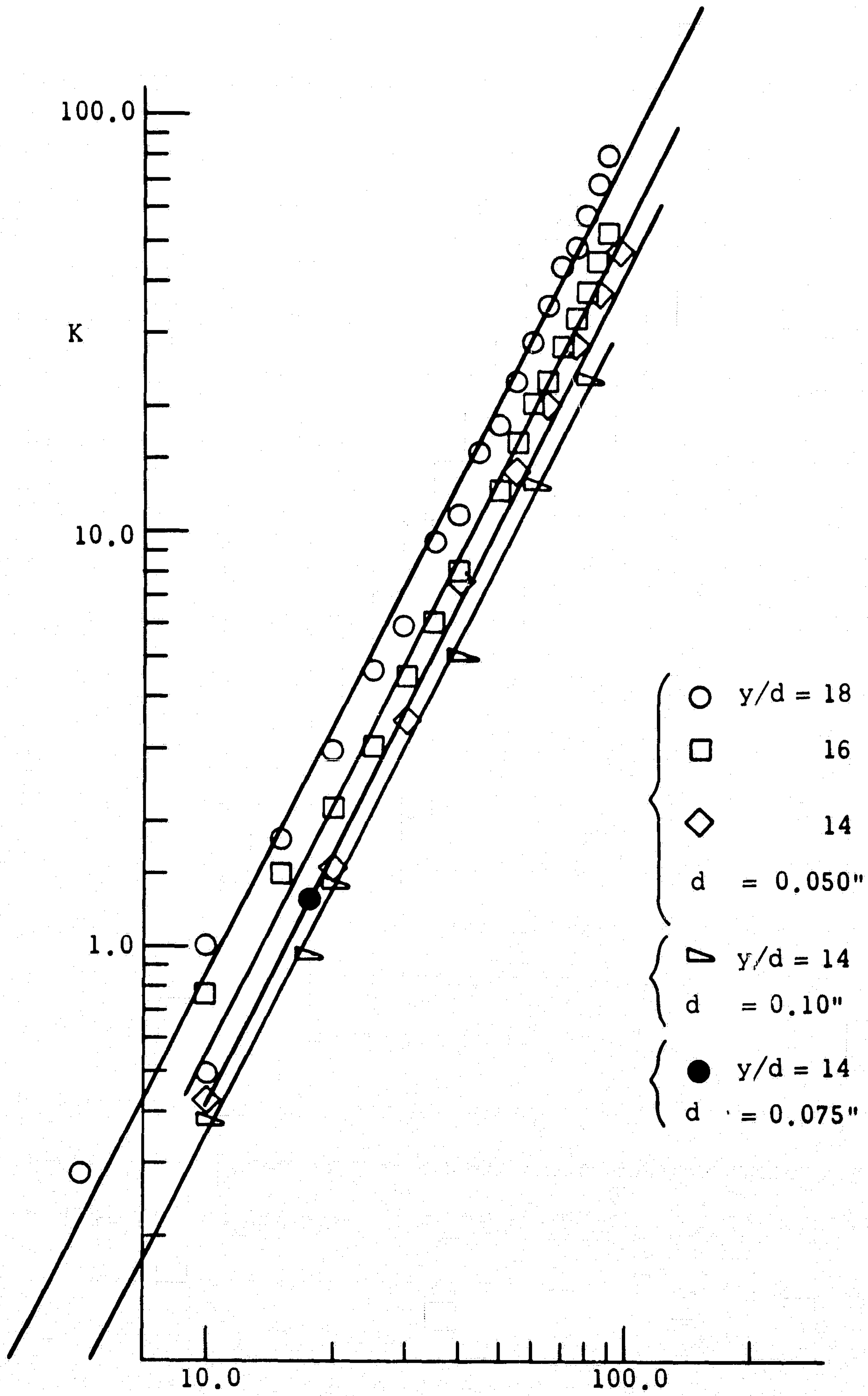

Figure 16.

CROSS FLOW WIND SENSOR JET WIDTH

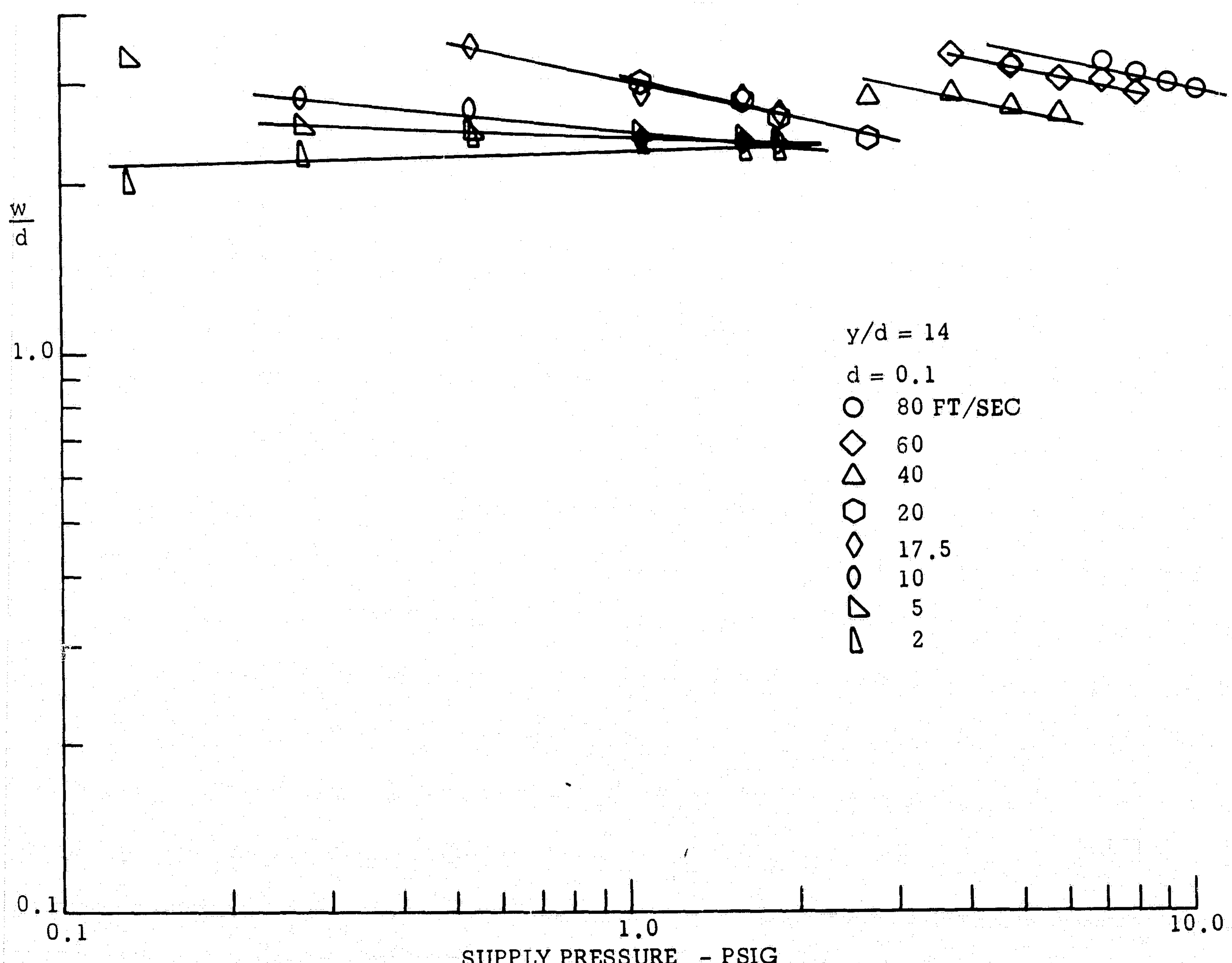

Figure 17.

CROSS FLOW WIND SENSOR

JET WIDTH VARIATION FOR DIFFERENT POWER NOZZLES

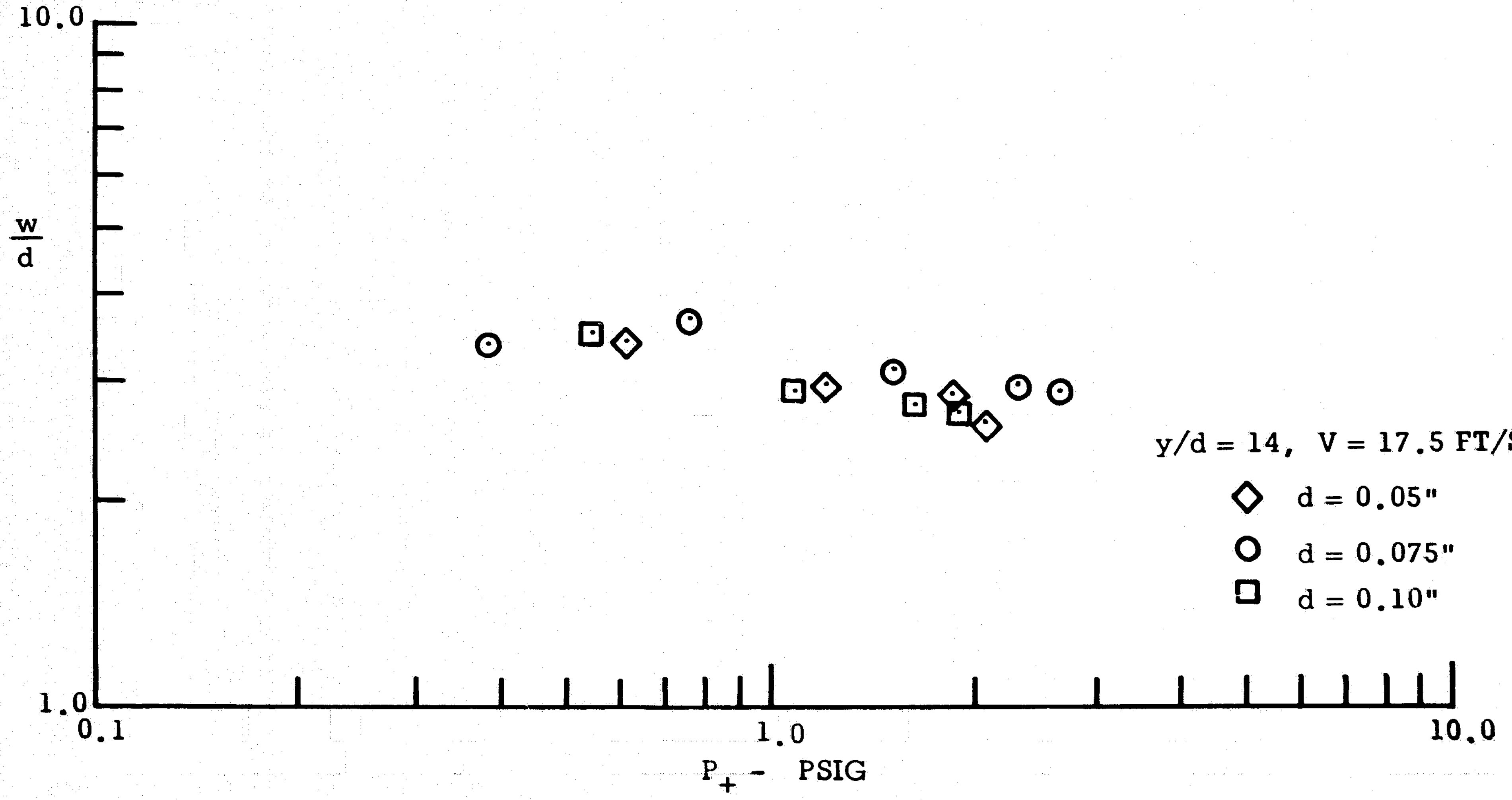

Figure 18.

CROSS FLOW WIND SENSOR SLOPE OF PRESSURE PROFILE

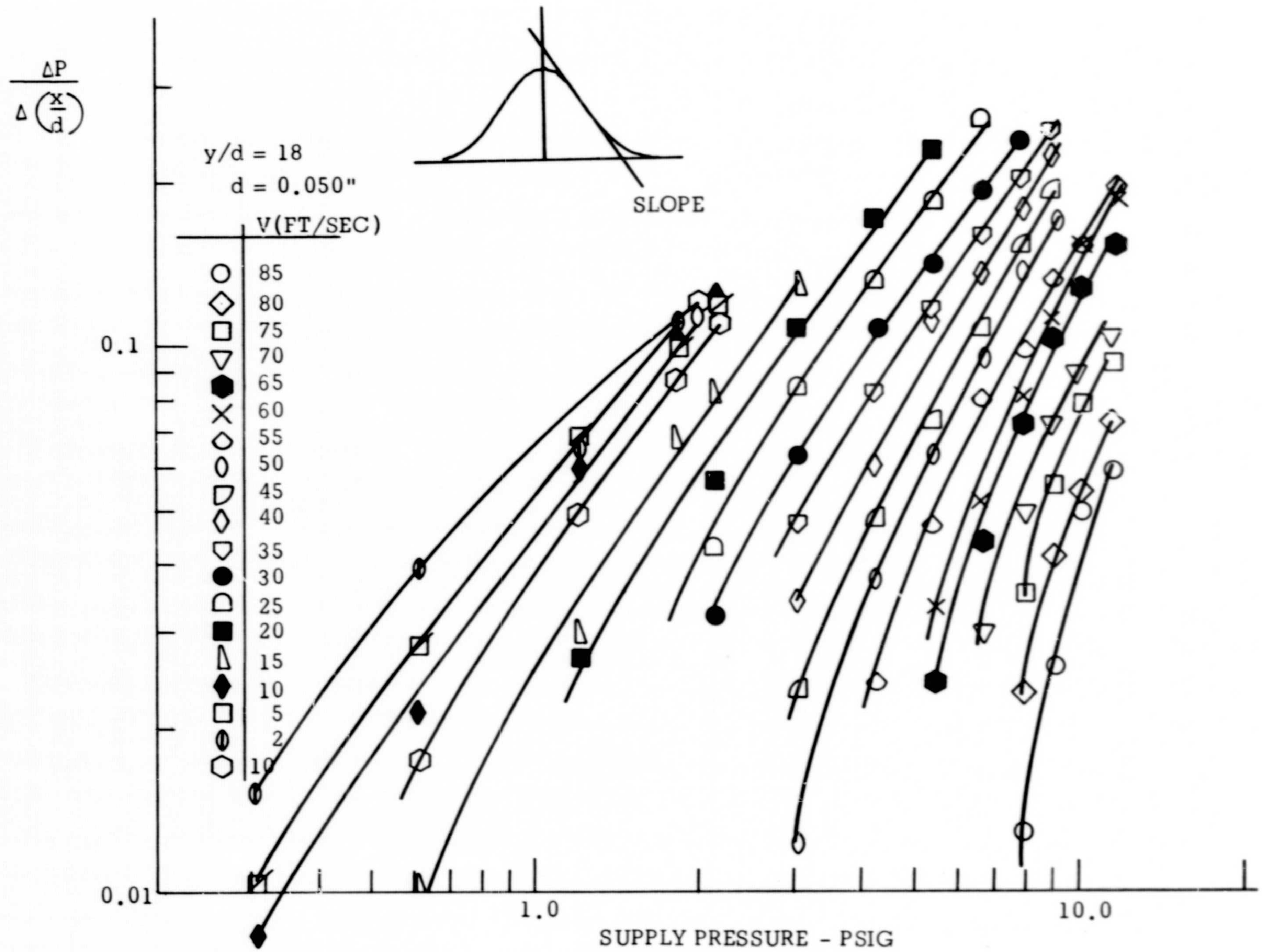

Figure 19.

Previous results show that certain jet characteristics behavior is independent of power jet nozzle diameter, d. However, the same is not true for the jet pressure profile slope as shown in Figure 20. It is also interesting that the behavior with increasing jet nozzle diameter is not monotonic. This is an area which requires further study. Tests of jets into still air confirm that such behavior is not uncommon (Reference 7).

The effect of shear losses can also be seen in Figure 21, which shows the normalized centerline pressure, P_{CL}/P_{+}, versus supply pressure. As the wind velocity increases, the pressure recovery rapidly decreases because of increased energy dissipation.

From the set of data of which Figures 15 through 21 are typical, the proper distance between power nozzle and receiver, separation between receivers, output pressure level and gain of the cross flow wind sensor can be determined.

c. Threshold

Data to this point have been recorded from the basic pressure profiles such as Figure 14, obtained in the general purpose model. However, at low velocities, the pressure profile curves are almost superimposed, making graphical discrimination difficult. A third cross flow sensor was therefore made, incorporating geometry determined from the previous two models. This was a fixed geometry model used specifically for threshold testing. The interaction region in this model was housed in a tubular structure, similar to that which might be used in a final instrument configuration. The distance between power nozzle and receiver is 18d, and the receivers are set symmetrically 3d apart. Tests were run with this model at velocities near the threshold velocity, the results of which appear in Figure 22. The data show that below a wind speed of about 0.26 ft/sec, the output pressure is essentially the same as at zero velocity. 0.26 ft/sec can, therefore, be taken to be the threshold of this model which compares well with the specified threshold, V = 0.33 ft/sec.

d. Empirical Analysis of Data

Using the reduced data previously shown, an analysis was made to correlate these data with empirical equations. This provides a design tool by showing functional dependence of the variables.

CROSS FLOW WIND SENSOR

PRESSURE PROFILE SLOPE VARIATION
FOR DIFFERENT POWER NOZZLES

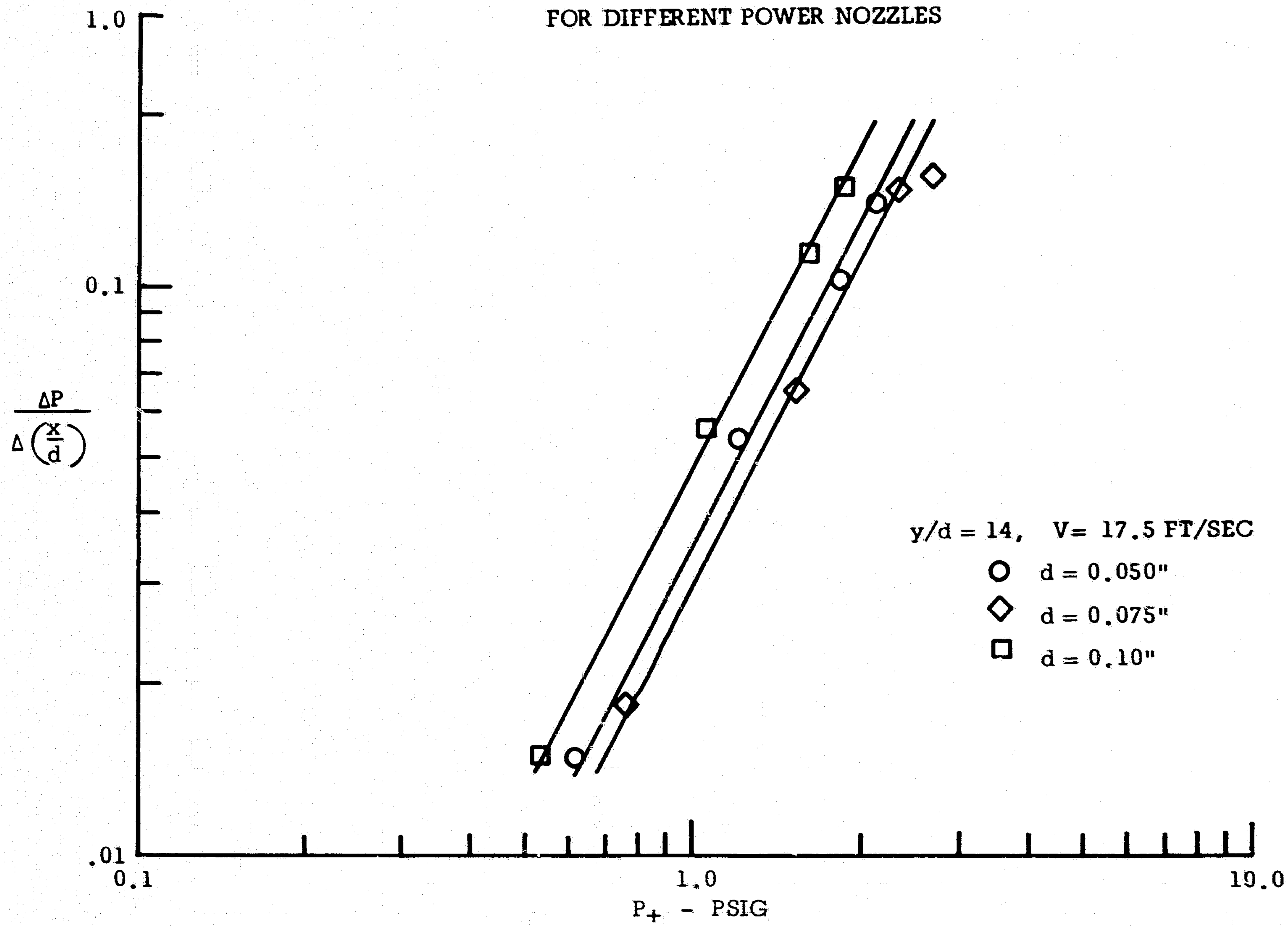

Figure 20.

31153

CROSS FLOW WIND SENSOR CENTERLINE PRESSURE RECOVERY

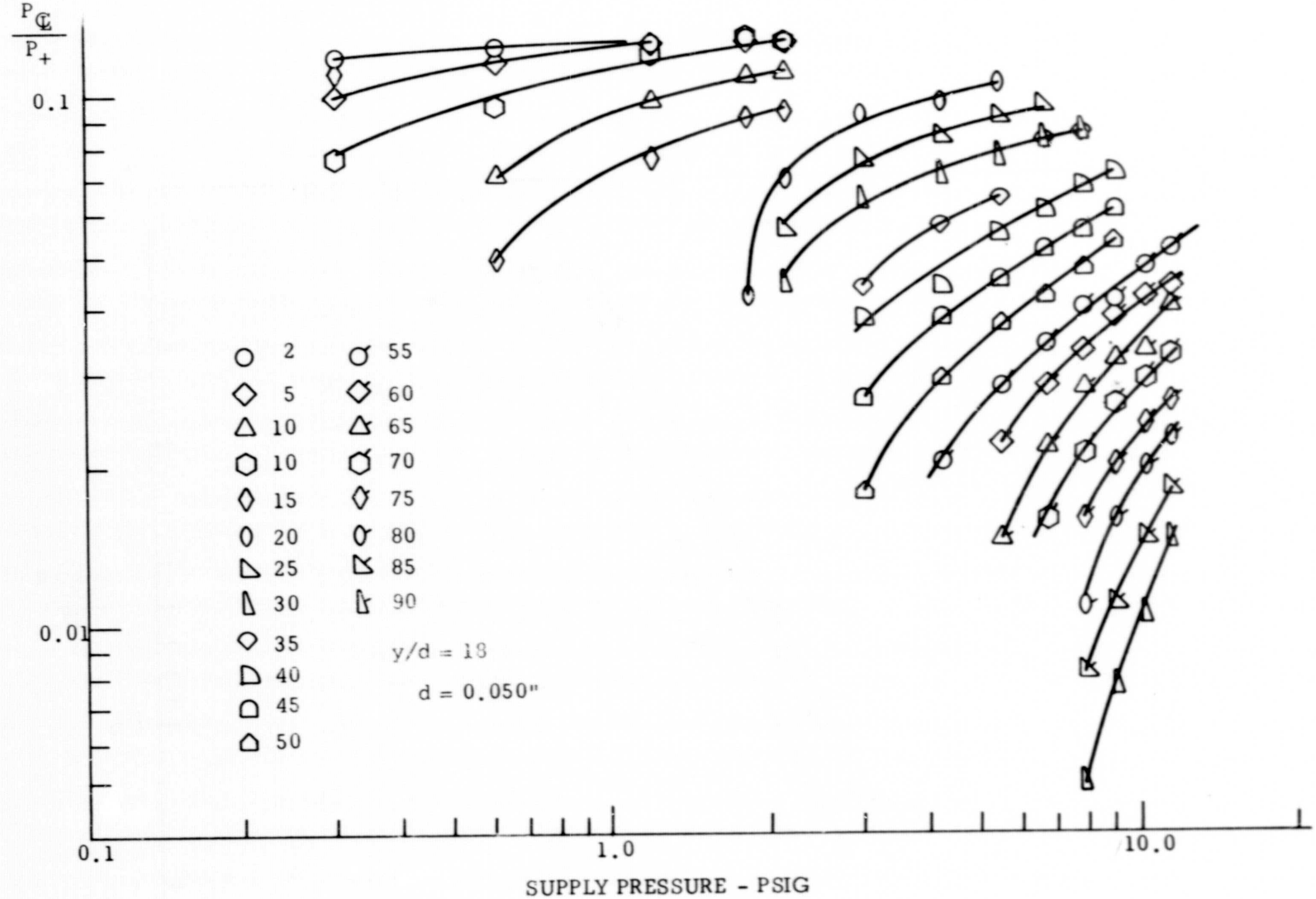

Figure 21.

31117

FIXED GEOMETRY CROSS FLOW SENSOR

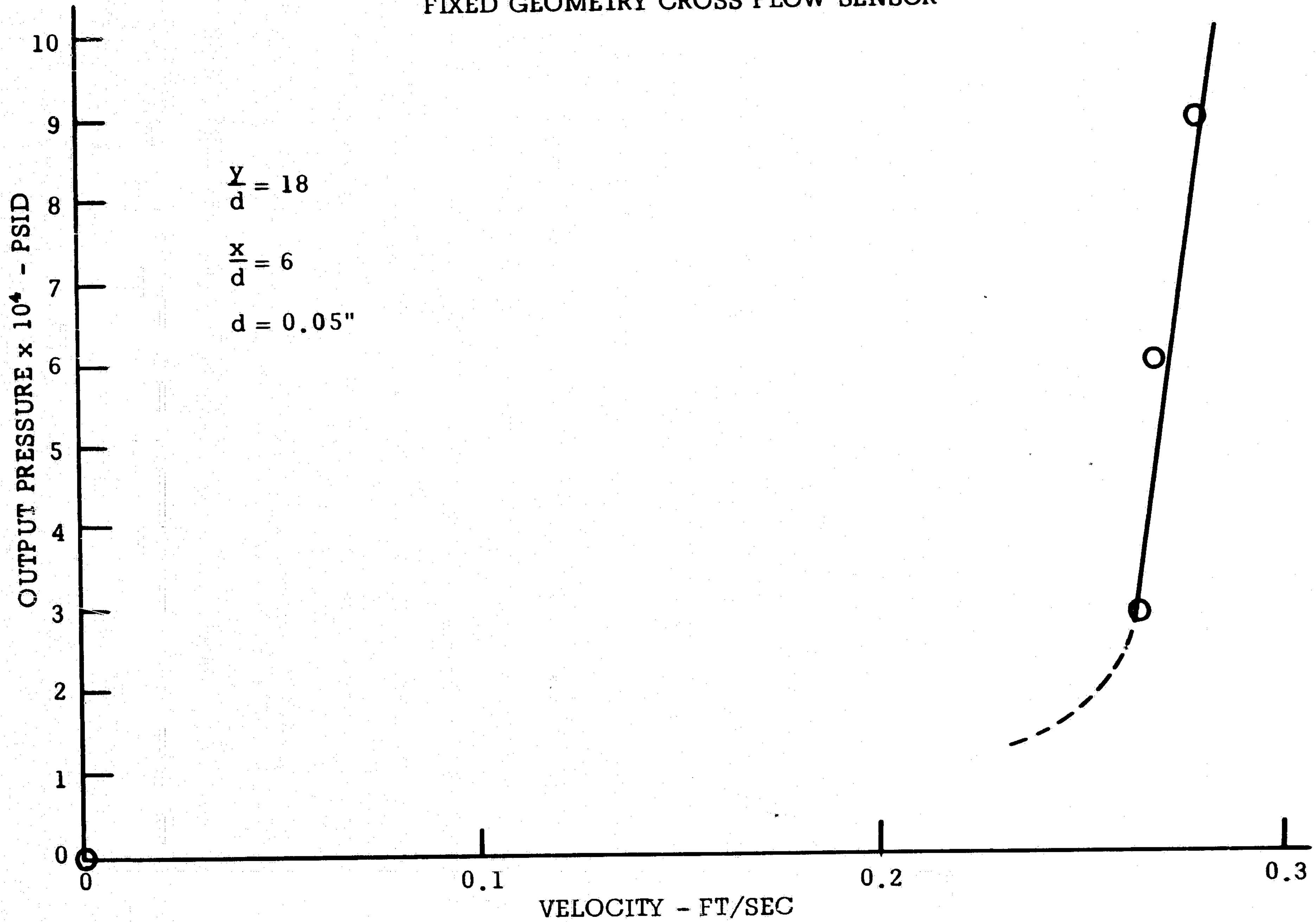

Figure 22.

From the wind tunnel data, and from appropriate cross-plotting of these data, an empirical relationship

$$\Delta P = \Delta P\,(V,\ y/d,\ P_+)$$

can be found. The differential output pressure is given by

$$\Delta P = \frac{\Delta P}{\Delta\left(\frac{x}{d}\right)}\ \Delta\left(\frac{x}{d}\right) \tag{1}$$

Figure 15 provides the expression for $\Delta\left(\frac{x}{d}\right)$

$$\Delta\left(\frac{x}{d}\right) = \frac{K}{P_+}$$

The constant of the hyperbola, K, is next found from Figure 16, which included all test results similar to that shown in Figure 15. The constant, K, is approximated by

$$K = a\,V^2\ . \tag{2}$$

Although the actual diameter of the power nozzle does not influence the constant, it is affected by the spacing between power nozzle and receiver. This latter effect may be represented by

$$a = 4.31 \times 10^{-5}\left(\frac{y}{d}\right)^2 - 3.18 \times 10^{-4}\,\frac{y}{d} + 5.553 \times 10^{-6} \tag{3}$$

This is obtained from Figure 16 and the fact that when $y/d = 0$, the deflection x/d is zero, and hence a must also be zero. The above quadratic formula is a "least squares" fit of the data.

x/d is thus, completely determined:

$$\frac{x}{d} = \left(4.31 \times 10^{-5}\left(\frac{y}{d}\right)^2 - 3.18 \times 10^{-4}\,\frac{y}{d} + 5.553 \times 10^{-6}\right)\frac{V^2}{P_+}\ . \tag{4}$$

From Figure 19, the term $\frac{\Delta P}{\Delta\,(x/d)}$ can be represented quite well by

$$\frac{\Delta P}{\Delta\left(\frac{x}{d}\right)} = b\,P_+^{\,n} \tag{5}$$

where b is determined by the vertical location of a particular curve on the graph (i.e., the velocity) and n is determined by the slope of the individual curves.

Figure 23 shows a plot of n vs. velocity. Whereas n varies substantially with velocity, it is not possible to detect a change with the spacing y/d within the scatter of data. A least squares fit of the data points shows that a cubic equation fits extremely well over the entire range. The cubic equation obtained is:

$$n = 4.2 \times 10^{-6} V^3 - 3.964 \times 10^{-4} V^2 + 2.74 \times 10^{-2} V + 1.023 \quad .$$

The "constant" b is shown in Figure 24. Observe that this term covers a wide range, and is dependent on the spacing between power nozzle and receiver. In order to effectively reduce the range of b, it is useful to replot the data as $\log_{10}(1/b)$ vs. velocity. By subtracting a constant determined by trial and error, the curves of Figure 25 can be made to conform to a straight line, Figure 26, which an empirical relationship can be easily deduced:

$$\left(\log_{10} \frac{1}{b}\right) - m = cV \qquad (6)$$

where c and m depends on the spacing y/d.

After performing a least squares fit to determine the appropriate expression for c and m as functions of y/d, the term b becomes:

$$b = 10^{-(cV + m)} \qquad (7)$$

where $c = .000375(y/d)^2 - .00975\,(y/d) + .093$

$m = .022125(y/d)^2 - .6552\,(y/d) + 5.787$ for $y/d > 15$

$= 0.94$ for $y/d < 14$.

The above empirical relationships may be combined:

$$\Delta P \frac{\Delta P}{\Delta (x/d)} \; \Delta\left(\frac{x}{d}\right) = a b P_+^{(n-1)} V^2 \qquad (8)$$

where $a = 4.31 \times 10^{-5} \left(\frac{y}{d}\right)^2 - 3.18 \times 10^{-4} \frac{y}{d} + 5.553 \times 10^{-6}$

$b = 10^{-(cV + m)}$

$n = 4.2 \times 10^{-6} V^3 - 3.964 \times 10^{-4} V^2 + 2.74 \times 10^{-2} V + 1.023$

EMPIRICAL CONSTANT FOR SLOPE OF PRESSURE PROFILE

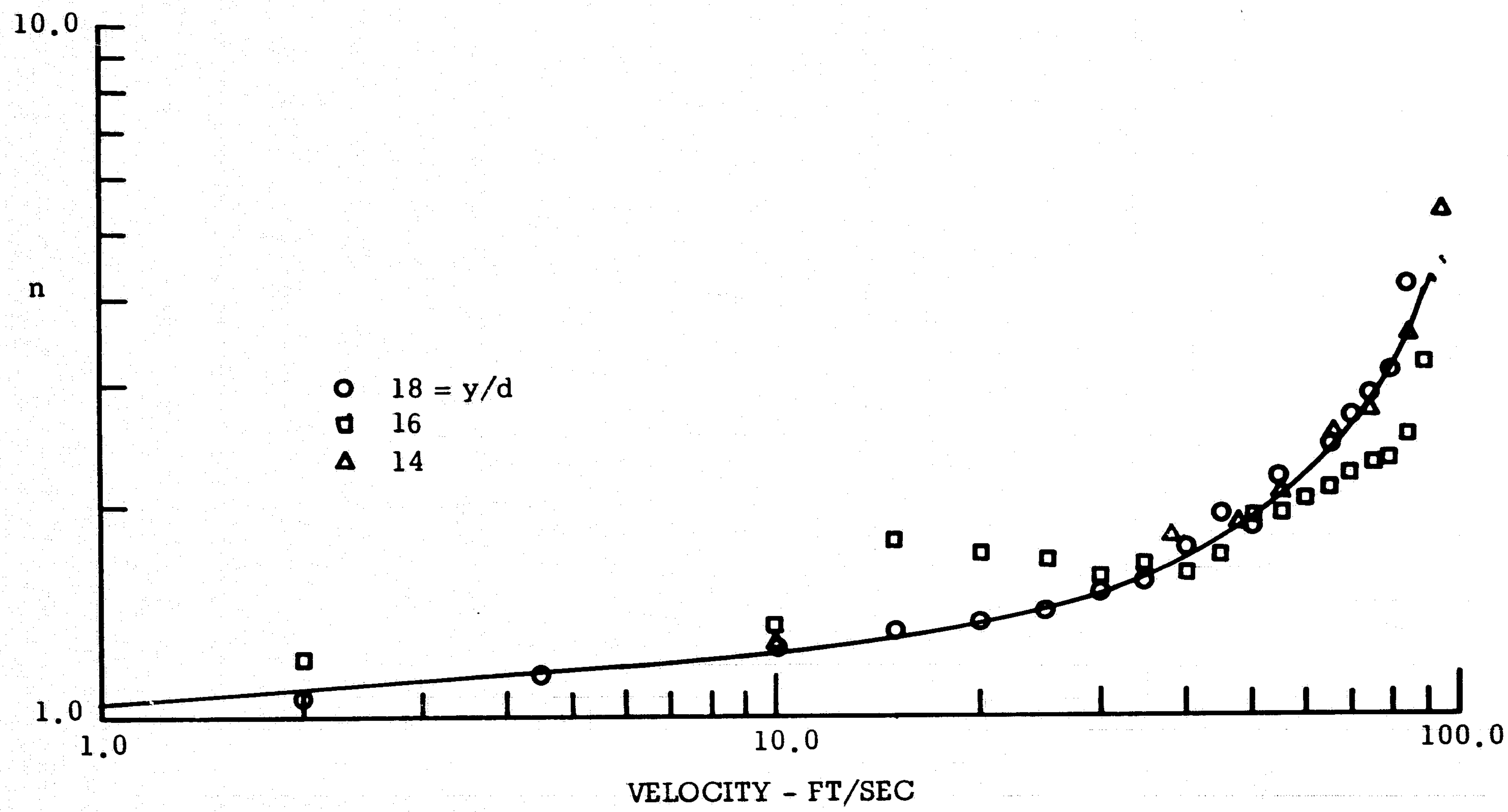

Figure 23.

EMPIRICAL CONSTANT FOR PRESSURE PROFILE SLOPE

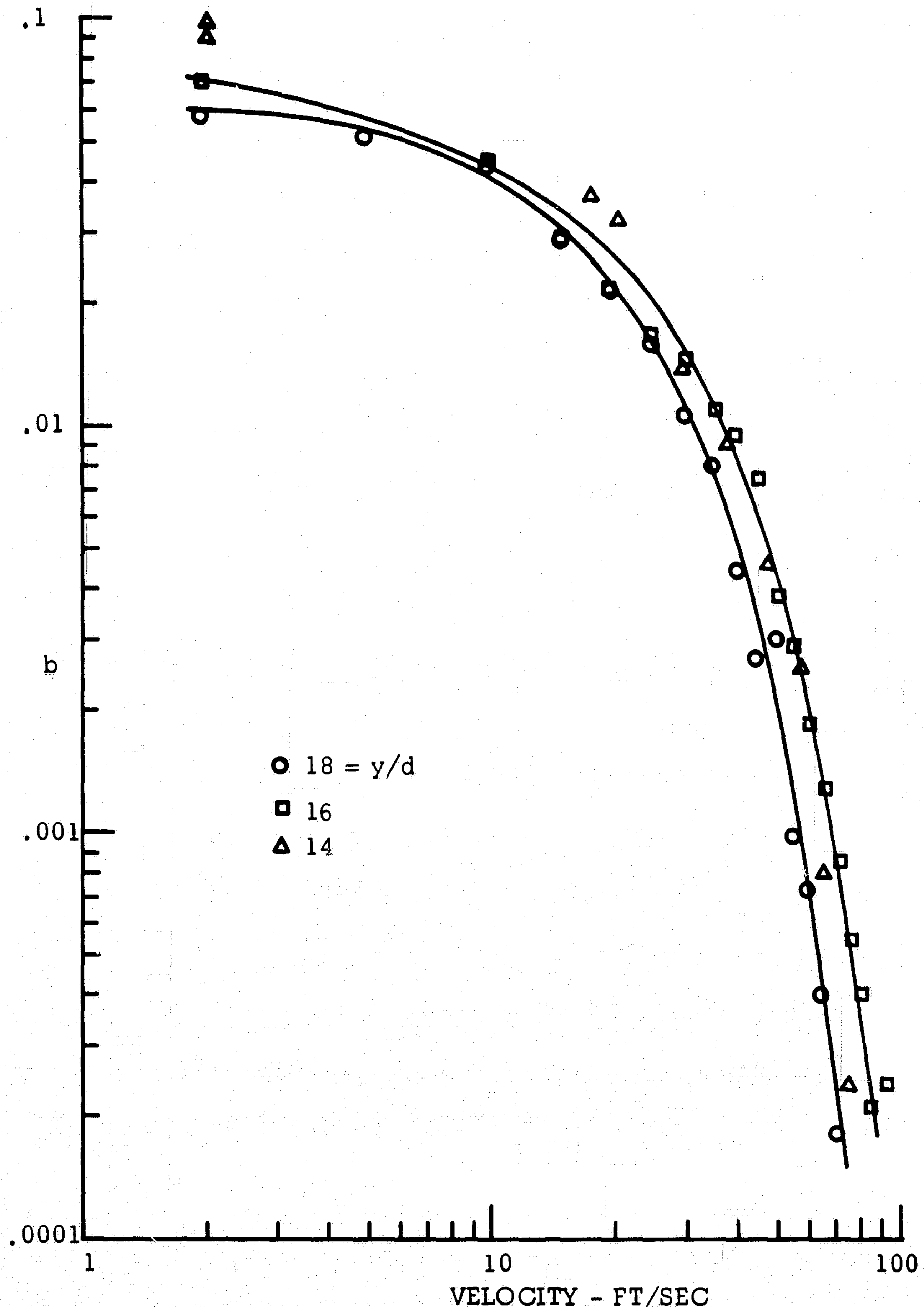

Figure 24.

EMPIRICAL CONSTANT FOR PRESSURE PROFILE SLOPE

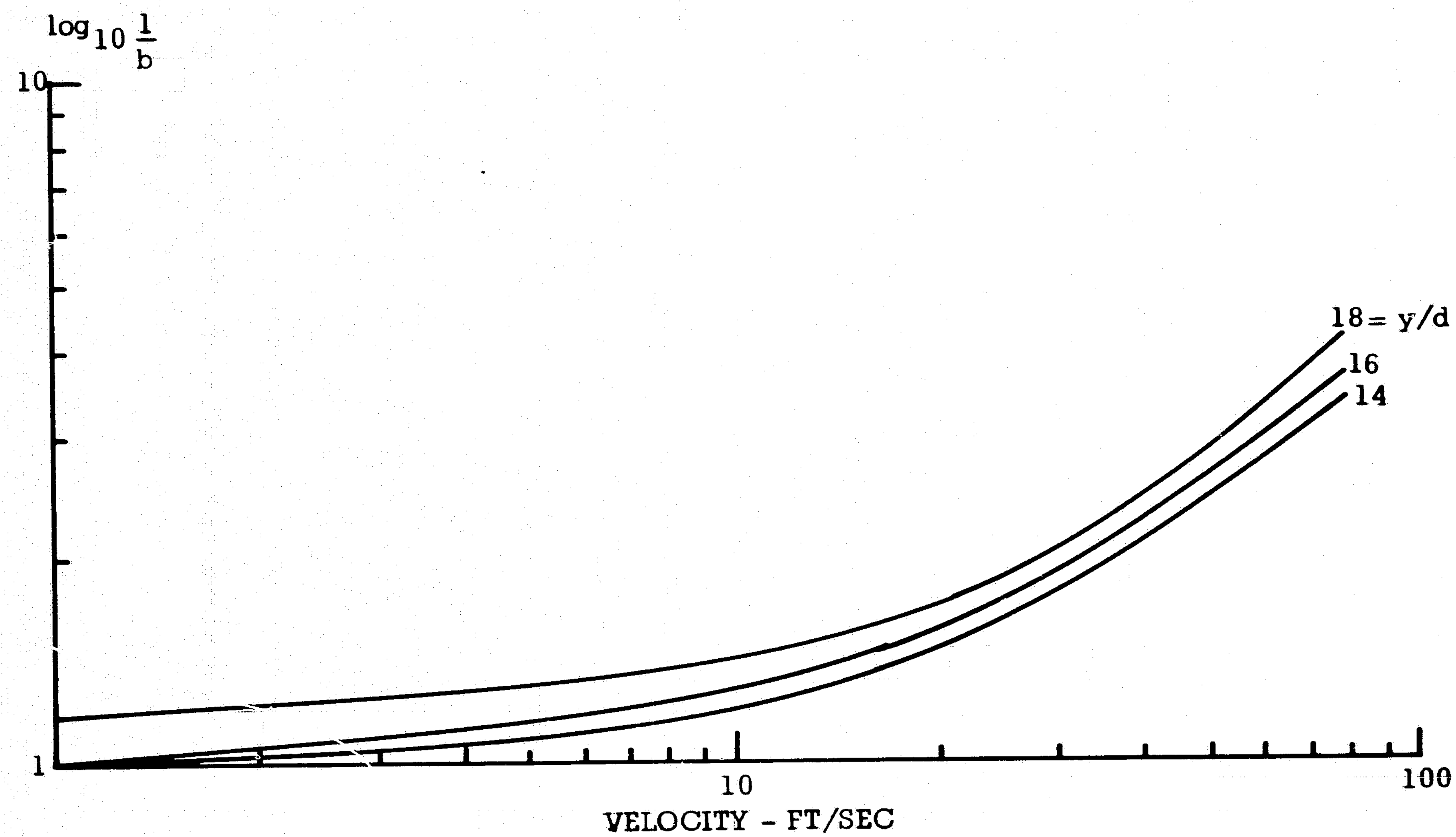

Figure 25.

EMPIRICAL CONSTANT FOR PRESSURE PROFILE SLOPE

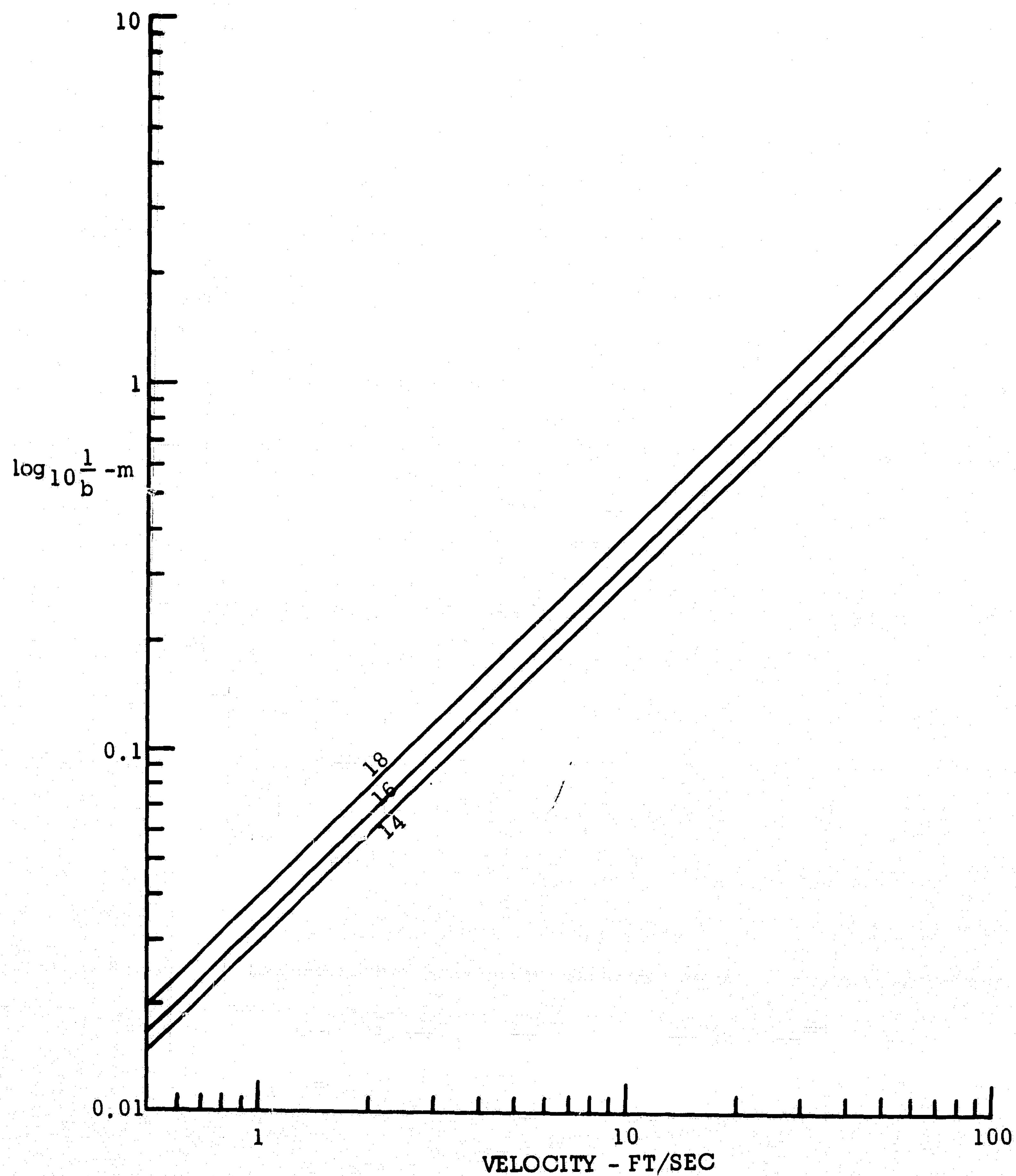

Figure 26.

The results of this analysis, and the results obtained from the data itself are shown in Figures 27a, b, c. Each of the curves show the correct trend, but there is a discrepancy in the magnitudes of the predicted ΔP. This is attributed to the value of b which is determined empirically from Figure 24.

As can be seen from Figure 26, a slight error in velocity can easily cause a factor of two error in b. Unfortunately, the scatter in the experimental data precludes a more accurate determination of b and hence ΔP.

Equation 8 is nonetheless significant in that is shows to what extent such design parameters as spacing between power nozzle and receiver, supply pressures, and velocity affect the output pressure.

2. Closed Loop Operation

The cross flow sensor can be operated in a closed loop mode. This is suggested by the strong dependence of ΔP on P_+ in equation 8. To demonstrate this approach, tests were run at the low speeds of the BFC-built wind tunnel. The schematic of the experimental arrangement is shown in Figure 28. A fluidic Operational Amplifier, "Op-Amp",* (Reference 8) was employed, as shown, in the feedback path. The receiver of the wind sensor serves as the input to the Op-Amp, and the system output is that of the Op-Amp, which by its high gain serves to maintain the receiver pressure at a constant value. Using this scheme provides the advantages of higher power output of the Op-Amp.

This device is capable of driving several other fluidic components at a higher pressure, thereby making fluidic computation of wind vector components an easier task.

The test results of the closed loop operation, for a single bias pressure, appear in Figure 29. Insofar as this method is beyond the scope of the present work, no attempt was made at optimization. Hence, the range presented is unduly short.

*The Operational Amplifier is a direct-coupled feedback amplifier having high open-loop gain.

DIFFERENTIAL OUTPUT PRESSURE vs VELOCITY

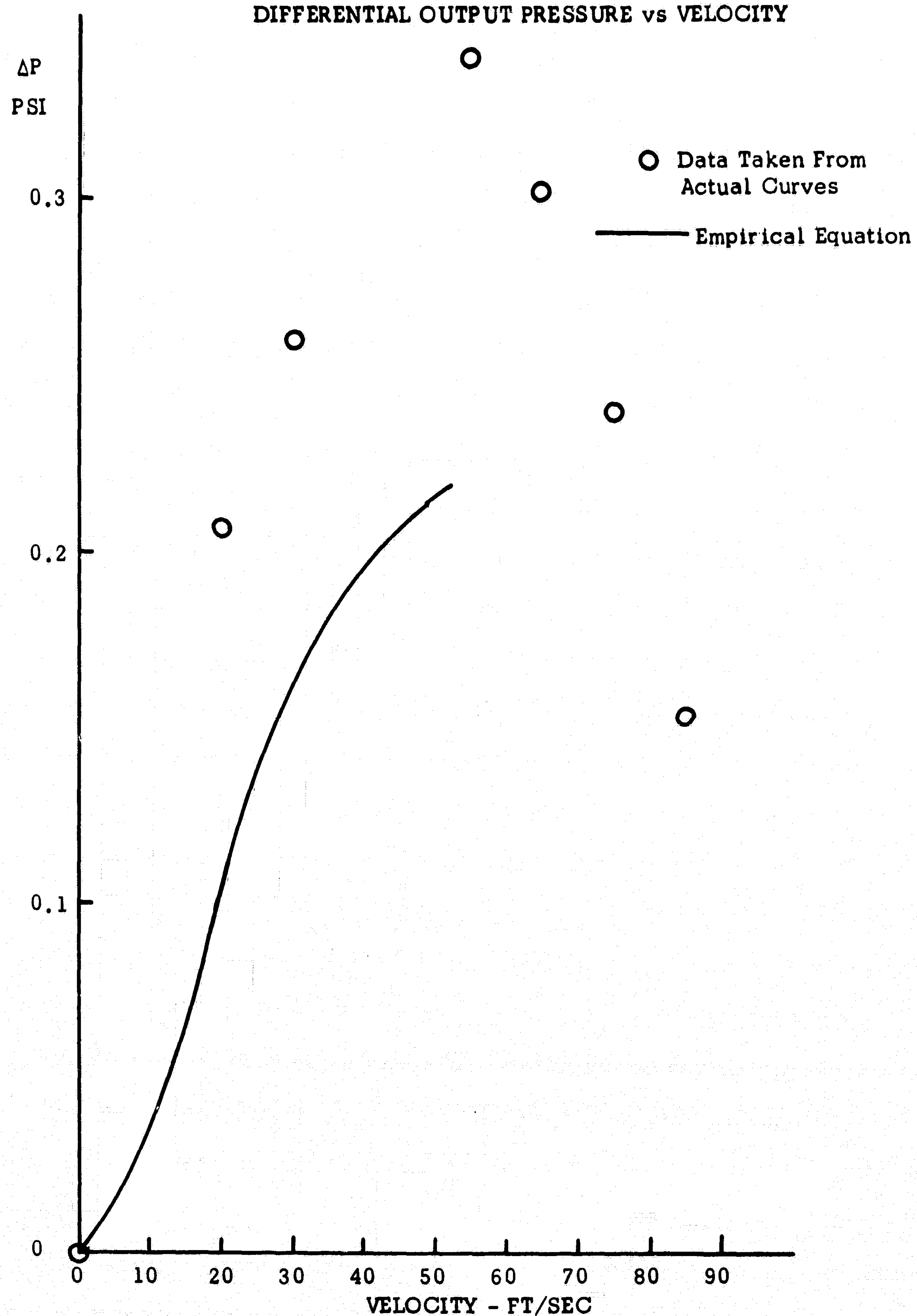

Figure 27a.

DIFFERENTIAL OUTPUT PRESSURE vs. VELOCITY

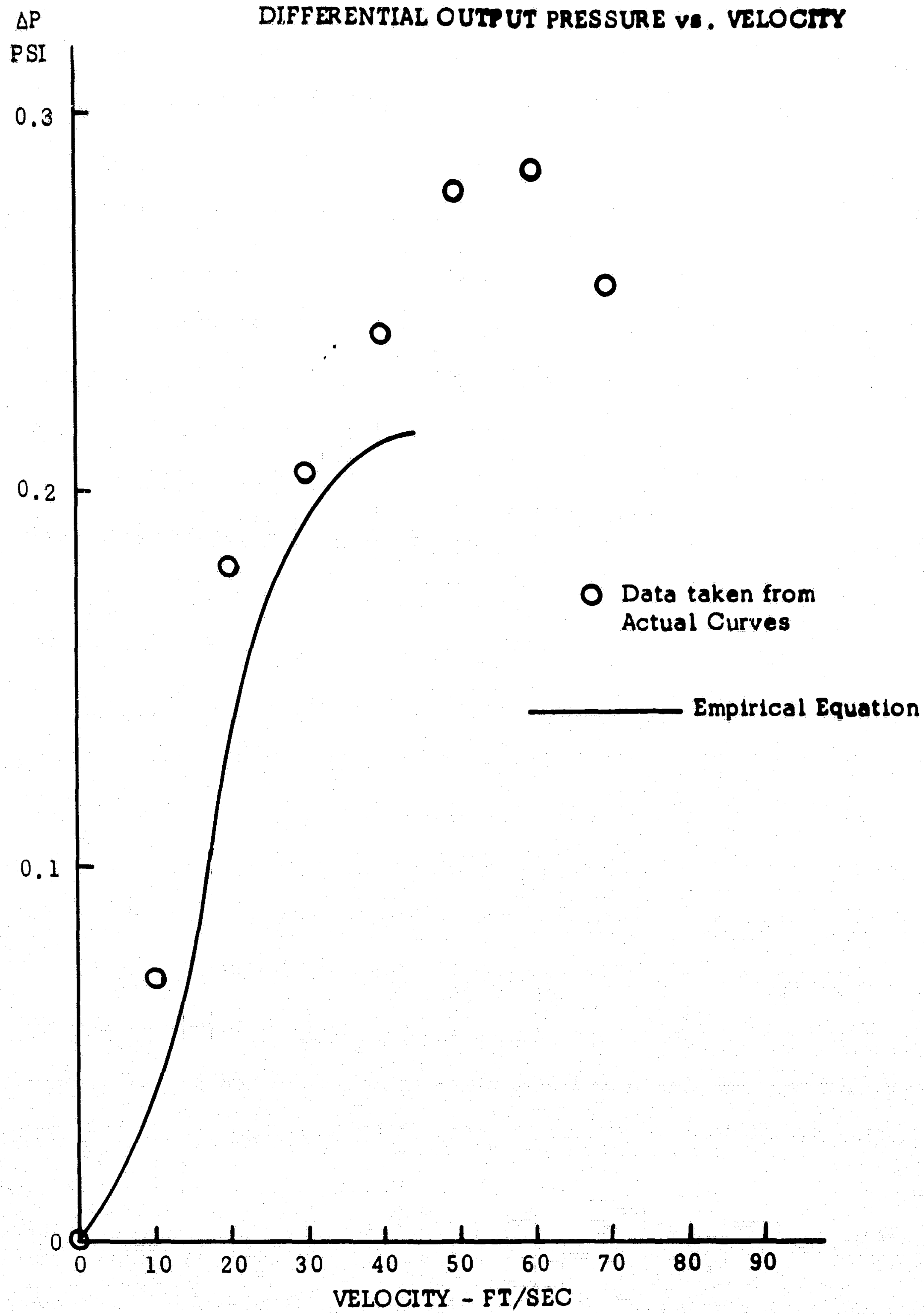

Figure 27b.

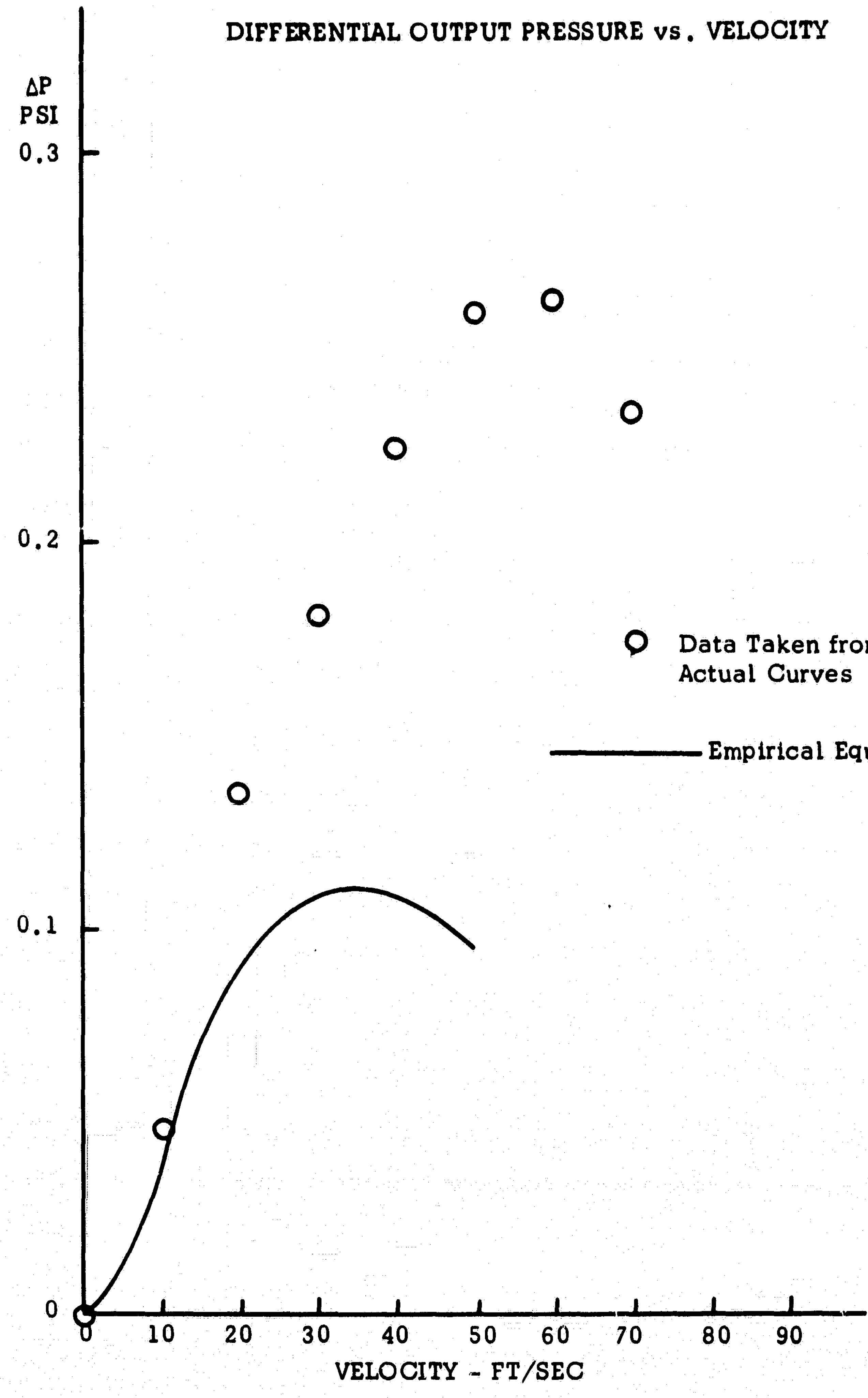
DIFFERENTIAL OUTPUT PRESSURE vs. VELOCITY
ΔP
PSI
0.3
0.2
0.1
0
0
10
20
30
40
50
60
70
80
90
VELOCITY - FT/SEC
Data Taken from
Actual Curves
Empirical Equation

Figure 27c.

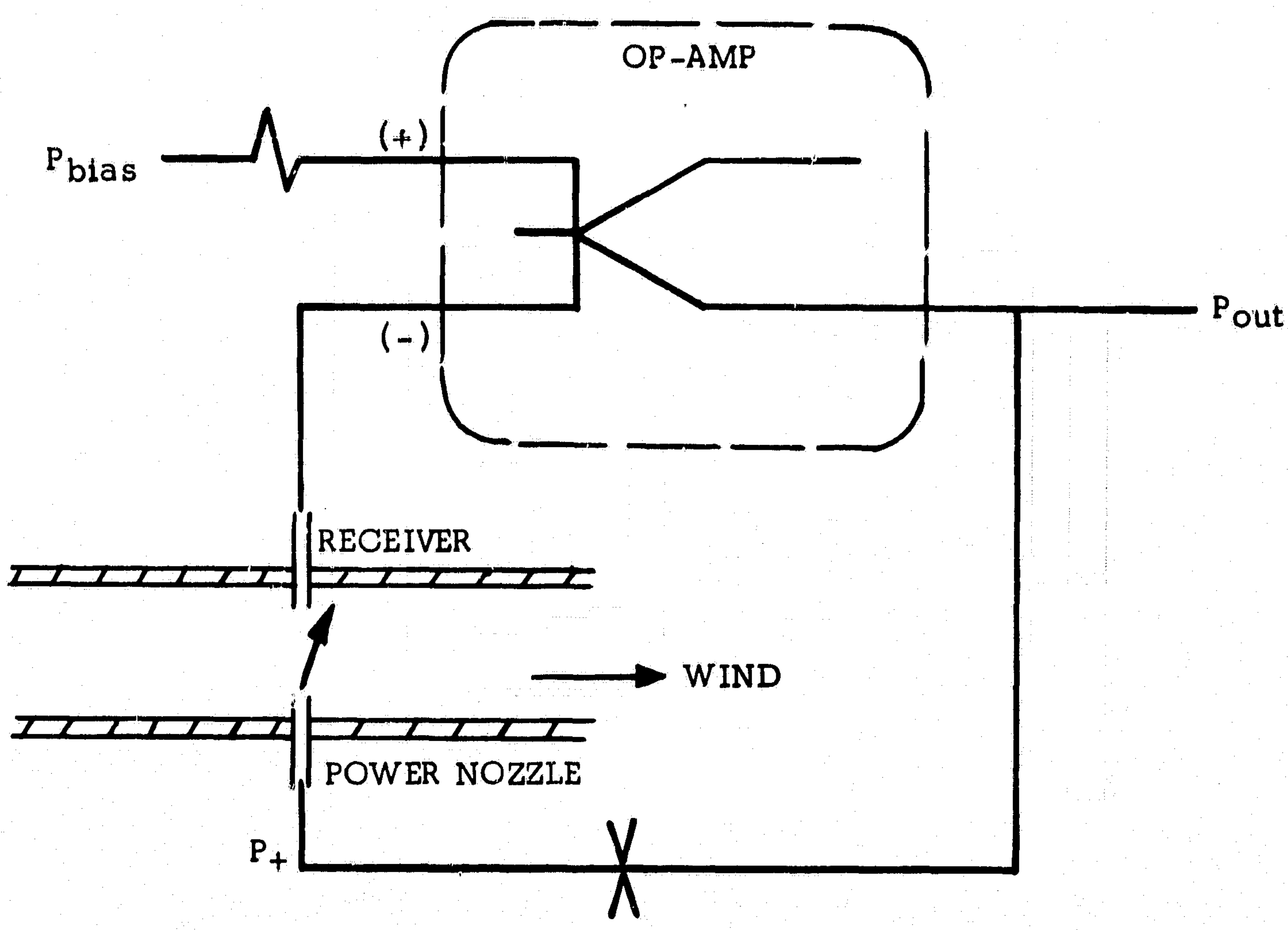

SCHEMATIC OF CLOSED LOOP OPERATION OF CROSS FLOW WIND SENSOR

Figure 28.

OUTPUT OF FLUIDIC OPERATIONAL AMPLIFIER

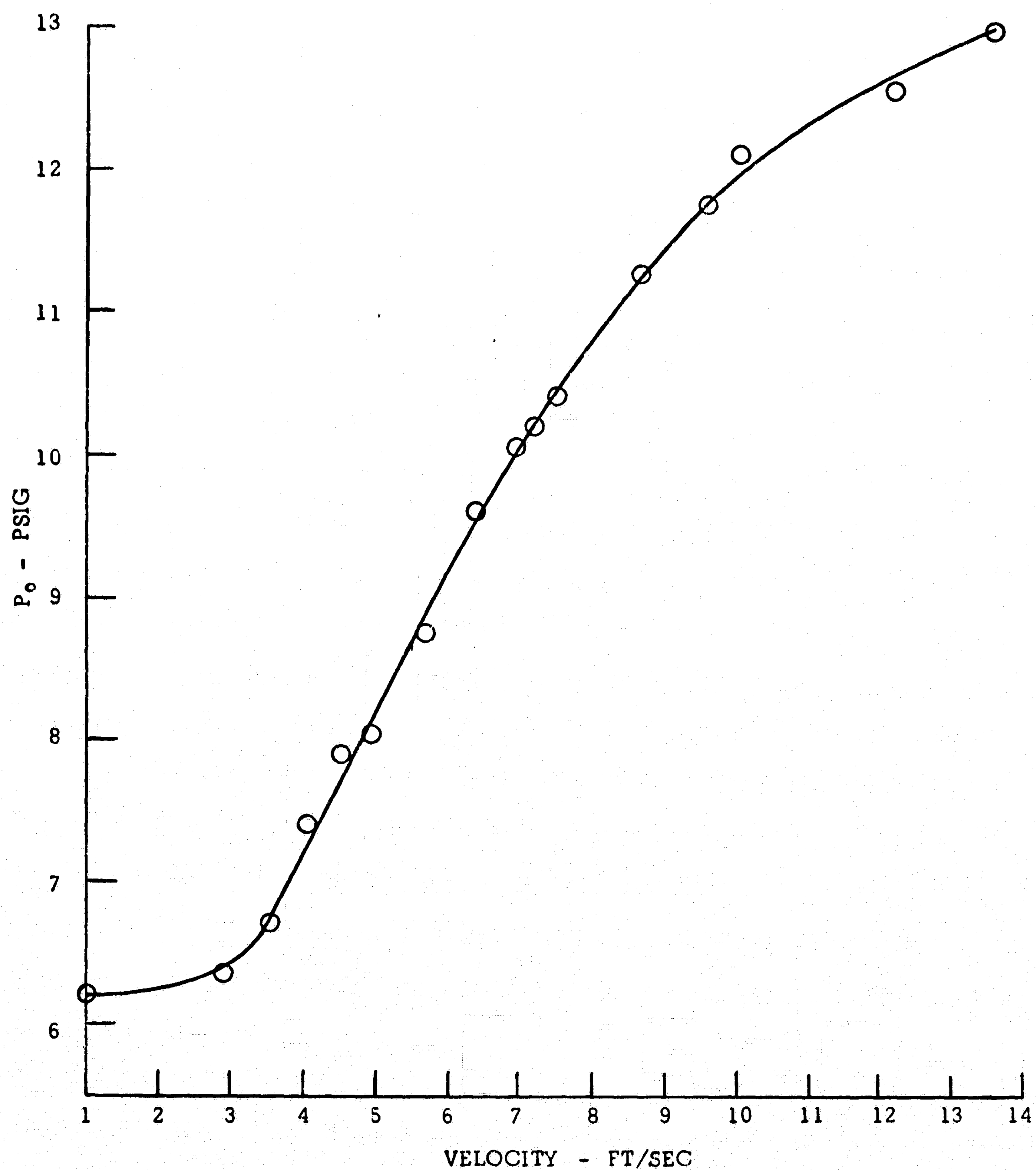

Figure 29.

C. Parallel Flow Wind Sensor

Whereas the previously discussed wind sensor is based on momentum interaction principles, the second approach investigated is based on viscous action between a jet and the surrounding wind. As an introduction to this approach, consider the case of a free jet exhausting into still air. At the nozzle exit plane, the velocity is uniform across the jet.

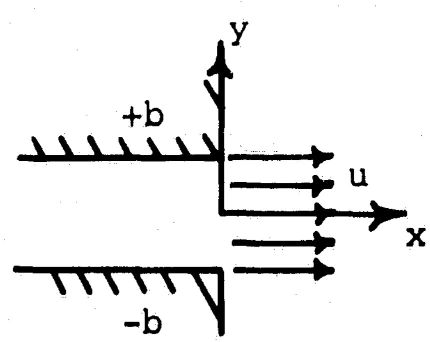

i.e., $u = \text{Const}$ for $-b < y < b$

$u = 0$ for $|y| > b$

For $x > 0$, this initially uniform velocity undergoes a gradual transition to a bell-shaped profile. At these values downstream $(x>0)$, $u>0$ for $y > b$ due to viscous action. The resulting profile appears as

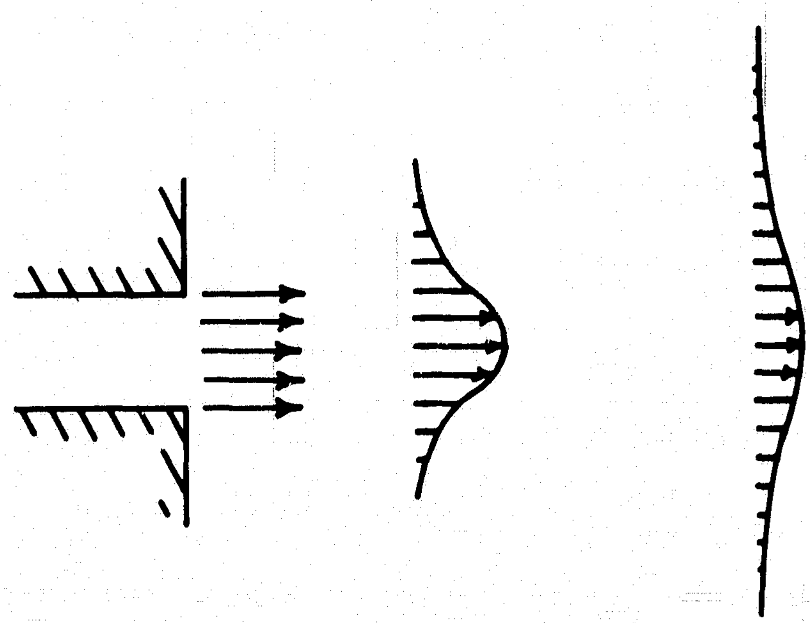

If the jet velocity, u, is small compared to the free stream (wind) velocity, V, the problem can be treated mathematically using perturbation techniques (Reference 5). Unfortunately, this solution is not valid if u and V are of opposite sign, thereby excluding the possibility of bi-directional operation of the wind sensor. The problem is not amenable to an analytical approach, and resport is made to wind tunnel testing.

1. Model Description

Two models of this parallel flow concept were made. As was previously done, the first model was built allowing maximum versatility. Using this model, basic jet pressure profile data were recorded. The model is shown in Figure 30a, which shows the configuration mounted on the wind tunnel wall. There are two nozzles with centerlines which are mutually parallel to each other and to the wind direction. The supply pressure can be applied to either nozzle, and therefore, data can be recorded with the jet blowing into and with the wind.

Figure 30b shows the mechanism which provides motion in two directions, one of which is transduced into an electrical signal by a linear motion potentiometer. This test setup was used to obtain pressure profile data, which was recorded for varying supply pressures and distance between nozzle over the velocity range $10 < V < 90$ ft/sec. An X-Y plot with zero velocity is shown in Figure 31. This establishes the datum from which the effects of the wind may be determined. Two sets of profiles are shown, one using each nozzle as the supply. They differ in amplitude at corresponding pressures because pressure was measured upstream of the line fittings which are not identical for each nozzle. This discrepancy only exists in the raw data, and has been corrected in the data reduction. Figure 32 shows the jet profile blowing with and against a 35 ft/sec wind. The distance between power nozzle and receiver for this case is 20 nozzle diameters. By comparing these profiles with the profile having the same supply pressure in Figure 31, the change in the recoverable pressure due to a 35 ft/sec wind in either direction can be determined.

From these basic profiles, the centerline pressure was plotted vs. supply pressure, holding the velocity constant at incremented values in wind speed from 10 to 90 ft/sec. Figure 33 shows the results of these tests for the jet flow in both directions.

Differential Pressure From Bridge Circuit -- The difference between receiver pressures at the same supply pressure and corresponding velocity represents the differential output obtainable from a bridge-type configuration shown below. The differential output thus obtained is shown in Figure 34.

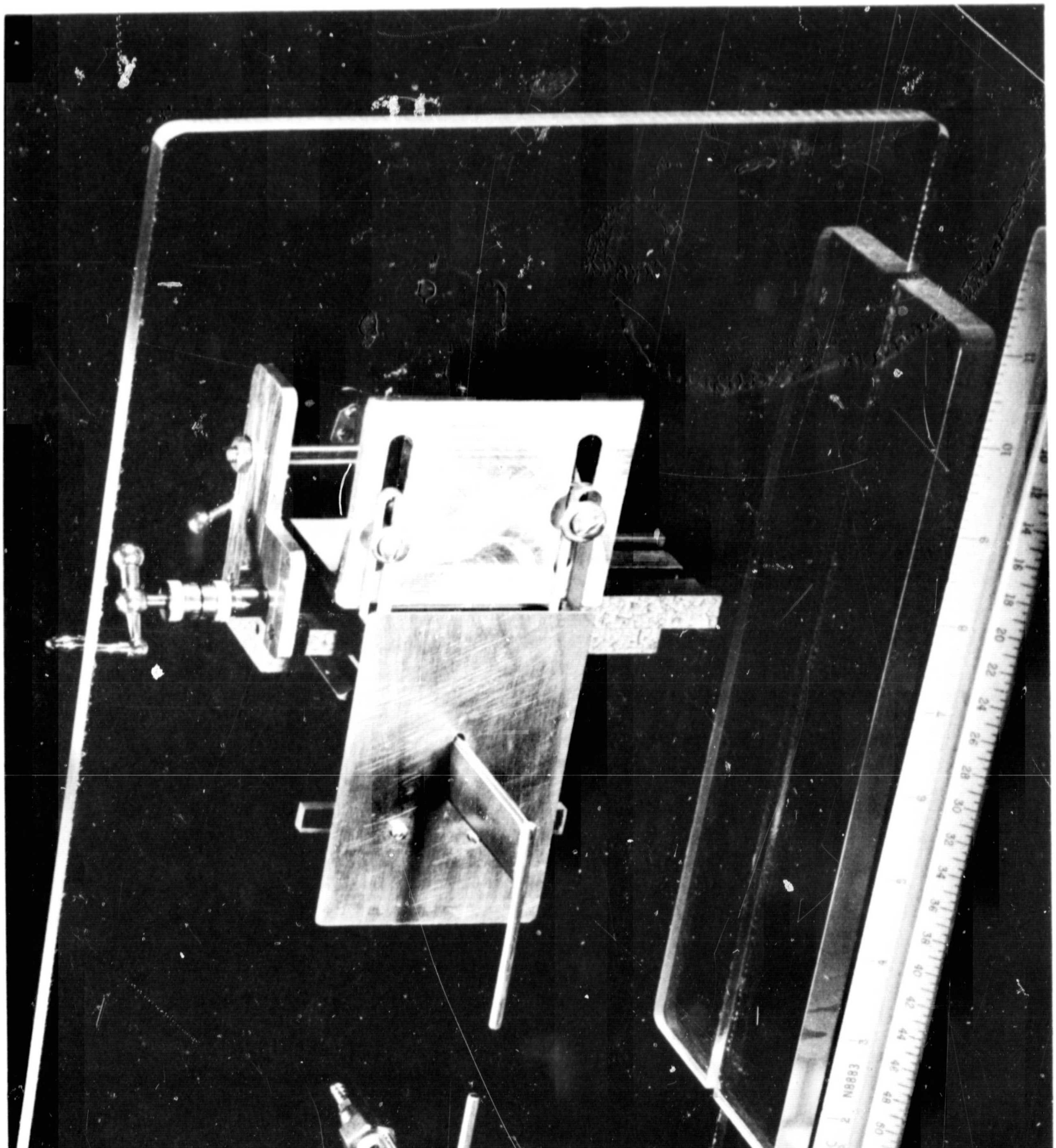

FIGURE 30a. PARALLEL FLOW WIND SENSOR MODEL

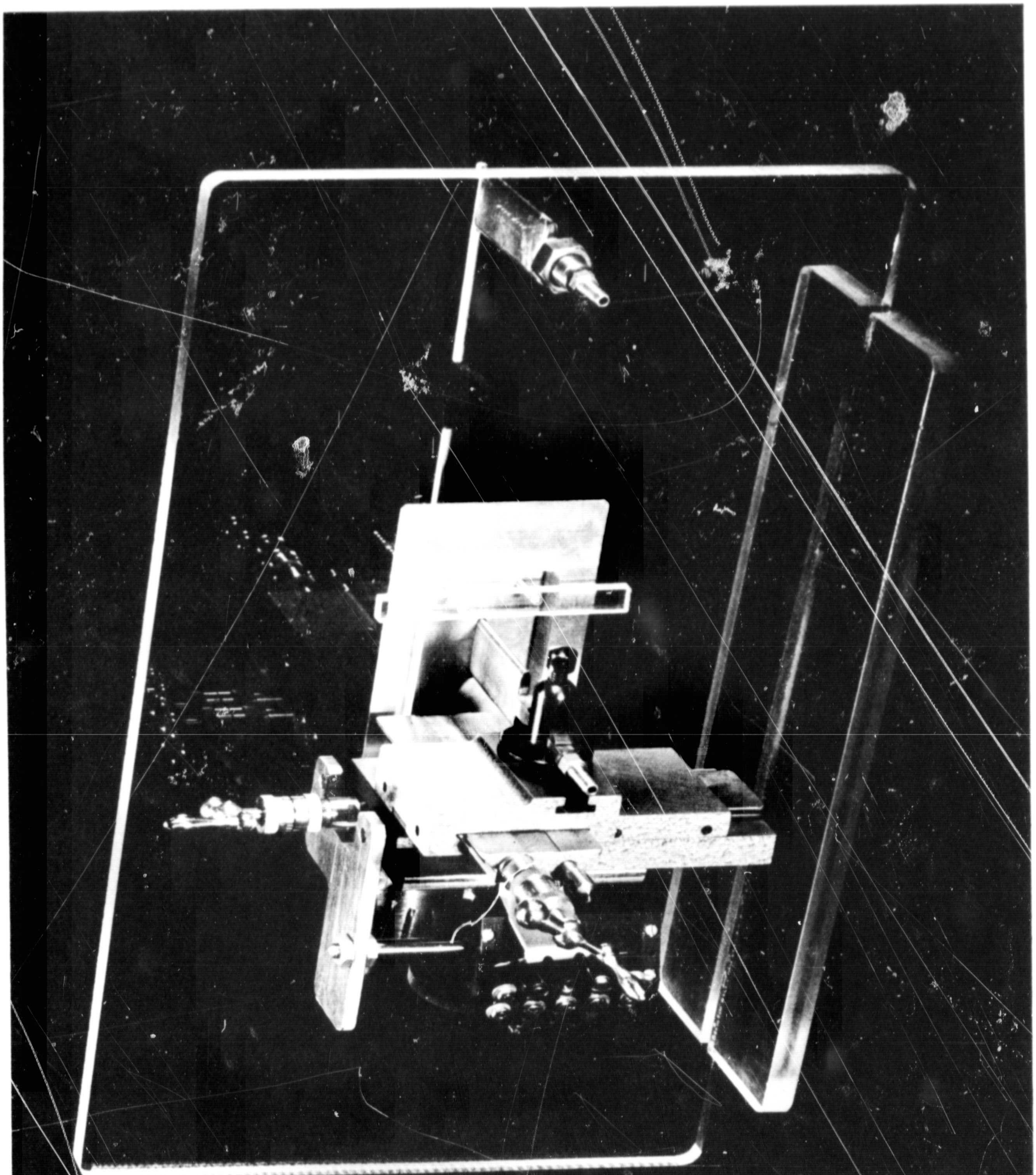

FIGURE 30b. PARALLEL FLOW WIND SENSOR MODEL

31182

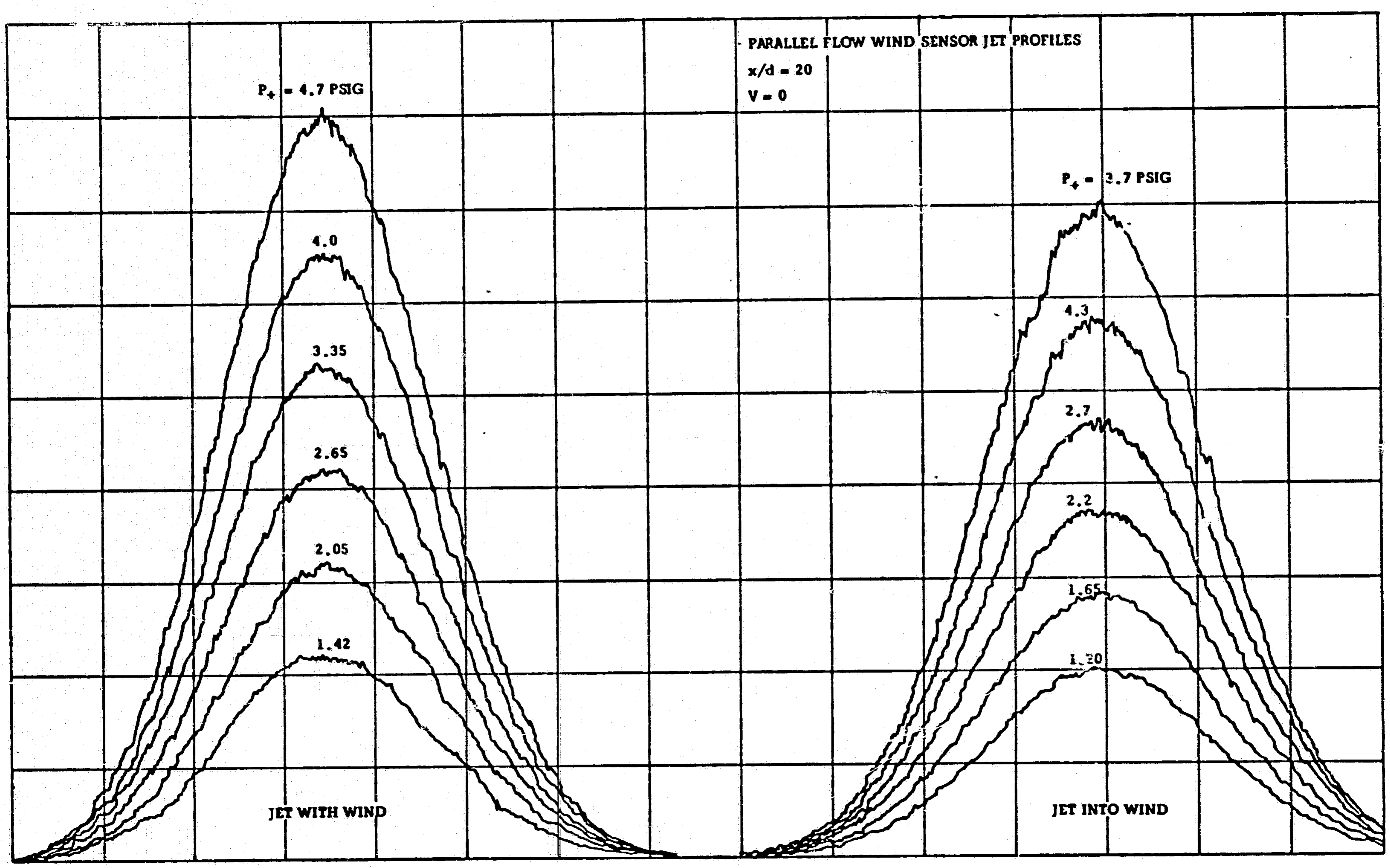

Figure 31.

31127

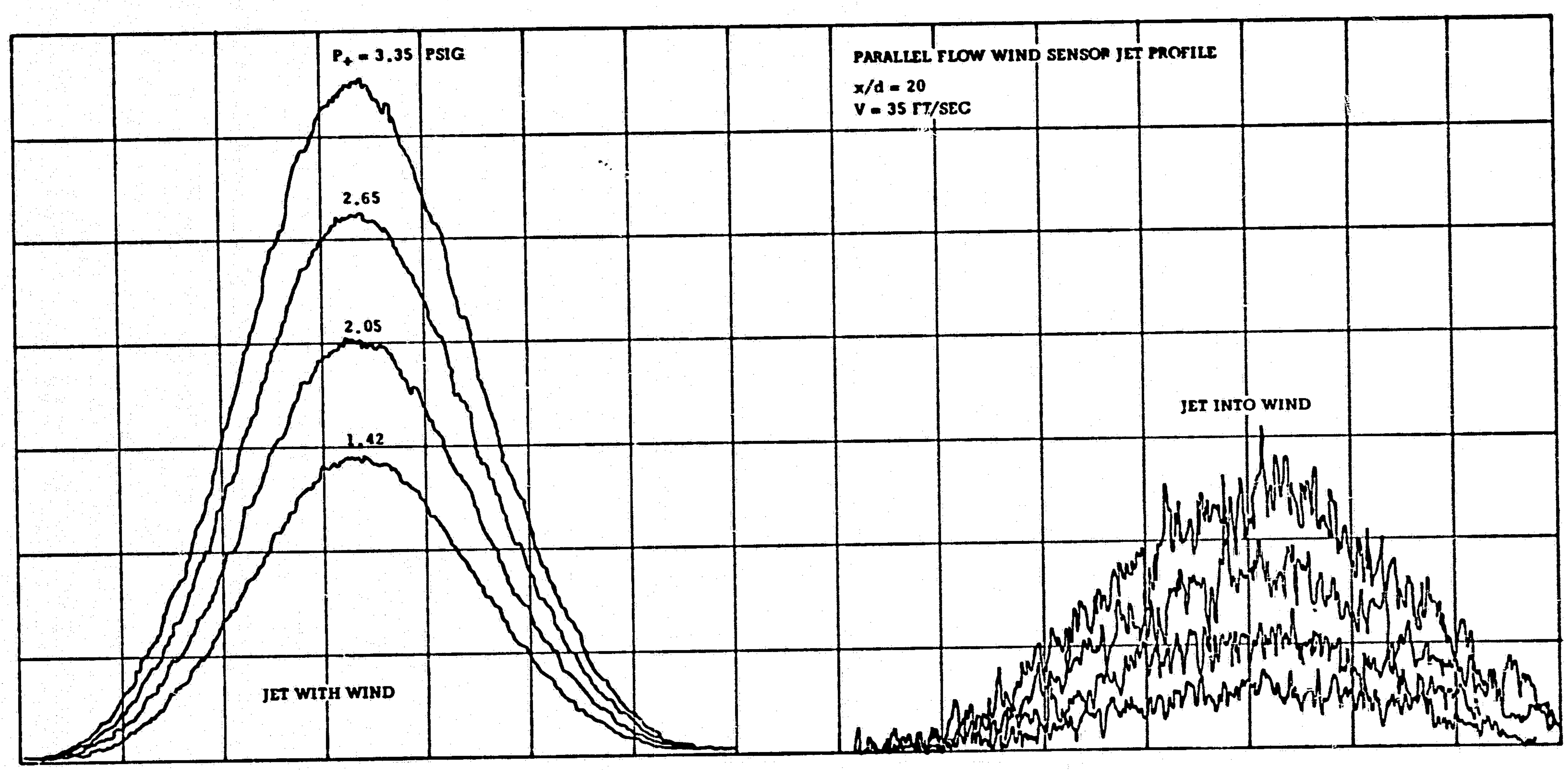

Figure 32.

31128

PARALLEL FLOW WIND SENSOR PRESSURE RECOVERY
FOR JETS BLOWING WITH AND AGAINST WIND

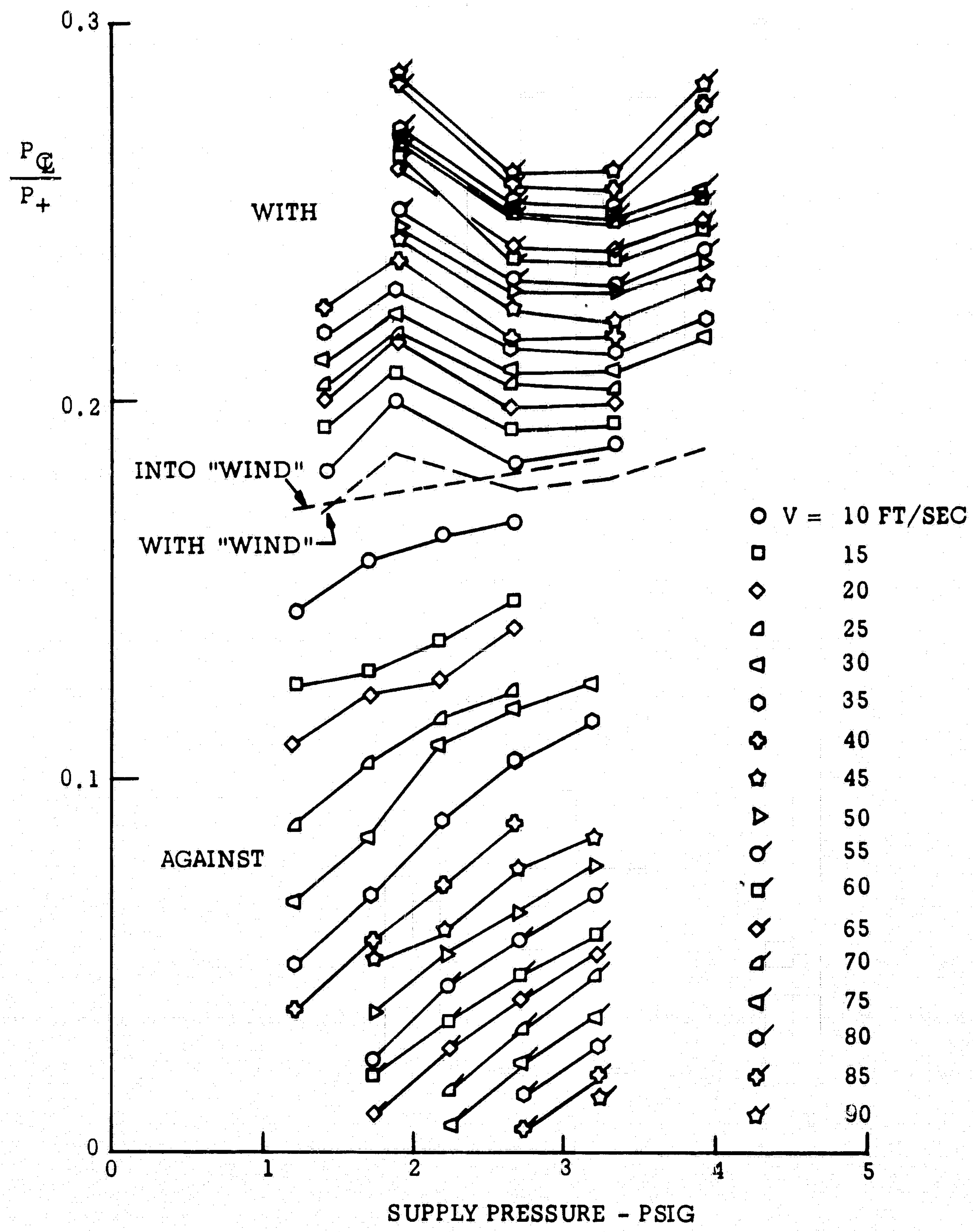

Figure 33.

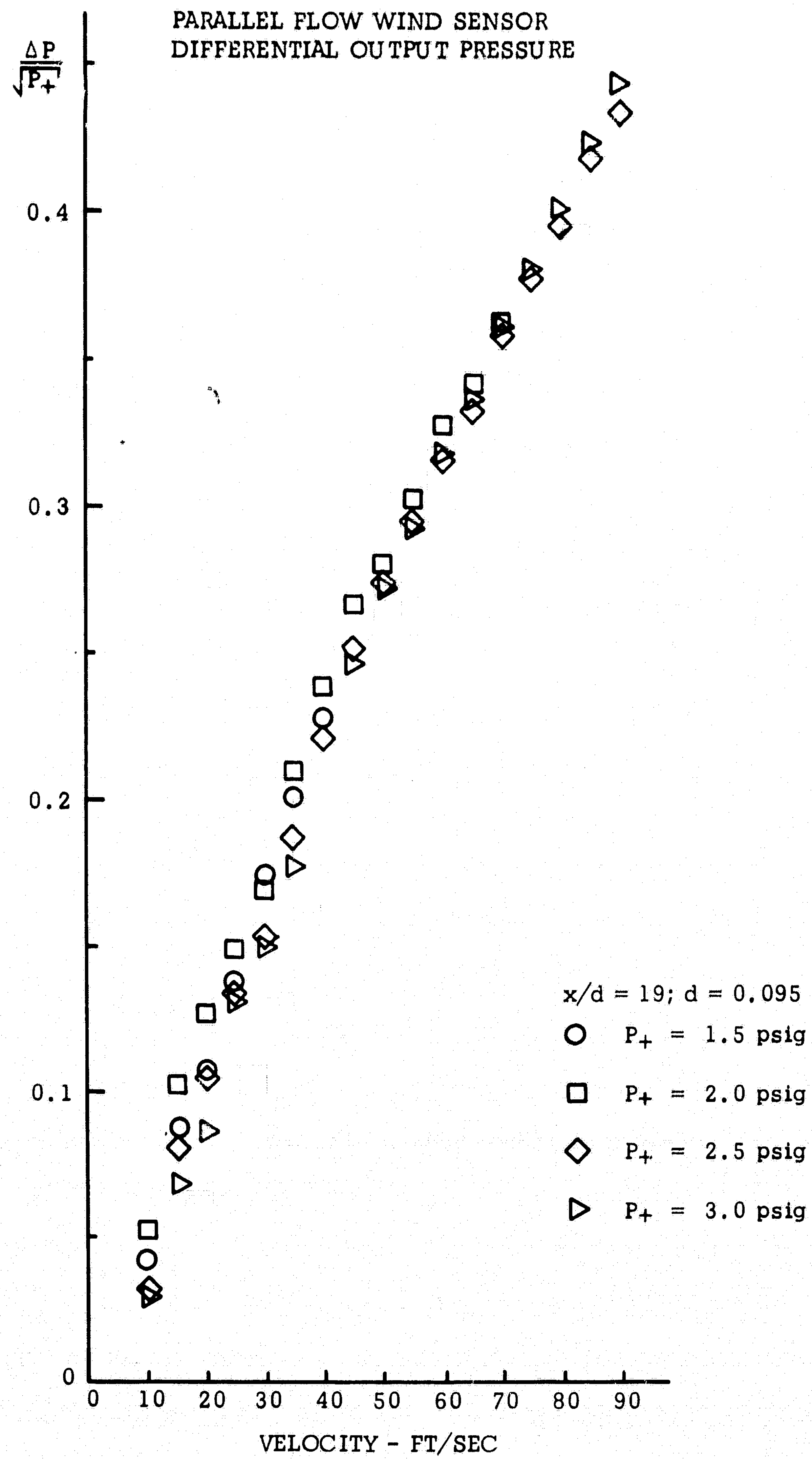
PARALLEL FLOW WIND SENSOR
DIFFERENTIAL OUTPUT PRESSURE
$\frac{\Delta P}{\sqrt{P_+}}$
0.4
0.3
0.2
0.1
0
0
10
20
30
40
50
60
70
80
90
VELOCITY - FT/SEC
x/d = 19; d = 0.095
P_+ = 1.5 psig
P_+ = 2.0 psig
P_+ = 2.5 psig
P_+ = 3.0 psig

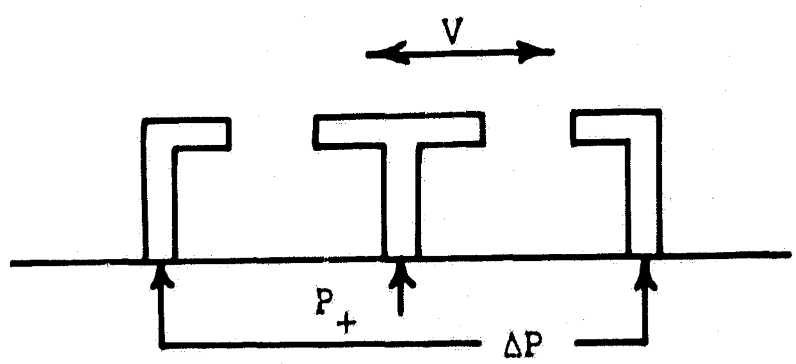

Through the use of modulating the power jet by the viscous action of the flowing wind, one essentially moves up the "Pitot tube" square law to an operating point not at the wind velocity but rather at the power jet velocity. Moving farther up the curve, i.e., increasing supply pressure, increases the slope $d\Delta P/dV$ and thus the sensitivity of the sensor. This behavior was observed in Figure 4.

The bridge-type configuration shown above was tested in the low speed regime at Bowles Fluidics Corporation. The results of the low speed testing and the higher speed testing are shown in Figure 35. The curve is remarkably linear over the entire velocity range.

2. Empirical Analysis of Data

Because the mechanism by which the parallel flow wind sensor operates, namely velocity gradient between the power jet and the free stream, it is appropriate to normalize the output pressure by a representative velocity. The normalizing factor chosen is $\sqrt{P_+}$ which is proportional to the supply velocity. Figure 34 shows a typical result, from which it can be concluded that variation in supply pressures have been accounted for with this factor. The output characteristic is essentially a linear function, and one may therefore describe the behavior of a parallel flow wind sensor simply by

$$\frac{\Delta P}{\sqrt{P_+}} = KV$$

where $K = K(x/d)$

From the remainder of the data of which Figure 34 is typical, the slope of the output is measured and plotted in Figure 36. This curve shows that the optimum spacing between power nozzle and receiver to be 18d.

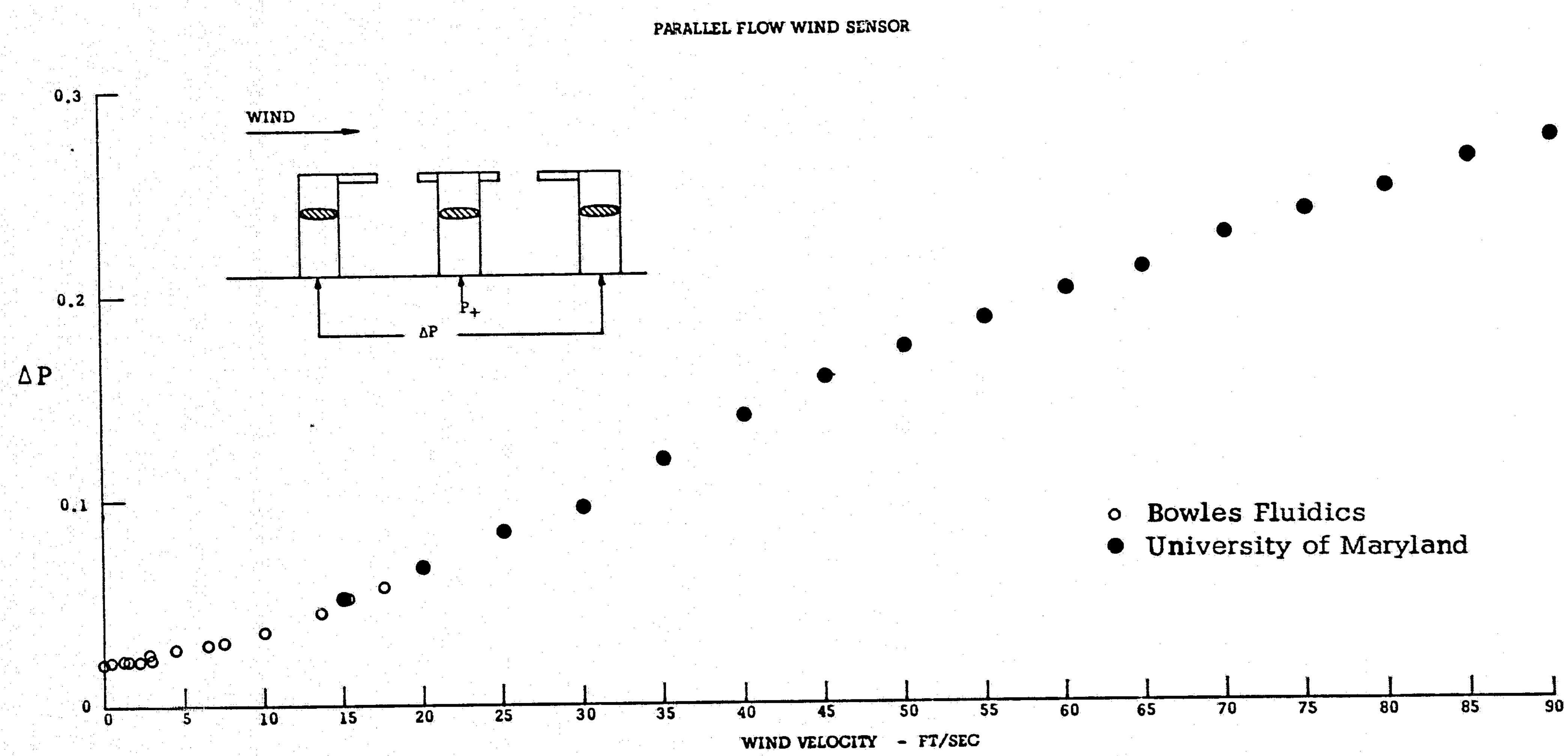
PARALLEL FLOW WIND SENSOR
WIND
P+
ΔP
ΔP
0.3
0.2
0.1
0
0
5
10
15
20
25
30
35
40
45
50
55
60
65
70
75
80
85
90
WIND VELOCITY - FT/SEC
o Bowles Fluidics
● University of Maryland

Figure 35.

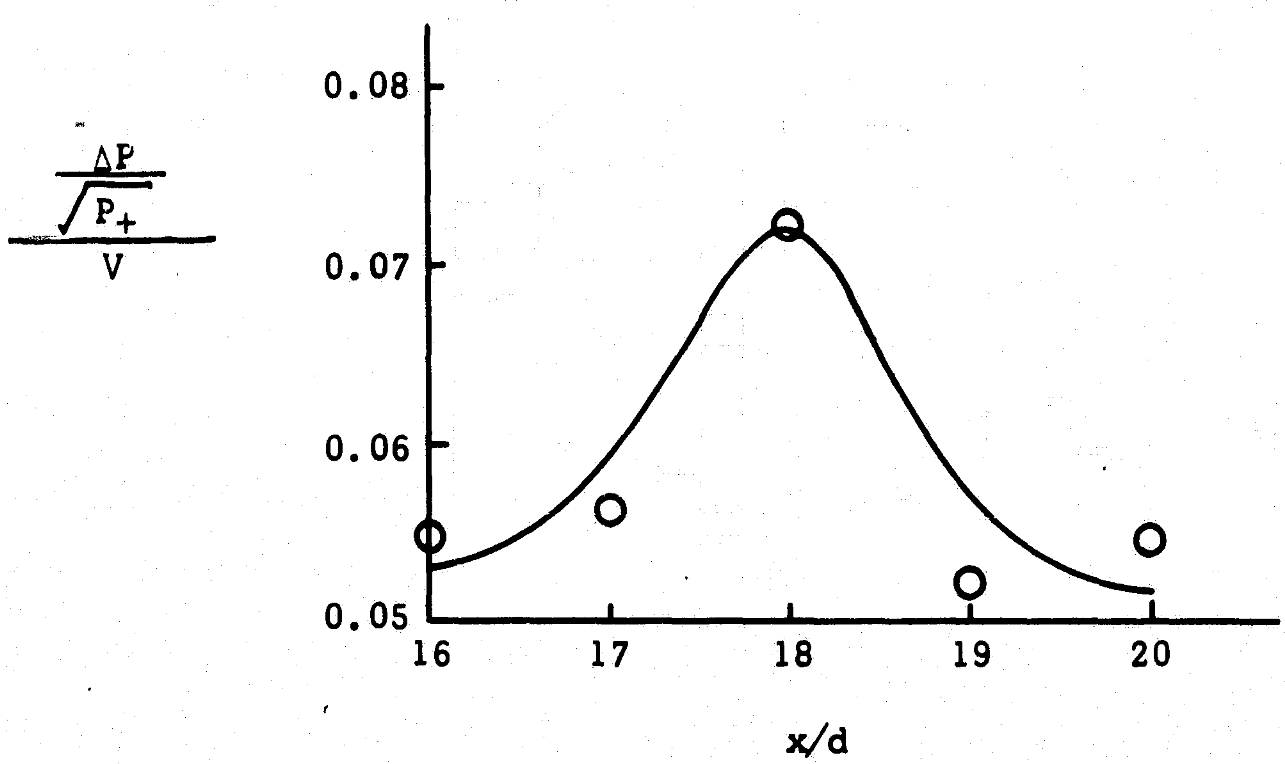

Figure 36

GAIN OF WIND SENSOR VS DISTANCE FROM POWER NOZZLE TO RECEIVER

D. Comparison of Sensors

Comparison of the Fluidic sensors tested and also a conventional Pitot tube is aided by Table I which shows the important factors in selection of a wind velocity sensor.

1. Pitot Tube

The prescribed range ($0.3 < V < 90$ ft/sec) of velocity cannot be met by the Pitot tube. Whereas it can read well beyond the specified 90 ft/sec (nearly up to 800 ft/sec), it is hampered at the low end by its square law behavior. The limit to the velocity which can be sensed is usually that of the pressure transducer or manometer, but manufacturers of the Pitot tubes caution that viscous effects become significant at or below velocities in the order of 10 ft/sec. Over the velocity range $12 < V < 90$ ft/sec the output pressure range is $0.00119 < \Delta P < 0.0845$ psid. The sensitivity of the device depends on the velocity, because of the square law.

2. Parallel Flow Wind Sensor

The parallel flow wind sensor provides a linear output pressure over the prescribed velocity range. With a supply pressure between 1-3 psig, the maximum output pressure is in the range 0.3 - 1 psid. A typical curve of pressure versus velocity was shown in Figure 35.

3. Cross Flow Sensor - Open Loop

The range of operation of the cross flow sensor in the open loop mode is limited by the fact that the jet profile must remain in the vicinity of the receivers. Although the receivers can be separated, the sensitivity then decreases, and is least where the wind velocity is smallest. At this small velocity is where sensitivity is especially needed because of the square law operating characteristic.

4. Cross Flow Sensor - Closed Loop

Although the range of the closed loop mode of operation of the cross flow sensor which was tested is limited, it does possess some qualities worth discussing. First of all, the output pressure is sufficiently high to drive other fluidic elements, which when considered in addition to its high fanout capability,

TABLE I

SUMMARY OF WIND SENSORS

	Pitot Tube	Cross Flow	Parallel Flow
Air Speed Range (ft/sec)	12 (minimum)	0 - 90	0 - 90
Maximum Pressure Signal at V = 0- ft/sec (psid)	.0637	0.5 to 1	.3 to 1
Supply Pressure (psig)	none	10 to 15	1 to 3
Velocity at 0.25% of full scale output pressure (ft/sec)	4.5	1.29	0.63
Threshold Tested (ft/sec)	-	0.26	0.28
Pressure-vs-Velocity Characteristic	Square Law	Modified Square Law With Saturation	Approx. Linear (Finite Slope at V = 0)

provides unique advantages from the standpoint of using this sensor in more complex systems. This must be a factor in use for computing to determine the wind direction. The sensitivity of this approach is far greater than that achieved by any of the others considered. Finally, over the range of operation, the output signal is proportional to the wind velocity. Since it was not a specific goal of this program to investigate this type of operation, no optimization was carried out. In particular, only a single receiver of the sensor was used to drive the Op-Amp, the other input being a bias pressure. The range of the Op-Amp is determined by such things as this bias pressure, and therefore, the range observed in testing thus far is not an indication of the potential of this scheme for wind sensing.

SECTION IV

CONCLUSIONS AND RECOMMENDATIONS

A. Conclusions

The following conclusions are noted from the results of this research study:

1. Fluidic techniques can be used for directly sensing wind speeds down to below 1/3 ft/sec. Compared to Pitot tubes, relatively high output signal pressures are achieved because of amplification produced by interaction between the wind and air jets.

2. Two fluidic concepts were verified as suitable for a wind sensor instrument. They are:

- Cross flow concept -- in which an air jet, perpendicular to the wind, is deflected by the wind by momentum exchange forces. The deflected jet produces a changing pressure in a receiver in a manner similar to the operation of a conventional fluidic analog amplifier. The receiver pressure is the measure of wind speed. The range of this type sensor may be extended by the closed loop mode of operation.

- Parallel flow concept -- in which an air jet, parallel to the wind, has its velocity modulated by the wind by viscous forces. The modulated jet velocity is detected as a changing pressure in a receiver which in turn is a measure of wind speed. This represents a new fluidic concept for achieving amplification.

3. The parallel flow concept has the following advantages over the cross flow concept.

- Better linearity
- More dynamic range
- Lower required supply pressure for a given maximum wind speed.

Because of these advantages, it is concluded that the parallel flow concept is better suited for aircraft use.

4. Mounting a sensor in a simple, straight collecting tube is generally satisfactory for measuring actual wind speeds over angles-of-attack up to 40 degrees in any direction from the tube centerline. A different external configuration will be needed to directly measure wind components.

5. The major problem experienced is the relatively high noise content in the output of the parallel flow sensor. The worst noise condition occurs when the wind is blowing against the jet. Much of the noise appears to have frequency components below 1 hz. Therefore, filters, which would attenuate this noise, might also filter out useful transient information. Consequently, filtering may not be a satisfactory solution.

6. The testing conducted during this program was performed at essentially standard conditions of sea level pressure and temperatures in the range of 70 to 80°F. Consequently, conclusions about performance under altitude or widely varying temperature conditions cannot be made at this time.

B. Recommendations

Because fluidic low speed wind sensing was demonstrated to be feasible, and furthermore, because the simplicity of the fluidic concepts offer potential cost and reliability advantages over comparable mechanical and electronic devices, it is recommended that research and development be continued. A meaningful program would have as its objective the demonstration of a multi-axis flight test model. Based on the results of this study and the above conclusions, the following specific steps are recommended.

1. Conduct a noise investigation to determine the noise sources. This can be done using various flow visualization techniques in both air and scaled water models. Secondary flows, primarily vortex formations inside the tube, are the probable causes of noise. By locating the vortices it will then be possible to formulate designs to either stabilize their positions or reduce their strength. Both of these actions would improve the signal-to-noise ratio.

2. Conduct an investigation of external configurations to determine the best method for sensing the wind speed component. The goal for this purpose would be a configuration which produces an output signal proportional to wind speed and the cosine of the angle-of-attack.

3. Design, fabricate, and test a flyable model of a single axis parallel flow sensor. This effort would provide an early investigation of this concept under flight conditions. Calibration of the model should be first done in a wind tunnel and then compared in flight with Pitot sensor and radar measurements. Altitude performance would also be studied during this testing. This effort would be necessary to consider design means for interfacing the sensor with the aircraft including the power supply and read out devices. Pitot reaction to the concept and performance of the flyable model might also be obtained.

4. Conduct analytical and experimental investigation of performance over variable pressure and temperature conditions. The testing of these effects should be carried out under laboratory conditions rather than in flight tests in order to get controlled test conditions. This investigation should also include a study of how the sensor's power supply pressure should be controlled during altitude conditions to obtain the desired performance.

5. Design, fabricate and test a flyable multi-axis low speed wind sensor model. This instrument would utilize the best design techniques as determined by the previous steps and would serve to demonstrate a complete two- or three-axis system.

APPENDIX A

DESIGN OF A LOW SPEED WIND TUNNEL

A. Introduction

Historically, the wind tunnel is a device for testing aircraft and their components under laboratory conditions. By virtue of their applications, their speeds range from approximately 10 mph to hypersonic velocities. More recently, four very low speed wind tunnels have been built for testing of burning rates, flame intensities and combustibility of organic foliage found in our national forest (References 9, 10). With these tunnels, speeds as low as 0.55 ft/sec have been obtained.

The major difficulty in low speed wind tunnel design is not that of moving the air, but rather one of measuring its velocity. This attests to the need for a low speed wind sensor as described in the body of this report.

B. The Bowles Fluidics Corporation Low Speed Wind Tunnel

Even the lowest speed of the aforementioned wind tunnels is a little high to satisfy the prescribed minimum velocity. Furthermore, the difficulties associated with testing of basic configurations suggest that it is desirable to work locally. For velocities above 10 ft/sec, the University of Maryland (which is located near Bowles Fluidics) will suffice, but for testing at lower velocities, it was decided to build a simple wind tunnel to operate over the range $0.3 < V < 15$ ft/sec.

The basic philosophy of the Bowles-built wind tunnel is to measure the mass flow rate through a metering orifice and relate this to the velocity in the test section. The velocity thus obtained is the average velocity and therefore, this must be modified to account for the boundary layer growth in the test section. In order to insure uniform flow outside of the boundary layer, a large stilling chamber is employed at the tunnel entrance. This is particularly important at the low wind velocities which may be less than the stray currents in the laboratory. The wind tunnel is open circuit and draws still air through the test section to minimize the turbulence level. Several alternate orifices (each of different diameter) were used so that a sizable pressure differential existed throughout the velocity range. These orifices were corrected for Reynolds number effects to provide greater accuracy. Velocity was regulated by varying a bypass area at the fan entrance.

The wind tunnel is shown in Figure A-1 without the settling chamber. At right is the Plexiglas test section (18" x 24"), which was designed to account for boundary layer growth. The calculations are based on an exact solution of the boundary layer equations for the entrance region of a channel (Reference 11). The flow next passes through a transition section into a circular pipe. This pipe is several diameters long in order to prepare the flow for the orifice. Corner taps on either side of the square-edged orifice provide the differential pressure. The flow then continues through another equal length of pipe before entering the fan. Immediately before the fan is a sliding segment of tube which varies the flow which passes through the wind tunnel. The fan is running with full flow at all times. Hanging below the tunnel are the various orifices used.

Figure A-2 shows the settling chamber in position at the entrance to the test section. The material of this section is a dense material composed of fine fibers. The size of the unit was determined by having the structure sufficiently far from the test section entrance so that the velocity was sufficiently low. The criterion for the maximum permissible velocity through the settling chamber was that for which vortex shedding would not occur on the fibers of the chamber. Inside the settling chamber is a short curved entrance section to the test section. (This is not visible in the photographs.) It was found that this was necessary in order to avoid flow separation at the entrance.

At the maximum velocity of this tunnel, the speed was checked against a Pitot tube and found to be in agreement. At the lower velocities, some hot wire measurements were made, and these indicate that the flow is uniform across the tunnel to within a few percent. It is, therefore, concluded that this wind tunnel is ideally suited to testing as low as 0.3 ft/sec wind velocity.

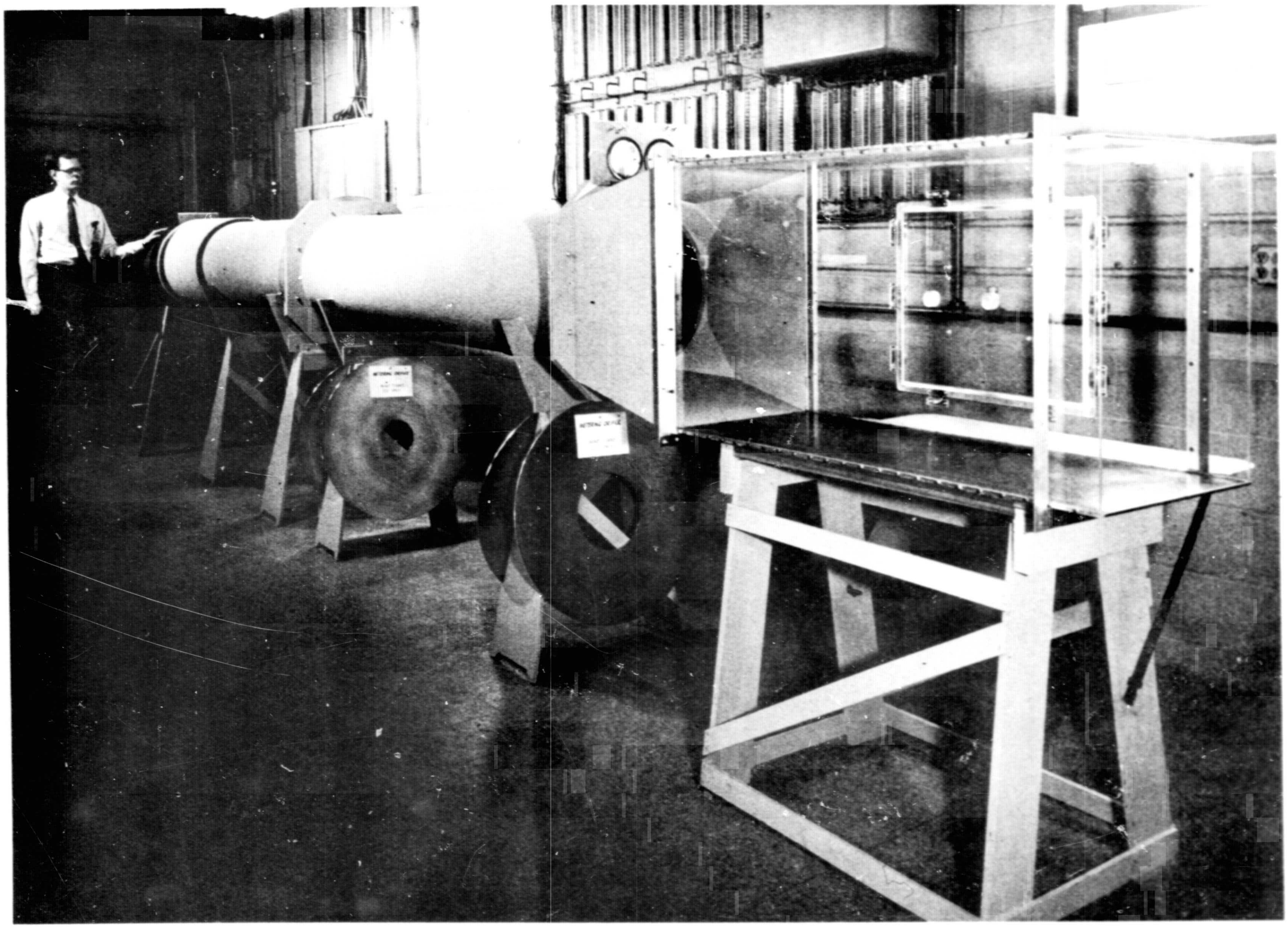

FIGURE A-1. LOW SPEED WIND TUNNEL

31183

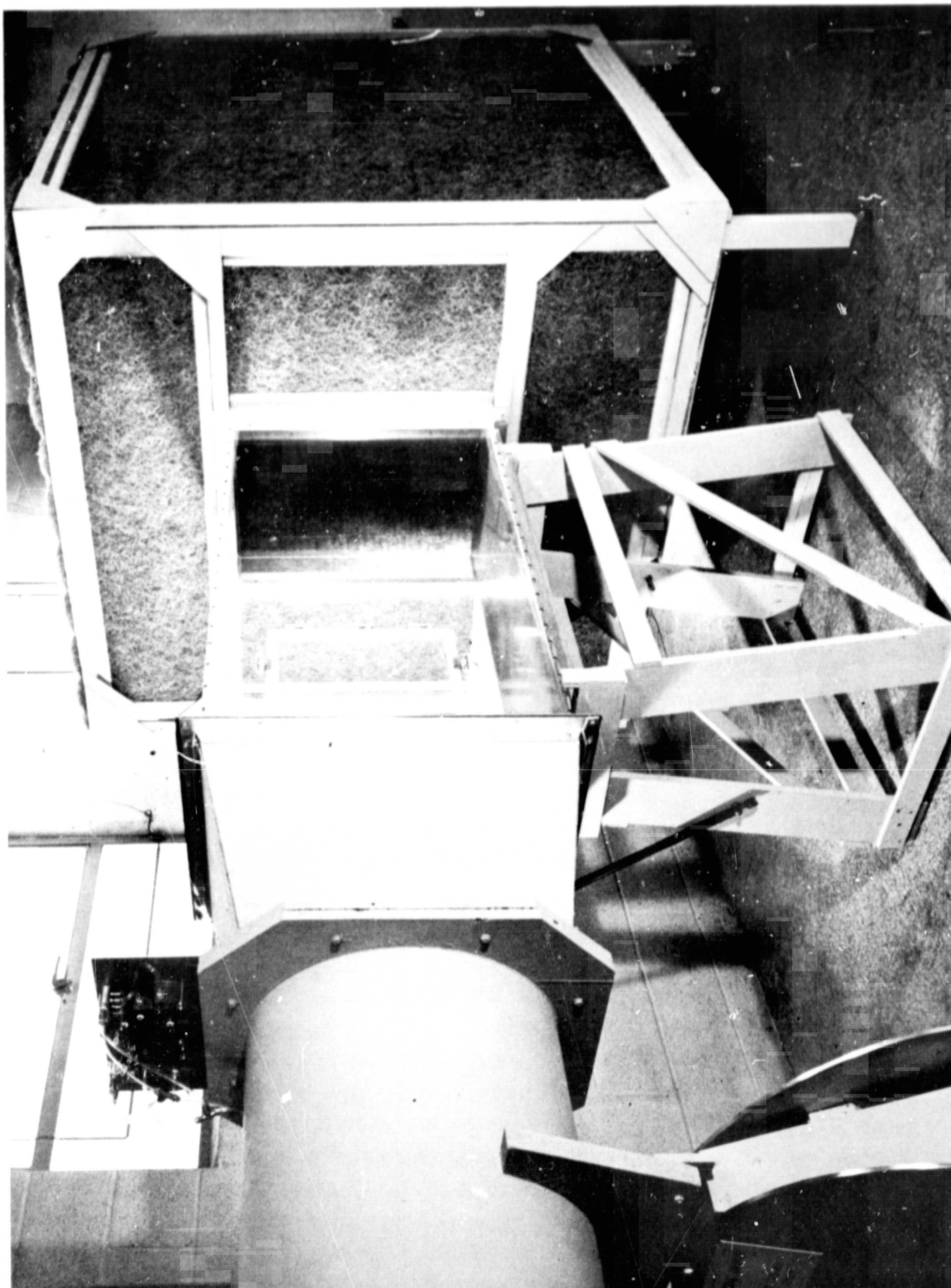

FIGURE A-2. LOW SPEED WIND TUNNEL SETTLING CHAMBER

31178

APPENDIX B

NEW TECHNOLOGY

Significant improvement was made in the technology of low speed air velocity measurement (p. 15). Specifically, this was done employing a new approach to fluidics in the parallel flow sensor; viz, modulating a jet velocity by viscous interaction between the jet and its surroundings (p. 64).

Improvement was also made in extending the potential range of the cross flow wind sensor by utilizing a fluidic operational amplifier in a closed loop mode of operation (p. 44).

REFERENCES

1. Merriam, K. G. and Spaulding, E. R., "Comparative Tests of Pitot-Static Tubes," NACA TN-46, 1935.

2. Salter, C., Warsap, J. H., and Goodman, Miss D. G., "A New Design of Pitot-Static Tube with a Discussion of Pitot Static Tubes and Their Calibration Factors," NPL Aers. Rept. 1013 - A.R.C. 23, 760, 1962.

3. Pope, Alan, "Wind Tunnel Testing," John Wiley & Sons, Inc., New York, 1961, p. 89.

4. Abramovich, G. N., "The Theory of Turbulent Jets," MIT Press, Cambridge, Massachusetts, 1963.

5. Pai, Shih-I, "Fluid Dynamics of Jets," Van Nostrand Co., Inc., New York, 1954.

6. Analysis of a Jet in a Subsonic Crosswind," NASA SP-218, Langley Research Center, 1969.

7. Neradka, V. F., and Turek, R. F., "Flueric Variable Gain Component Feasibility Study," Bowles Fluidics Corporation Report R-1-17-69.

8. Del Toro, Vincent and Parker, Sydney R., "Principles of Control Systems Engineering," McGraw-Hill Inc., New York, 1960, p. 544.

9. Anderson, H. E. and Rothermel, "Influence of Moisture and Wind Upon the Characteristics of Tree Burning Firs," Reprint from the 10th Symposium (International on Combustion), London, 1964.

10. Milburne, R. A., "The Design and Calibration of a Very Low Speed Open Circuit Wind Tunnel," M. E. Thesis, University of Oklahoma, Norman, Oklahoma, 1965.

11. Schlicting, H., "Boundary Layer Theory," McGraw-Hill, Inc., New York, 1958.